Dipartimento di Ingegneria dell'Informazione

Scuola di Dottorato di Ricerca in Ingegneria dell'Informazione
Indirizzo: Bioelettromagnetismo e Compatibilità Elettromagnetica

Ciclo XX

Tesi di Dottorato

Performance assessment of DVB-T and wireless communication systems by means of cross-layer measurements

Dottorando: Ing. Daniele Fortin

Supervisori: Ch.mo Prof. Matteo Bertocco

Dott. Ing. Alessandro Sona

Direttore della Scuola: Ch.mo Prof. Silvano Pupolin

Gennaio 2008

Alla mia famiglia, a Lucia

Sommario

Oggetto di questa tesi è lo studio e l'applicazione di metodologie di misura per l'analisi di segnali a modulazione digitale, utilizzati per comunicazioni wireless e per il broadcasting televisivo. L'obiettivo è sviluppare metodi che permettano di effettuare una stima efficace delle prestazioni dei sistemi di trasmissione - ricezione, al variare dei parametri di trasmissione e delle condizioni del canale trasmissivo. In questo modo è possibile ottenere indicazioni utili per l'ottimizzazione della configurazione di trasmissione e della pianificazione delle reti, riducendo al minimo l'impatto ambientale ed allo stesso tempo mantenendo un determinato livello di qualità del servizio. Le metodologie sviluppate, definite cross-layer measurements, prevedono che l'analisi del segnale sia effettuata simultaneamente a differenti livelli del sistema, in modo tale da ottenere una correlazione tra parametri stimati a livello fisico e parametri relativi a livelli superiori, quali transport, network e livello applicativo. Tali metodologie sono state applicate a un sistema di trasmissione DVB-T per il broadcasting televisivo (Parte I), in collaborazione con Digilab, Centro di competenza per le comunicazioni digitali di Bolzano, ed inoltre sono state utilizzate per la valutazione della coesistenza tra un sistema WLAN IEEE 802.11b ed una rete wireless di sensori IEEE 802.15.4 (Parte II).

Abstract

This thesis deals with the study and the application of measurement methods for the analysis of digitally modulated signals, deployed for wireless communications and television broadcasting. The goal is to develop methods allowing to efficiently assess the performance of transmission - reception systems upon the varying of transmission parameters and of the channel. In this way guidelines for the optimization of transmission set-up and of the network planning can be obtained, thus reducing the environmental impact of EM fields and at the same time providing an adequate quality of service. The methods developed, known as *cross-layer measurements*, provide an analysis of the signal to be simultaneously carried out at different layers. In this way correlation relationships between physical layer parameters and higher layer ones (transport, network, application) can be obtained. These cross-layer measurements are applied to a DVB-T transmission platform (Part I), in collaboration with Digilab, Bozen, and furthermore, they are deployed for the assessment of coexistence problems of IEEE 802.11b and IEEE 802.15.4 wireless networks (Part II)

Contents

Part I

Performance assessment and optimization of DVB-T systems

Introduction

Digital terrestrial television (DTT), also known as DVB- T (Digital Video Broadcasting-Terrestrial) television, is nowadays an efficient communication technology for broadcasting television (TV). Many countries in Europe are quickly moving toward DTT: necessary infrastructures are being realized, basic DVB-T applications are being developed and, above all, relevant problems are going to be solved. Concerning the last point, some problems are related to the setup and location of repeaters, gap fillers and other peripheral apparatuses within coverage areas; this task is rather complex and time consuming, involving a large amount of parameters, boundary conditions, and constraints to be considered. Other problems refer to in-channel interference. Such interference can be produced by digital or analogue TV networks of other broadcasters, or can be due to spurious components from different transmitters, located in the proximity to the ones of interest, as well as to radiated emissions from electrical and electronic appliances operating in the nearness of victim receivers. To provide an optimized setup of a DVB-T system, the effects of such interference should be known and carefully accounted for. Few application notes are available in literature to the purpose; they, however, cover only a partial set of practical guidelines. As a matter of fact, in [19] interesting results are given, but they concern measurements performed only in the presence of impulsive interference and only at application layer through estimates of visual errors on the decoded picture. In [28], major effects of impulsive noise in a UHF (Ultra High Frequency) channel are analyzed only theoretically, through statistical models. In [29], some models are proposed for predicting in-channel and adjacent channel Phase Altering Line (PAL) interference effects on digital terrestrial television. In this work, the effects produced on DVB-T systems performance both by Additive White Gaussian Noise (AWGN) and impulsive interference are experimentally assessed. In particular, a cross-layer approach is applied involving the following two layers: physical layer, with relevant quantities such as received power, signal-to-interference ratio (SIR) and modulation error ratio (MER); application layer, through objective video quality estimates of the whole video stream received. Two main goals are pursued. From one side,

results showing how some parameters of DVB-T systems vary in the presence of interference are gained. From the other side, information and hints useful for characterizing and optimizing DVB-T system performance are deduced; special attention is paid to the role played by code rate.

Part I of the thesis, dealing with the definition and the application of cross-layer measurement method for the performance assessment of a DVB-T system performance, is organized as follows. In Chapter 1 the OFDM modulation technique, used for DVB-T signal transmission, is introduced. Chapter 2 deals with the main features of the DVB-T standard. In Chapter 3 the main typologies of in-channel interfering signals, AWGN and impulsive noise, are briefly described. Cross-layer measurements and the corresponding parameters are detailed in Chapter 4: signal power, modulation quality and video quality. The hardware and software components of the testbed are described in Chapter 5 and in Chapter 6 the results of the experiments performed upon the varying of the transmission configuration and the type of interference are presented.

Chapter 1

OFDM modulation technique

1.1 Introduction

In the modern information technology scenario, the demand and usage of new efficient standards for wireless communication networking is rapidly increasing. The mobile telephony, with voice, video and data applications, exploits consolidated digital modulation techniques: GSM, GPRS and UMTS are standards supporting long range wireless communication, mobility, robustness to channel degradation, low energy consumption. At present, wireless broadband communications are widely used to support networking (WLAN) as well as audio and video broadcasting (DVB) that require higher data rates and also higher quality of service with respect to mobile telephony. A widespread diffusion of these services, i.e. the increasing number of Wi-Fi hot-spots, the use of wireless to implement the last mile, the planned switch-off of analogue TV replaced by digital terrestrial TV, and in the very near future the diffusion of mobile multimedia terminals, are ongoing.

These wireless communication services are based on digital modulation techniques that provide both large data rates and robustness to radio channel impairments, like the multicarrier modulation techniques; in particular the orthogonal frequency division multiplexing (OFDM) is the most commonly employed. In this Chapter the main features of OFDM and the implementation of an OFDM system using the discrete Fourier Transform are described.

1.2 From single-carrier to multicarrier modulation

In classical digital communications systems, single-carrier modulation techniques are utilized. Single-carrier systems convey information by varying frequency, phase, or amplitude of a periodic waveform, i.e. a sinusoid, used as carrier signal. The messages produced by the input source are converted

into a sequence of bit. The information bits are grouped and mapped into a finite number of symbols, whose values are used to modulate the analog carrier. As higher data rates are used, the duration of one bit or symbol of information becomes smaller and the required bandwidth increases. This leads to greater susceptibility of the transmitted signal to interferences from other signal sources and to radio channel impairments.

The Frequency Division Multiplexing (FDM) is a technique that extends the concept of single-carrier modulation toward the *multicarrier modulation*. A multicarrier modulation is a transmission technique where a single datastream is split into a number of lower rate streams, that are transmitted over a number of carriers. It is obtained by modulating in parallel these carriers, denoted as *subcarriers*, using blocks of K symbols. Each subcarrier is modulated with a separate symbol; consequently, the symbol period is longer than the symbol period of a single-carrier system transmitting at the same rate. The K resulting signals are then frequency-multiplexed: in a classical FDM system the total signal frequency band is divided into K non-overlapping frequency subchannels to avoid interchannel interference, as represented in Fig.1.1. The main advantages of FDM systems are the robustness to multipath delay spread, due to symbol duration increase, and robustness to radio channels impairments like frequency selective fading or narrowband interference. In fact, in a single-carrier system a single narrowband interferer can cause a severe performance degradation while in a multicarrier system, only a few subcarriers will be affected.

1.3 Orthogonal Frequency Division Multiplexing

The **Orthogonal Frequency Division Multiplexing (OFDM)** is an improved form of FDM providing an optimized occupation of the frequency spectrum. As highlighted in Fig.1.1 a drawback of the FDM is the inefficient use of the available spectrum, due to the required frequency separation between adjacent subcarriers. This fact can be overcome by an overlapping multicarrier modulation technique, like OFDM. In order to avoid intercarrier interference (ICI) introduced by channel overlapping, orthogonality between the different modulated subcarriers is required. The use of orthogonal subcarriers allows the spectra to partially overlap, thus increasing spectral efficiency, while keeping the possibility to recover the individual signals of the subcarriers without adjacent carrier interference.

1.3.1 Orthogonality

The definition of orthogonality states that two signals are orthogonal if their scalar product is zero, meaning that if these signals are multiplied together

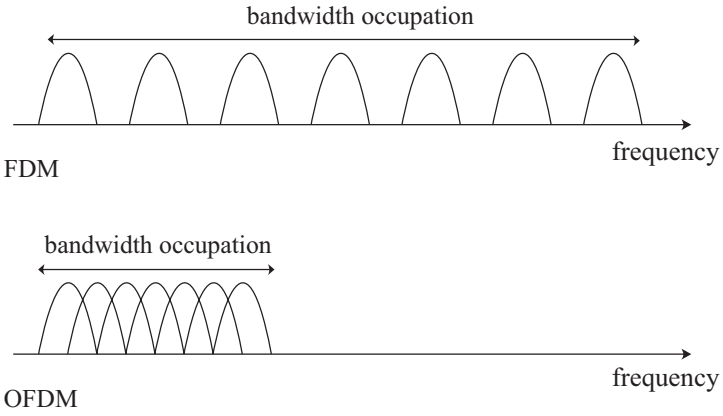

Figure 1.1 Spectral occupation of FDM and OFDM systems.

and integrated over a given interval, then they are orthogonal in that interval if the result is zero. The OFDM technique provides that the frequency of each subcarrier is selected to form an orthogonal signal set. Orthogonality condition is satisfied by the set of subcarriers when each subcarrier has an integer number of cycles in the interval T_o and the number of cycles between adjacent subcarriers differs by one. In Fig. 1.2 it is reported an example of orthogonal sinusoids in the time domain. The three sinusoids have frequency $f_m = m \cdot 1/T_o$ respectively with $m = 1, 2$ and 3. In the frequency domain the spacing between these carriers is equal to $1/T_o$.

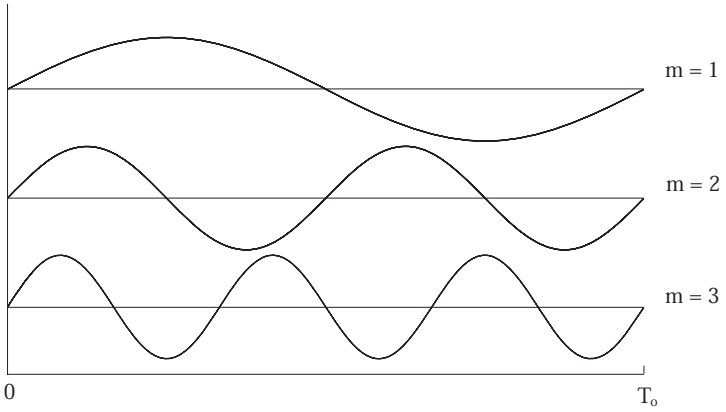

Figure 1.2 Example of orthogonal sinusoids with frequency $f_m = m \cdot \frac{1}{T_o}$.

The OFDM signal consists of a sum of the subcarriers from the orthogonal

set, each of which is individually modulated by using phase shift keying (PSK) or quadrature amplitude modulation (QAM), as represented in the simplified scheme of Fig.1.3. When the OFDM signal is received, each carrier is down-

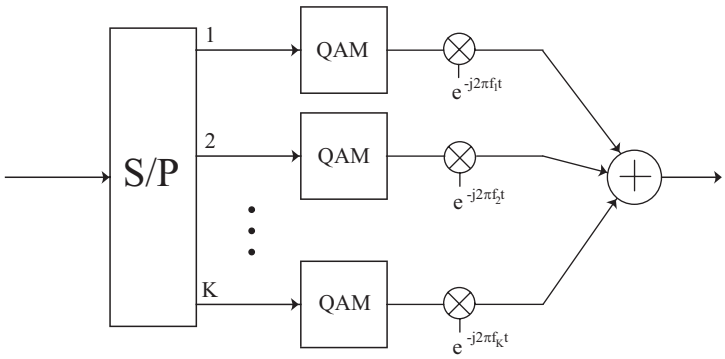

Figure 1.3 A simplified scheme of OFDM modulator. The frequency of the K subcarriers is $f_1, f_2, \ldots, f_K$ respectively.

converted by the receiver, that acts as a bank of demodulators. The resulting signal is integrated over a symbol period to produce the original set of data. For a given subcarrier translated down to DC, the integration process gives the QAM value for that particular subcarrier, while for all the other subcarriers the integration process results in zero contribution, due to orthogonality. In this way, all the K symbols of a transmitted block can be recovered from the K modulated subcarriers.

It is useful to consider the orthogonality property of the subcarriers also in the frequency domain. For a single OFDM subcarrier with frequency equal to f_1, the transmitted pulse can be modeled in the time domain as a sinusoid multiplied by a *rect* function with length equal to the symbol period T_o. In the frequency domain the resulting spectrum has a *sinc* shape centered at the subcarrier frequency f_1. The sinc has nulls for all frequencies that are an integer multiple of $1/T_o$, i.e. at the adjacent carrier frequencies. Consequently, at the maximum of each subcarrier spectrum all other subcarriers spectra are zero. Fig.1.4 shows an example of the resultant overlapping sinc spectra of five subcarriers with frequency equal to $f_m = m \cdot 1/T_o$ with $m = 1, \ldots, 5$ respectively. The figure highlights that the peak of each spectrum corresponds to the zero crossings of the adjacent sincs. At the receiver side the spectrum values are calculated at those points that correspond to the peaks of individual subcarriers; in this way, each subcarrier can be demodulated without interference from the other subcarriers.

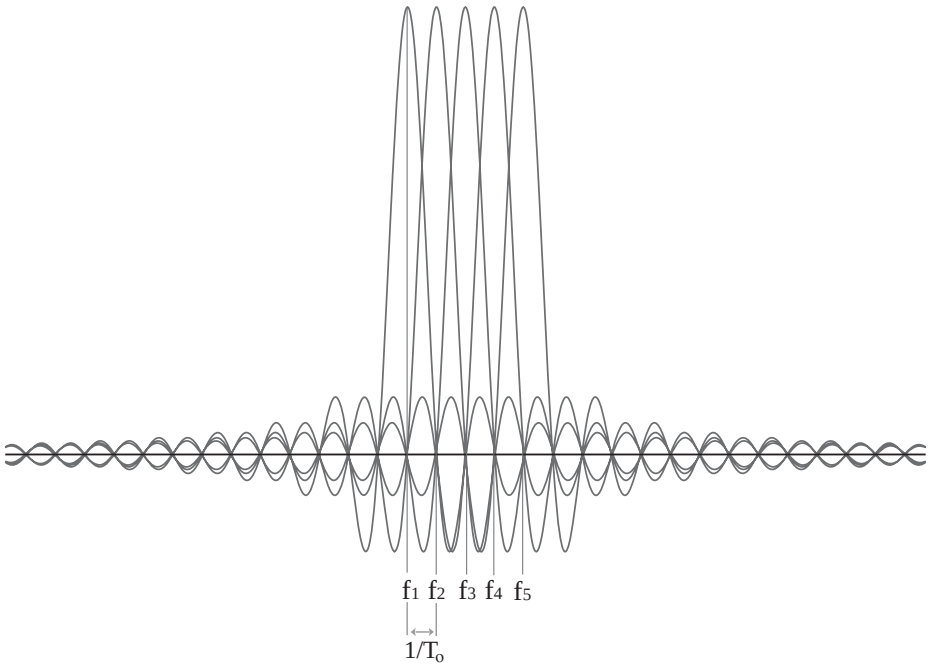

Figure 1.4 Overall spectrum of five orthoghonal subcarriers with frequency equal to $f_m = m \cdot 1/T_o$ for $m = 1, \ldots, 5$ respectively.

1.3.2 Implementation of an OFDM system using the IDFT

Since an high number of subcarriers is used to exploit the advantages of a multicarrier modulation technique like OFDM, an efficient implementation of the system is required. In fact, when thousands of subcarriers are employed, like for example in DVB-T systems, it is unthinkable to use banks of thousands QAM modulators and oscillators working in parallel, as sketched in Fig.1.3.

An efficient implementation of OFDM can be realized in the digital domain by using the *discrete Fourier Transform* (DFT) and its inverse (IDFT). Let's consider a OFDM system with K subcarriers, where T is the QAM symbol duration, T_U is the OFDM symbol period ($T_U = KT$) and a_k is the complex QAM symbol value. One OFDM symbol starting at $t = 0$ can be expressed, for $0 \leq t \leq T_U$, as:

$$s(t) = \Re e \left\{ \sum_{k=-\frac{K}{2}}^{\frac{K}{2}-1} a_{k+\frac{K}{2}} \cdot e^{j2\pi f_k t} \right\} = \Re e \left\{ \sum_{k=-\frac{K}{2}}^{\frac{K}{2}-1} a_{k+\frac{K}{2}} \cdot e^{j2\pi (f_0 + \frac{k}{T_U})t} \right\} \quad (1.1)$$

where $f_k = f_0 + \frac{k}{T_U}$ and f_0 is the carrier frequency; $f_{-\frac{K}{2}}$ is the frequency of the

first subcarrier, $f_{\frac{K}{2}-1}$ is the frequency of the K-th subcarrier. Let's consider the index n instead of k, with $n = k + \frac{K}{2}$, $n = 0, \ldots, K-1$. Using the complex baseband notation the OFDM symbol can be expressed as:

$$s(t) = \sum_{n=0}^{K-1} a_n \cdot e^{j2\pi \, \frac{n}{T_U} \, t} \tag{1.2}$$

The time discrete equivalent results:

$$s(m\,T) = \sum_{n=0}^{K-1} a_n \cdot e^{j2\pi \, \frac{n\,m}{K\,T}} \quad \text{with} \quad m = 0, \ldots, K-1 \tag{1.3}$$

and the m-th sample, s_m, can be written as:

$$s_m = \sum_{n=0}^{K-1} a_n \cdot e^{j2\pi \, \frac{n\,m}{K}} \quad \text{with} \quad m = 0, \ldots, K-1 \tag{1.4}$$

It corresponds to the inverse discrete Fourier Transform (IDFT) of the vector $\underline{a} = [a_0, a_1, \ldots, a_{K-1}]$, which is the block of K QAM input symbols that constitute an OFDM symbol. The IDFT can be implemented very efficiently by the inverse fast Fourier Transform (IFFT). This transform is used at the OFDM transmitter to map input data into a set of orthogonal subcarriers. In the same way, the discrete Fourier Transform (DFT) is used at the OFDM receiver to process the received subcarriers and recover the data. The OFDM system treats the QAM symbols at the transmitter as though they are in the frequency-domain. The QAM symbols are used as the inputs to an IFFT block that converts the signal into the time domain. The IFFT takes in a block of K symbols at a time where K is the number of subcarriers in the system. Each of these K input symbols, with symbol period of T seconds, acts like a complex weight for the corresponding sinusoidal basis function. Since the input symbols are complex, the value of the symbol determines both the amplitude and phase of the sinusoid for that subcarrier. The IFFT output is the summation of all K sinusoids. Thus, the IFFT block provides a simple way to modulate data onto K orthogonal subcarriers. The block of K output samples from the IFFT make up a single OFDM symbol, whose duration is equal to KT. At the receiver, an FFT block is used to process the received signal and bring it into the frequency domain. In ideal conditions, the FFT output will be the original symbols sent to the IFFT at the transmitter [1], [2].

1.3.3 Guard interval

As stated before, one of the main advantages of OFDM systems is high immunity to multipath. In wireless systems multiple delayed versions of the signal

arrive at the receiver, due to reflections off objects or buildings of the transmitted signal, that cause intersymbol interference (ISI). ISI occurs when, for example, the first samples of a symbol are received simultaneously to the last samples of the previous symbol, as sketched in Fig.1.5. To efficiently avoid intersymbol interference, a guard time is introduced for each OFDM symbol. The *guard interval* is a relevant feature of OFDM systems, in particular of DVB-T (Sec. 2.2), that plays a fundamental role in mitigating negative effects of echoes and multipath. In order to preserve the orthogonality between the subcarriers, the guard interval consists of a cyclic extension of the transmitted symbol and is inserted before it [1]. For this reason it is also referred to as *cyclic prefix*. The first samples of each received symbol, corresponding to the guard interval, are discarded at the receiver as they do not contain useful data. If the guard interval is larger than the delay of the multipath component, each symbol is not distorted by the delayed version of the previous one and the effects of ISI can be avoided. Fig.1.5 highlights the effect of the guard interval

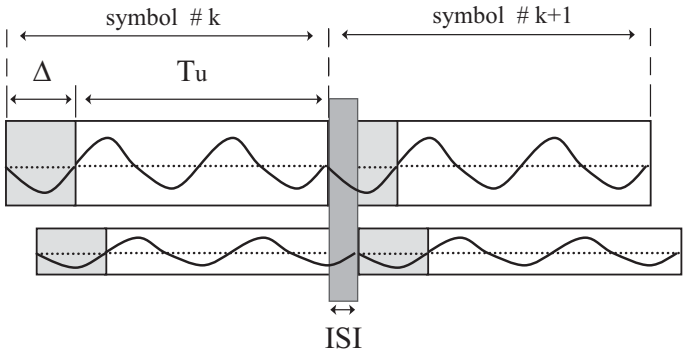

Figure 1.5 Example of intersymbol interference (ISI) between $k-th$ received symbol and $(k+1)-th$ received symbol. T_U is the useful symbol duration, Δ is the guard interval duration.

against ISI. A signal and its delayed and attenuated replica are reported, with a useful symbol duration T_U and the guard interval duration equal to Δ; the guard interval is represented in light grey. The first samples of the $(k+1)-th$ symbol are degraded by the last ones of the delayed $k-th$ symbol in the ISI time region, represented in dark grey. As the ISI region is shorter than Δ, the symbol only interferes with itself and not with the previous one, which leads only to a scaling and rotation of the symbol of the resulting signal. If the multipath delay becomes larger than the guard interval, orthogonality is lost, because in that case the phase transitions of the delayed replica are not discarded at the receiver and fall within the FFT interval.

In OFDM system design, the choice of the guard interval duration Δ re-

quires a tradeoff between the maximum tolerable delay spread and the bit rate. Since the guard interval does not contain useful information the bit rate is reduced upon the increasing of Δ.

Further details on OFDM modulation technique can be found in [1], [2], [3].

Chapter 2

DVB-T standard

2.1 Introduction

Digital Video Broadcasting (DVB), is a set of internationally accepted open standards for digital television, maintained by the DVB Project. The Digital Video Broadcasting Project is an industry-led consortium of over 260 broadcasters, manufacturers, network operators, software developers, regulatory bodies and others in over 35 countries. These standards are published by a Joint Technical Committee (JTC) of European Telecommunications Standards Institute (ETSI), European Committee for Electrotechnical Standardization (CENELEC) and European Broadcasting Union (EBU).

The three key DVB standards concern the delivery of digital TV to the consumer via the traditional broadcast networks and define the physical layer and data link layer of the distribution system:

- DVB-S for satellite networks
- DVB-C for cable networks
- DVB-T for terrestrial networks

In addition to these, a range of supporting standards has been developed for elements such as service information, interfacing, return channel standards and Multimedia Home Platform (MHP). Furthermore DVB Project developed standards for the delivery of DVB services over fixed and wireless telecommunications networks, e.g. DVB-H mobile TV for handheld devices, DVB-IPTV for TV via Internet Protocol networking [4].

2.2 DVB-T

In the ETSI 300 744 standard [5], the DVB-T system is defined as *the functional block of equipment performing the adaptation of the baseband TV signals from the output of the MPEG-2 transport multiplexer, to the terrestrial channel characteristics.* The system is designed for digital terrestrial television services to operate within the existing VHF (Very High Frequency) and UHF (Ultra High Frequency) spectrum allocations for analog transmissions, 50-230 MHz and 470-870 MHz respectively. The DVB-T standard is based on the Orthogonal Frequency Division Multiplexing (OFDM) multicarrier modulation scheme with concatenated error correcting coding, also referred to as COFDM (where "C" stands for *coding*). The transmission data stream is distributed over a set of orthogonal subcarriers, equally spaced in pre-assigned VHF and UHF channels, characterized by a bandwidth equal respectively to 7 MHz and 8 MHz. Each subcarrier is then digitally modulated according to a QPSK, 16-QAM or 64-QAM scheme. The number of subcarriers can be set according to two modes of operation: *2K mode* and *8K mode*; in fact the DVB-T system may employ either $K_{tot} = 2048$ subcarriers in the 2K mode, or $K_{tot} = 8192$ subcarriers in the 8K mode. The corresponding number of *active* subcarriers is respectively 1705 and 6817, while subcarriers dedicated to useful data are 1512 in 2K mode and 6048 in 8K mode. Exclusively for use in DVB-H systems, a third transmission mode with 3409 active subcarriers, *4K mode*, is defined.

The processes applied to the input data stream are listed in the following and sketched in Fig. 2.1:

- transport multiplex adaptation and randomization for energy dispersal
- outer coding
- outer interleaving
- inner coding
- inner interleaving
- mapping and modulation
- Orthogonal Frequency Division Multiplexing (OFDM) transmission

2.2.1 MPEG-2 Transport Stream

The input baseband signal of a DVB-T system is a MPEG-2 multiplex transport stream (TS). The TS is a continuous sequence of packets with a fixed length of 188 bytes. The first 4 bytes of each packet constitute the header,

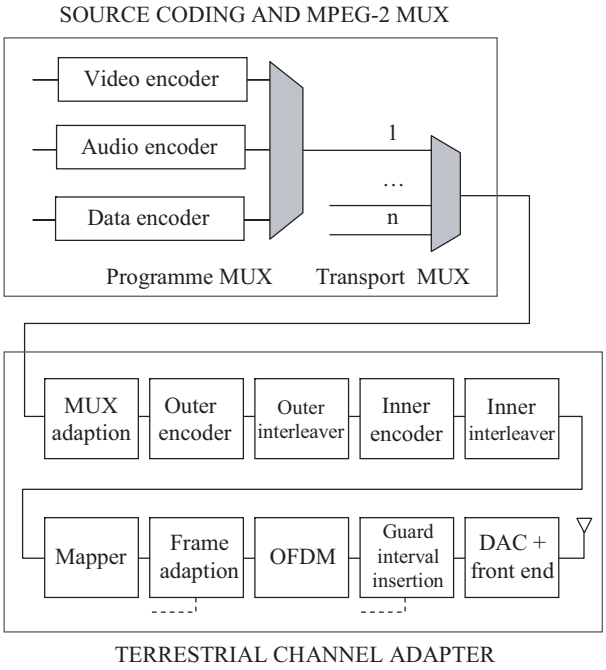

Figure 2.1 Block diagram of a DVB-T transmitter.

containing the synchronization byte and the packet identifier (PID), the following 184 bytes are used for the payload. In addition to video and audio streams the payload of the TS may be composed by other components like teletext data, subtitling, additional services and also IP packets encapsulated over MPEG [7].

2.2.2 Channel Coding: Outer Code, Inner Code

Before the baseband signal can be transmitted, a forward error correction (FEC) is required in order to enable the receiver to correct errors that may occur in the transmission path, due to noise and other interferences. To maximize commonality with the Satellite baseline specification and Cable baseline specifications the outer coding and outer interleaving are common, and the inner coding is common with the Satellite baseline specification. Before the coding an energy dispersal process is applied: the data at the baseband interface is combined with the bit stream of a pseudorandom noise generator to achieve a flat power-density spectrum.

Outer Coding and Interleaving

The outer error protection is implemented with a byte-oriented block code. For each block, i.e. the TS packet constituted by 188 information bytes, 16 error correcting bytes are calculated and appended to that packet. To achieve this, a Reed-Solomon (204, 188, t = 8) shortened code is used, derived from the original systematic Reed-Solomon (255, 239, t = 8) code. After the coding process convolutional byte-wise interleaving is applied to the error protected packets: an outer convolutional interleaver rearranges the bytes of the packets in order to facilitate the correction of long burst errors.

Inner Coding and Interleaving

A second level of error correction, denoted as inner coding, is subsequently applied. In particular, a punctured convolutional coding with code rate m/n, i.e. the ratio between number of useful bits, m, and number of useful plus redundancy bits, n, is applied to the input binary sequence. Therefore, $n-m$ redundancy bits for error correction are added to each group of m useful bits. The system allows for a range of punctured convolutional codes, based on a mother convolutional code of rate 1/2 with 64 states [5]. Puncturing is a technique used to obtain a m/n code rate, from the basic rate 1/2 code, thus reducing the amount of redundancy. It is reached by deletion of some bits at the encoder output according to a fixed puncturing matrix [5]; in this way not all of the calculated output bits are transmitted. This allows selection of the most appropriate level of error correction for a given service or data rate: in addition to the mother code of rate 1/2 the system allows punctured rates of 2/3, 3/4, 5/6 and 7/8. The choice of code rate allows to match the needs of error protection and throughput. In particular, 1/2 is the best choice in terms of robustness against errors, but worst in terms of useful bit rate. On the contrary, 7/8 is efficient in terms of throughput but less robust to errors and interference. If two level hierarchical transmission (Subsection 2.2.3) is used, each of the two parallel channel encoders can have its own code rate.

An inner interleaver follows the inner error protection; it consists of block-based bit-wise interleaving and block-based symbol interleaving. In the bit-wise interleaving process the input is demultiplexed into v sub-streams, where $v = 2$ for QPSK, $v = 4$ for 16-QAM, and $v = 6$ for 64-QAM. Each sub-stream is then processed by a separate bit interleaver where 126 successive input bits are grouped into one block and are then interleaved within this block. The purpose of the symbol interleaver is to map v bit words onto the 1512 (2K mode) or 6048 (8K mode) data carriers per OFDM symbol, where each OFDM symbol is constituted by the sequence of the 1705 or 6817 data symbols of the corresponding active subcarriers. The symbol-wise interleaver acts on blocks

of 1512 or 6048 data symbols by changing their sequence. The result on the DVB-T signal is frequency interleaving inside an OFDM symbol [7].

2.2.3 Modulation: OFDM

The choice of the OFDM modulation technique is due to the very different characteristics of the terrestrial channel with respect to both the satellite and the cable channel. In fact the signal may be impaired by severe multipath propagation resulting both from the buildings inside urban areas and from the orography of the coverage areas. The OFDM modulation scheme provides high immunity to multipath fading and several other advantages: high data rate, efficient management of the frequency spectrum, coexistence of single frequency networks (SFN) with the conventional multifrequency ones (MFN), and low minimum levels of ratio C/N, between the carrier power C and the noise level N, required in order to guarantee an acceptable quality of service.

Mapping

Subsequently to the inner interleaving the symbol mapping process is performed. Each data subcarrier of the OFDM signal is separately modulated using either QPSK, 16-QAM or 64-QAM scheme. The Gray mapping [5] is applied for the allocation of v sequential bits to one carrier, either $v = 2$ for QPSK, $v = 4$ for 16-QAM, or $v = 6$ for 64-QAM.

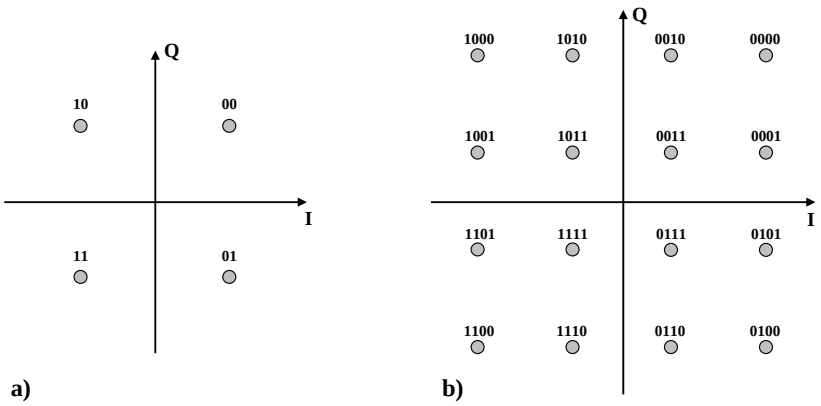

Figure 2.2 Constellations and corresponding Gray mappings of QPSK (a) and 16-QAM (b) schemes.

The system also allows a two level hierarchical modulation for the transmission of data streams with different priority levels. With this technique, two independent data streams are inserted in the same signal and mapped

using different modulation techniques, like for example QPSK for one stream and 16-QAM for the second stream. Consequently, the robustness against transmission errors is higher for the first stream (high priority) with respect to the second one (low priority). Furthermore, for hierarchical modulation non-uniform 16-QAM or non-uniform 64-QAM constellations may be deployed [5].

OFDM frame structure

The transmitted signal is organized in frames; each of them consists of 68 OFDM symbols and has a duration of T_F. Each symbol, constituted by a set of $K = 6817$ subcarriers in the 8K mode and $K = 1705$ subcarriers in the 2K mode, is transmitted with a duration T_S. It is composed of two parts: a useful part, with duration T_U, and a *guard interval* with a duration Δ. The guard interval consists in a cyclic continuation of the useful part, T_U, and is inserted before it (Fig. 2.3). Four values of guard intervals, expressed as a fraction of the useful part, may be used: $\Delta/T_U = 1/4, 1/8, 1/16$ or $1/32$. The flexibility of the guard interval allows to trade off between network topology and frequency efficiency, enabling the system to support different network configurations (cf. Parag. Network architectures: MFN, SFN) while keeping maximum frequency efficiency. The spacing between adjacent subcarriers is $1/T_U$ while the spacing

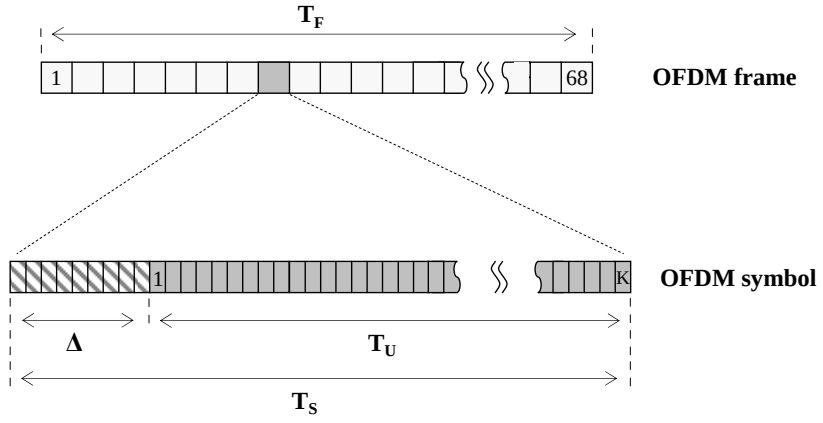

Figure 2.3 OFDM frame and OFDM symbol structure. K=1705 for 2K mode, K=6817 for 8K mode.

between the first and the last subcarrier is determined by $(K-1)/T_U$.

The standard [5] fixes the elementary period T, i.e. the duration of a single carrier data symbol, equal to $7/64$ μs for the 8 MHz channel, and equal to $1/8$ μs for 7 MHz channels. Taking into consideration only the 8 MHz channel,

the OFDM symbol duration is therefore:

$$T_U = K_{tot} \cdot T = \begin{cases} 2048 \cdot \frac{7}{64}\ \mu s = 224\ \mu s & \text{for 2K mode} \\ \\ 8192 \cdot \frac{7}{64}\ \mu s = 896\ \mu s & \text{for 8K mode} \end{cases}$$

the carrier spacing is:

$$1/T_U = \begin{cases} 4464\ Hz & \text{for 2K mode} \\ \\ 1116\ Hz & \text{for 8K mode} \end{cases}$$

and the spacing between the first and the last subcarrier is:

$$(K-1)/T_U = \begin{cases} 7.61\ MHz & \text{for 2K mode} \\ \\ 7.61\ MHz & \text{for 8K mode} \end{cases}$$

The numerical values of the OFDM parameters for the 8K and 2K modes for 8 MHz channels are summarized in Table 2.1.

Parameter	**8K mode**				**2K mode**			
Number of carriers K	6817				1705			
Duration of symbol part T_U	896 μs				224 μs			
Carrier spacing $1/T_U$	1116 Hz				4464 Hz			
Guard interval Δ/T_U	1/4	1/8	1/16	1/32	1/4	1/8	1/16	1/32
Duration of guard interval Δ (μs)	224	112	56	28	56	28	14	7
Symbol duration $T_S = T_U + \Delta$ (μs)	1120	1008	952	924	280	252	238	231

Table 2.1 DVB-T symbol parameters for 8K and 2K modes for 8 MHZ channels.

The availability of a number of configuration parameters allows to define several transmission setups, which provide different performance in terms of useful data rate and robustness against errors, interference, multipath, etc.. In Table 2.2 the useful data rates (in Mbps), for all combinations of guard interval, modulation and code rate, are reported for the case of 8 MHz transmission channel. The data rate is independent of the transmission mode (2K or 8K).

In the DVB-T standard [5], simulated performance of channel coding and modulation combinations are given. These results are reported in Table 2.3

Modulation	**Code Rate**	**Guard interval Δ/T_U**			
		1/4	**1/8**	**1/16**	**1/32**
QPSK	1/2	4.98	5.53	5.85	6.03
	2/3	6.64	7.37	7.81	8.04
	3/4	7.46	8.29	8.78	9.05
	5/6	8.29	9.22	9.76	10.05
	7/8	8.71	9.68	10.25	10.56
16-QAM	1/2	9.95	11.06	11.71	12.06
	2/3	13.27	14.75	15.61	16.09
	3/4	14.93	16.59	17.56	18.10
	5/6	16.59	18.43	19.52	20.11
	7/8	17.42	19.35	20.49	21.11
64-QAM	1/2	14.93	16.59	17.56	18.10
	2/3	19.91	22.12	23.42	24.13
	3/4	22.39	24.88	26.35	27.14
	5/6	24.88	27.65	29.27	30.16
	7/8	26.13	29.03	30.74	31.67

Table 2.2 DVB-T useful data rates (Mbps) for 8 MHz channels.

for the Gaussian channel and Ricean channel, in terms of required carrier-to-noise ratio C/N (dB) for non-hierarchical transmission to achieve a BER $= 2 \times 10^{-4}$ after the inner (Viterbi) decoder, Quasi Error Free (QEF)[1] after the Reed-Solomon decoder.

Gaussian channel is a communications channel subject to Gaussian noise (Sec. 3.2). Ricean channel is a model for transmission channel that has a line-of-sight component and several scattered of multipath components, which cause partial cancelation or fading of the radio signal at the receiver. Ricean fading occurs when one of the paths, typically a line of sight signal, is much stronger than the others. This fading characteristic exhibits a Ricean probability density function.

Reference signals and Transmission Parameter Signalling carriers

As reported above, only a part of the the active subcarriers is dedicated to useful data, that is 1512 subcarriers in 2K mode and 6048 subcarriers in 8K mode. In fact, an OFDM frame contains further information necessary at the receiver side. The additional carriers can be grouped as follows:

[1]Quasi Error Free (QEF) means less than one uncorrected error event per hour, corresponding to BER $= 10^{-11}$ at the input of the MPEG-2 demultiplexer.

Modulation	Code Rate	Gaussian channel	Ricean channel
QPSK	1/2	3.1	3.6
	2/3	4.9	5.7
	3/4	5.9	6.8
	5/6	6.9	8.0
	7/8	7.7	8.7
16-QAM	1/2	8.8	9.6
	2/3	11.1	11.6
	3/4	12.5	13.0
	5/6	13.5	14.4
	7/8	13.9	15.0
64-QAM	1/2	14.4	14.7
	2/3	16.5	17.1
	3/4	18.0	18.6
	5/6	19.3	20.0
	7/8	20.1	21.0

Table 2.3 Required C/N (dB) for BER $= 2 \times 10^4$ after Viterbi decoder, QEF after Reed-Solomon decoder.

- scattered pilot cells

- continual pilot carriers

- Transmission Parameter Signalling (TPS) carriers.

The scattered and continual pilots are used as reference signal for the channel equalization by the receiver. They are transmitted at boosted power level with respect to data subcarriers. The continual pilots occur at the same frequency on every symbol, while the scattered ones are allocated symbol by symbol on a different carrier, meaning that their frequency allocation is shifted of a constant value at each symbol (Fig. 2.4). The TPS carriers are used for providing to the receiver information about the actual operating parameters of the transmission scheme, i.e. channel coding (inner code rate), guard interval and modulation (QAM constellation, 2K or 8K mode, etc.). The TPS carriers are modulated by means of a differential binary phase shift keying (DBPSK) and all convey the same message. In Fig. 2.4 the frequency allocation versus time of the additional carriers inside the OFDM frame is schematically represented.

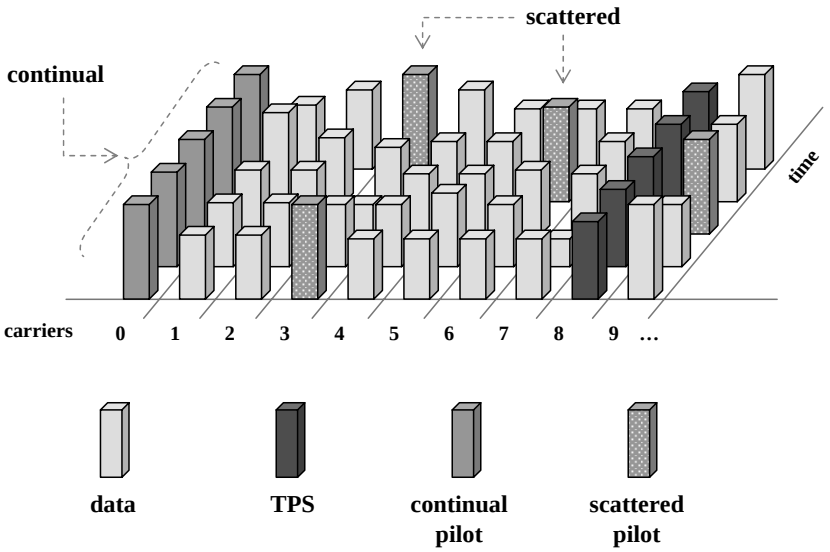

Figure 2.4 OFDM symbol subcarriers.

Network architectures: MFN, SFN

Multi-frequency network (MFN) is the configuration commonly used for analog television broadcasting. It is realized by several transmitters broadcasting a same signal on a number of different frequencies. This allows to avoid self-interference effects in the overlapping portions of coverage areas, due to the reception of delayed versions of the same signal (echoes).

A Single-frequency network (SFN) is a network architecture where several transmitters simultaneously broadcast the same signal over the same frequency channel. Consequently, it allows a more efficient utilization of the radio spectrum in comparison to MFNs. In high-data rate digital communications SFN transmission can be heavily affected by self-interference causing destructive interference and frequency-selective fading. Furthermore intersymbol interference may result from the effect of time spreading of the echoes, which can be considered analogous to multipath propagation effects.

The flexible guard interval specified by the DVB-T standard allows the system to effectively support both SFN and MFN network architectures. The guard interval, in fact, enables the system to support large area SFN configurations since the time overlapping of consecutive symbols is shorter than the guard interval inserted between them. In particular the 2K mode, providing shorter guard intervals (as reported in Tab. 2.1), is suitable for small SFN networks with limited transmitter distances. The 8K mode instead can be used both for single transmitter operation and for small and large SFN networks.

Chapter 3

Common interference

3.1 Introduction

The transmission medium utilized for radio communications commonly causes degradation of the received signal,which can be due to several phenomena like for example path loss, multipath, fading, presence of in-channel noise, time variance of the channel. A radio communication system may be affected by different kinds of noise, like thermal or atmospheric noise and man-made noise. The first one can be represented as an additive white Gaussian noise (AWGN) signal, while the second one can be both Gaussian and of shot nature. In particular the noise present in urban environments, created by for example electrical self-starter of cars, power lines, current switches, fluorescent lights, etc. can be effectively represented by an impulsive model.

Proper functioning of DVB-T systems can be affected by different types of in-channel interference. In this work, for the performance evaluation of the DVB-T transmission system, the presence of AWGN noise and impulsive noise has been considered, upon the varying of both the set-up of the transmitting platform and the noise type and power.

3.2 Additive White Gaussian Noise

Noise described by the Gaussian model is characterized by a Gaussian probability density function and a constant power spectral density, independent on frequency. Additive white Gaussian noise (AWGN) plays a fundamental role in all the experimental tests mandated to emulate communication channel background noise. It degrades slowly the quality of a digital communication system as its power level (N) relative to the signal level (C) increases, causing a reduction of the carrier-to-noise ratio (C/N) at receiver input. The main parameter of the AWGN is in fact the noise power in the frequency bandwidth

of interest, i.e. the bandwidth of the transmission channel.

The relevance of its effect on the performance of DVB-T systems mainly depends on the power level exhibited; if a given threshold value is not exceeded negligible effects are experienced.

3.3 Impulsive Interference

Impulsive interference is a phenomenon of certain interest in the digital terrestrial television field, as it is a critical interfering signal for TV systems. In the literature, interesting works supported by national television broadcasters, subsequently to the launch of DVB-T, are present. In particular [19] and [28] supported respectively by *BBC R&D* in UK and *Retevision* in Spain, concern measurement, characterization and modeling of impulsive interference in UHF channels. In [19] capture and statistical analysis of real impulsive interference are described in order to design a representative model to be used in simulation. The proposed model is validated by a campaign of measurements. In [28] the results of measurements and characterization of wide-band impulsive noise in "noisy" and "quiet" outdoor environments are presented.

Impulsive noise can be due to radiated emissions of electronic and electromechanic equipment, like industrial power switches, motors or micro controller-based devices. In an urban context, car traffic and ignition systems are also a potential source. These *outdoor* interference can be conveyed to a DVB-T receiver by the rooftop antennas. In a domestic DVB-T installation impulsive *indoor* noise can affect a receiver through entrance into downleads, cables or connectors. In this context the potential sources of impulsive interference are household appliances (washing machines, food mixers, irons, ovens, electric razors, etc.), central heating thermostats and light switches.

As documented in [19], the lack of a suitable time-interleaving scheme in the DVB-T specification makes the system rather sensitive to sources of interference of an impulsive nature. This kind of noise may affect a DVB-T system even in the presence of high signal-to-noise ratios. It can provoke significant losses of video quality although in the presence of low levels of bit error rate (BER).

3.3.1 Models for Impulsive Interference

Impulsive interference is usually modeled in the literature [28] as a random train of pulses, characterized by three random variables: the pulse amplitude, the pulse duration and the time interval between pulses. The model can be mathematically expressed as:

$$n(t) = \sum_i A_i \prod_{w_i} (t - \tau_i) \tag{3.1}$$

where A_i is the amplitude, w_i the duration and τ_i the arrival time of each pulse. These parameters account for many practical factors associated to the considered noisy environment. According to [19], the choice of statistical distribution provided in the literature for each parameter is based on models which are either too specific or excessively theoretical. Consequently the applicability to DVB-T issues is rather limited. Furthermore, as impulsive noise is characterized by a wide-band power spectral density, its bandwidth is typically much greater than that of the measuring system. The shape of the pulses is thus determined by the impulse response of the actual receiving or measuring system.

In the simplified model proposed in [19] impulsive interference is characterized as seen by a DVB-T receiver, rather than a generic measurement system. Impulsive interference is described as a process characterized by bursts containing one or more pulses. In Fig. 3.1 a graphical representation of the model

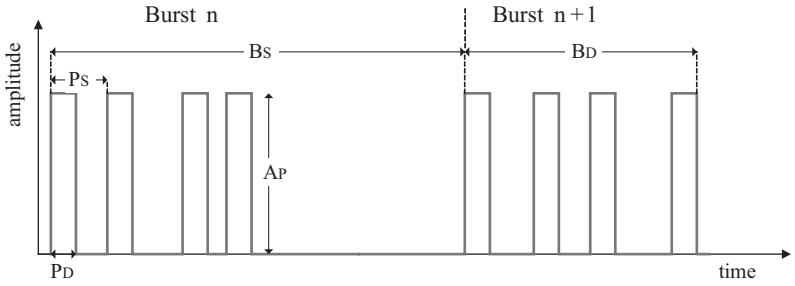

Figure 3.1 Model for impulsive interference.

is shown, where A_P is the pulse amplitude, P_S is the time interval between pulses within the same burst, B_S represents the time spacing between consecutive bursts, P_D and B_D are the duration of a pulse and a burst, respectively.

The pulse amplitude A_P is assumed to be constant within an impulsive event, due to the great and unpredictable variability encountered in measurements [1]. Pulse duration P_D is fixed at 250 ns, as single pulses within a burst are shaped by the impulse response of the tuner; this response spreads the energy of the incoming short impulses over approximately 250 ns. Time spacing between consecutive bursts B_S fixed at 10 ms. The time interval between pulses, P_S, follows a uniform distribution. The number of pulses per burst determines the duration of the burst B_D; it is also a major parameter discriminating the different types of interference source.

From the conclusion of [19], the effective duration of the burst is the param-

[1] For the purpose of this work, pulse amplitude is varied during experimental tests (Ch. 6) according to the selected interfering signal power.

eter that defines the performance of the DVB-T receiver. For this reason the key parameters chosen in this work for the performance assessment of a DVB-T system in the presence of in-channel impulsive interference are the noise power and the number of pulses per burst, as detailed in the following (Ch. 6). A further consideration on burst duration is necessary: it may become useless to set an extremely high number of pulses per burst because if B_D exceeds the length of a useful OFDM symbol (224 μs for 2K mode, 896 μs for 8K mode), impulsive noise can be treated as Gaussian noise.

3.3.2 Generation of Impulsive Interference

The generation of an AWGN signal can be provided by several digital signal generators available in the market with an I/Q arbitrary waveform generation option, that allow to set bandwidth and output power level. Impulsive interference is generated instead as gated Gaussian noise, which means that that each pulse is constituted by a wide-band AWGN signal with the duration of 250 ns. As pulses are grouped in bursts (Fig. 3.1) the resulting signal can be seen as if gating is performed twice: the first gating defines the burst duration and the time spacing between consecutive bursts, while in the second one Gaussian noise constituting a burst is gated to shape the pulses. In this second gating process the number of pulses per burst is defined.

The description of the procedure and the instruments used in this work for the generation of impulsive interference is provided in Sec. 5.3.

3.4 Interference from Analogue TV Signals

Another significative source of in-channel and adjacent-channel interference for DVB-T systems are the TV analogue PAL (Phase Alternating Line) signals [29]. Such interferences are more frequently due to the presence of analogue TV stations operating in areas close to the one covered by a DVB-T transmitter and exploiting the same frequency band. PAL video signals are typically composed by a vestigial sideband-amplitude modulated (VSB-AM) carrier for video and two frequency-modulated carriers for audio (mono and stereo), characterized by a fixed bandwidth and located at fixed frequency positions within a 7 MHz or 8 MHz channel in the VHF or UHF band, respectively.

Chapter 4

Cross-Layer Measurements

4.1 Introduction

In a digital communication system, like the DVB-T system, a number of flexible transmission parameters is available. Network designers and operators can set these parameters according to specific requirements in terms of robustness or throughput maximization. To investigate on the effectiveness of a given setup choice several indices (e.g. C/N, SNR, MER, BER, QoS, etc.) may be analyzed by measurements. Such indices, belonging to different layers of the system or to different levels of the same layer, provide information on the specific level they are related to; as a consequence they may not be exhaustive for an overall performance assessment. Thus, in order to find the best tradeoff between different configurations, a proper choice of the indices and suitable measurement methodologies are required.

In this work, a ***cross-layer*** measurement procedure is defined and applied to the DVB-T transmission-reception system. Cross-layer measurements consist of a set of measurements performed on parameters belonging to different levels of the ISO/OSI (International Standard Organization/Open Systems Interconnection) stack. They allow an efficient assessment of communication networks performance and drawbacks. The cross-layer approach provides for several measurements, to be concurrently carried out at different layers. It aims at experimentally correlating the major physical layer quantities to those characterizing key higher layer parameters, e.g. network, transport, application layer [8]. In particular, for the analysis of the DVB-T system two layers are considered in this work: physical and application layer. At physical layer, measurements of signal power, carrier-to-noise ratio (C/N) and carrier (signal)-to-interference ratio are carried out as detailed in Sec. 4.2. Other measurements at the same layer, focused on modulation quality of the down-converted baseband signal, involve parameters like Modulation Error Ratio

(MER) and Error Vector Magnitude (EVM), described in Sec. 4.3. At application layer, measurements are performed in terms of video quality of DVB-T streams. In particular, two different approaches can be followed: subjective analysis, based on a large number of interviews taken from a set of test viewers, or objective analysis, more efficiently obtained by means of algorithms applied to the received video stream. These latter measurements have been accomplished through Video Quality Metric (VQM) algorithms, based on models of ITU Recommendation BT.1683 [9]. An example of software tool based on these models is the VQM software [10], which provides video quality estimates rather close to those achievable by subjective analysis. In Sec. 4.4 traditional methods of video quality estimation and Video Quality Metric algorithms are reported and compared.

4.2 Physical Layer: RF Signal Power

The first physical layer parameters here considered are the radiofrequency (RF) signal power and the carrier-to-noise ratio at the receiver sites, which are commonly considered for the definition of the coverage area [11] . According to the DVB standard [6] definition, *the signal power of a terrestrial DVB signal is the mean power of the signal as would be measured with a thermal power sensor. In the case of received signals care should be taken to limit the measurement to the bandwidth at the wanted signal. When using a spectrum analyzer or a calibrated receiver, it should integrate the signal power within the nominal bandwidth of the signal* $n \times f_{spacing}$ *where* n *is the number of carriers* and $f_{spacing}$ is the frequency spacing between carriers. The method applied in this work for signal power measurement, known as *channel power* technique, complies with the DVB standard definition.

4.2.1 Measurement method: Channel Power

Measurements of the signal power P, at the DVB-T receiver input, have been carried out by using a superheterodyne spectrum analyzer (SSA). It has been estimated by applying the channel power method, which is based on the use of the spectrum analyzer in the conventional sweeping mode. The main idea is that the input signal power and the area of the mean trace that the analyzer displays are proportionally related [13].

The channel power method is based on the following post-processing formula [14]:

$$P = \frac{1}{ENBW} \frac{\Delta f}{M} \frac{1}{R} \sum_{k=1}^{M} X_k^2, \tag{4.1}$$

Abbreviation	Term	Definition
C/N (dB)	Carrier-to-noise ratio	The ratio of carrier or signal power to the white-noise power in a specified bandwidth, as measured on an RF spectrum analyzer or similar equipment.
C/N_0 (dB-Hz)	Carrier-to-noise - density ratio	The ratio of carrier or signal power to white-noise spectral density.
$C/(N+I)$ (dB)	Carrier-to-noise-plus-interference ratio	The ratio of carrier or signal power to the total noise power (including white noise and interference) in a specified bandwidth
E_s/N_0 (dB)	Energy-per-symbol to noise-density ratio	In digital modulation, the ratio of the average energy of a QAM symbol to the white-noise spectral density.
EVM (%)	Error vector magnitude	The ratio of RMS constellation error magnitude to peak constellation Percent symbol magnitude.
MER (dB)	Modulation error ratio	The ratio of average signal constellation power to average dB constellation error power.
SNR (dB)	Signal-to-noise ratio	(a) A general measurement of the ratio of signal power to noise power. (b) In a specific context, a measurement of the ratio of signal power to noise power made at baseband before modulation.

Table 4.1 Terminology for various signal-to-noise ratio concepts.

where Δf is the frequency span, $ENBW$ is the Equivalent Noise Band Width of the intermediate frequency (IF) filter, R is the input impedance of the instrument, while M is the number of the samples displayed at each sweep. The frequency span should be set equal to the bandwidth of the signal, centered at its carrier frequency. $ENBW$ is generally provided in the SSA data sheet, depending on the instrument characteristics. The input impedance of a SSA, also provided in the data sheet, is generally equal to 50 Ω. The terms X_k is the root-mean-square (RMS) average of X_{ki} $\{i = 1, \ldots, N_S\}$ and is defined as:

$$X_k = \sqrt{\frac{1}{N_S} \sum_{i=1}^{N_S} X_{ki}^2}, \tag{4.2}$$

where X_{ki} is the voltage of the k-*th* displayed sample acquired during the i-*th* sweep and N_S is the number of the performed sweeps. M and N_S have to be set by the operator to trade-off between the required measurement accuracy and the computational time, i.e. time necessary for the estimation, that clearly increases upon the increasing of M and N_S. Further details on the channel power method can be found in [14].

4.2.2 Carrier-to-Noise Ratio (C/N)

The ***carrier-to-noise ratio*** (C/N) is the ratio of wanted information power to unwanted interference power [6] or, more in detail, the ratio of a modulated signal power to the noise power in a specified bandwidth. This parameter is used for characterizing networks or individual devices performance and impairments. The term *carrier* instead of *signal* is used to distinguish this parameter, referred to the power of a radiofrequency (RF) passband signal, from the SNR, which is the *signal-to-noise ratio* of a baseband demodulated signal. C/N and SNR both represent a signal-to-noise ratio parameter, but the first in the RF domain while the second in the baseband domain.

Actually, when dealing with modulation schemes like QPSK, QAM or OFDM, which is the case of DVB-T signals, it is incorrect to describe the modulated signal as *carrier*, because the output is a suppressed-carrier doublesideband RF signal. In the DVB standard [6], for example, the parameter C is referred to as "RF/IF power" for a major clarity. Notwithstanding the terms "carrier" or "modulated carrier" are commonly used to address a modulated RF signal.

Definition

Carrier-to-noise ratio (C/N) is defined as follows:

$$C/N\ (dB) = 10 \log \frac{C}{N} = 10 \log \left(\frac{V_{carrier_{RMS}}}{V_{noise_{RMS}}} \right)^2 \tag{4.3}$$

where C and N are the scalar power levels of the carrier and noise respectively, $V_{carrier_{RMS}}$ and $V_{noise_{RMS}}$ are the RMS voltage values of the carrier signal and noise respectively.

Effect of Noise Floor on C/N and Power Measurements

In the measurement of C/N on a spectrum analyzer, when C/N values are very low, i.e. lower than 10 dB [15], the effect of thermal noise underlying the signal must be taken into account. In fact when measuring the carrier power C, the actual value corresponds to the sum of the signal power plus the noise power, i.e. expressing this measurement in linear units of power C+N, and the effective estimated carrier-to-noise ratio is not C/N but (C+N)/N. Consequently, when $N \ll C$ the following approximation can be used:

$$\frac{C+N}{N} \simeq \frac{C}{N} \tag{4.4}$$

while in the other case the real C/N must be determined as:

$$\frac{C}{N} = \left(\frac{C+N}{N} \right) - 1 \tag{4.5}$$

The following general rule is provided in [15]: if the signal is at least 15 dB above the noise, the measurement offset will be less than about 0.1 dB and a correction is not necessary. If the signal is at least 10 dB above the noise, the measurement offset will be less than about 0.5 dB. For measurement of system noise power that is less than 10 dB above the spectrum analyzer noise floor, a correction is required to avoid the noise-floor contribution.

4.3 Physical Layer: Modulation Quality

4.3.1 Modulation Error Ratio (MER)

The ***modulation error ratio*** (MER) is a measure of the quality of a digitally modulated signal, commonly used to assess the performance of transmitters and receivers in a digital communication system. It is represents the signal-to-noise ratio of a digitally modulated **baseband** signal. It is recalled that MER is the quantity recommended by the DVB-T standard ETSI TR 101 290 [6] to provide a "figure of merit" analysis of the signal, so it is of primary importance in the assessment of the performance of a DVB-T system.

The relevance of this index is highlighted by the fact that, in a digital communication system, it is not unusual to have low QoS at application layer and still obtain estimated C/N and signal RF power to be over the minimum required levels. This condition is generally due to the presence of impairments that can't be seen on a spectrum analyzer (like poor in-channel frequency response, in-channel interference below the signal power level, etc.) and are not detected by channel-power and C/N measurements. MER instead looks at the demodulated complex baseband constellation symbols. It indicates the mean deviation of the received I/Q values from ideal signal states thus providing a measure of signal quality. It is therefore a direct measure of modulation quality and, as these demodulated symbols produce correct bits or bit errors at the receiver output, it has a direct linkage to bit error rate and to the QoS at the application layer.

Sometimes MER is specifically referred to as *receive modulation error ratio* (RxMER) when it is measured in a received, after demodulation, and *transmit modulation error ratio* (TxMER) when measured at a transmitter output by an ideal test receiver.

Definition

MER is defined as the ratio of the average constellation symbol power to the average constellation error power. In Fig. 4.1, a detailed representation of a single constellation point on the I-Q diagram is shown, where I_j and Q_j are the coordinates of the ideal symbol vector. The error vector is also highlighted in the figure: it represents the distance of the j-th received symbol from the corresponding ideal target symbol. The difference between the position of j-th received symbol and the ideal one determines the non-null values of δI_j, δQ_j.

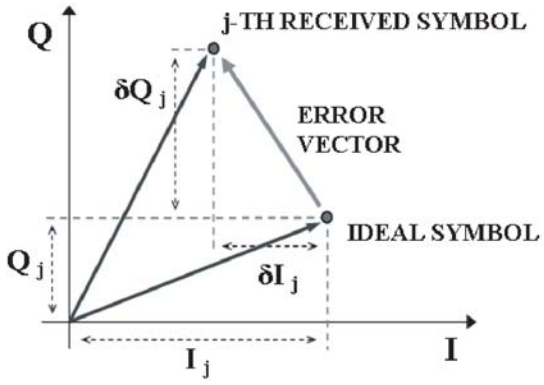

Figure 4.1 Error vector on the I-Q constellation diagram.

The mathematical definition of MER (in decibels) is the following:

$$MER = 20 \log_{10} \left\{ \frac{\sqrt{\sum_{j=1}^{N} (I_j^2 + Q_j^2)}}{\sqrt{\sum_{j=1}^{N} (\delta I_j^2 + \delta Q_j^2)}} \right\} \tag{4.6}$$

where I and Q are the real (in-phase) and imaginary (quadrature) coordinates of each ideal target symbol vector, and δI and δQ are the real and imaginary parts of each modulation error vector. N is the number of data points in the measurement sample; the considered sample should be long enough so that all the constellation symbols are equally likely to occur.

MER Measurement

In a digital QAM receiver, the received QAM symbol, or *soft decision*, is passed to the slicer, which selects the nearest ideal symbol, or *hard decision*, from the QAM constellation. The input and output of the slicer are complex vectors, each represented by two components: magnitude and phase, or equivalently, real (I) and imaginary (Q) parts. In ideal conditions, the received symbol would lie exactly on one of the constellation points, and the magnitude of the error would be zero. Real-world impairments cause instead most of the received symbols to be spread out from the ideal symbols, forming a small "cloud" in the constellation diagram around each ideal symbol. As a consequence, received symbol vectors are different than ideal. Subtracting the ideal symbol vector from the received symbol vector, gives the error vector at each symbol time. The average power of the error vector is computed by taking the complex magnitude-squared of the error vector and averaging it over a given number of symbols N. MER is then calculated by dividing the average signal power by the average power of the error vector. The implicit assumption is that the error vector from the nearest symbol nearly always equals the true error vector from the correct reference symbol.

Factors Affecting MER Measurement

Several factors must be accounted for when performing MER measurements.

- Statistical variation: the number of samples N over which the MER is averaged affects the reliability of the measurement. The considered sample should be long enough so that all the constellation symbols are equally likely to occur. Conversely, a smaller number of symbols allows the observation of transients in the MER measurement, which can highlight the effects of burst noise.

- Unequal occurrence of symbols: the average constellation power is a constant for each constellation. In the definition of MER provided by the ETSI standard [6] the average constellation power is computed by taking the complex magnitude-squared of the received ideal symbols and averaging it over a given number of captured symbols N. For low N (for example, $N < 100$) the result may be unreliable because of unequal occurrence of symbols: in some cases, many large QAM symbols (near the outer edges of the constellation) or many small QAM symbols (close to the center of the constellation) may happen to be transmitted.

- Implementation-loss MER ceiling: even if the input E_s/N_0 is very high, the MER reading will saturate at a value reflecting the implementation loss of the receiver. The receiver contributes noise to the MER measurement because of front-end noise figure.

- Symbol-error MER floor: the slicer produces the hard decision by taking the soft decision and finding the nearest ideal constellation point. If the wrong constellation point is chosen, a symbol error occurs. The error vector magnitude then indicates the distance to the nearest symbol point, which may be closer than the correct symbol, meaning that the error will seem smaller than it really is, and the MER will seem better than its true value. As a general rule, the MER measurement is not valid when the input E_s/N_0 is below the point that produces roughly a 1-percent symbol error rate (before FEC decoding).

- Impulsive noise: short bursts of noise may have unpredictable effects on the MER measurement. When impulsive interference hits, the MER will register a decrease, depending on the amount of averaging in the measurement and on the burst properties of the noise. In some instances, MER may change little in the presence of short bursts, because of the average measurement over many symbols, while QoS is instead heavily reduced.

4.3.2 Error Vector Magnitude (EVM)

The ***error vector magnitude*** (EVM) is a measurement metric closely related to MER, also used to quantify the quality of a digitally modulated signal. As shown in Fig. 4.1, the error vector is the vector drawn between the ideal symbol position and the received symbol position in the constellation diagram.

Definition

EVM is defined as the ratio of the error vector magnitude to the magnitude of the vector to the outermost state of the constellation, reported as a percentage.

$$EVM = (E_{RMS}/S_{max}) \times 100\% \tag{4.7}$$

where E_{RMS} is the RMS error vector magnitude and S_{max} is the maximum symbol magnitude. The mathematical definition of EVM is the following:

$$EVM_{RMS} = \sqrt{\frac{\frac{1}{N}\sum_{j=1}^{N}(\delta I_j^2 + \delta Q_j^2)}{S_{MAX}^2}} \times 100\% \tag{4.8}$$

Error vector magnitude is directly connected to the received symbols constellation display, as there is a linear relationship between EVM and a constellation symbol point "cloud" size.

4.3.3 MER - EVM Correlation

Different approaches can be used to compare MER with EVM. In the following the one provided in [15] and the one provided in the ETSI TR 101 290 standard [6] are reported.

In [15] the *maximum-to-average constellation power ratio* (*MTA*), i.e. ratio of the peak constellation symbol power (denominator in Eq. 4.8) to the average constellation power (numerator in Eq. 4.6), is considered. The peak constellation power is the squared magnitude of the outermost QAM symbol, that for a square M-QAM constellation is computed as follows:

$$P_{peak} = 2(\sqrt{M} - 1)^2 \tag{4.9}$$

where M is the number of points in the constellation and the points are spaced by 2 on I and Q axis. In [16] the formula of average constellation power (averaged equally over all symbols in the constellation) is provided:

$$P_{avg} = \frac{2}{3}(M - 1) \tag{4.10}$$

The maximum-to-average constellation power ratio (MTA) for each M-QAM constellation can be then computed as follows:

$$MTA = \frac{P_{peak}}{P_{avg}} = 3\frac{\sqrt{M} - 1}{\sqrt{M} + 1} \tag{4.11}$$

and the formula for the conversion from MER to EVM follows:

$$EVM\ (\%) = 100 \times 10^{-(MER + MTA_{dB})/20} \tag{4.12}$$

where EVM (%) is error vector magnitude (percent), MER is modulation error ratio (dB) and MTA_{dB} is maximum-to-average constellation ratio expressed in dB. In Table 4.2 MTA values in dB, for M = 4, 16 and 64, are reported. The limit for very-high-order QAM approaches the values of 3, which in decibels is equal to 4.77 dB.

In [6] the parameter *peak-to-mean voltage ratio* (V) is considered. Taking both EVM and MER as simple voltage ratios, and multiplying MER numerator and denominator by $\sqrt{1/N}$, from 4.8 and 4.6 the following are obtained:

$$EVM_V = \frac{\sqrt{\frac{1}{N}\sum_{j=1}^{N}(\delta I_j^2 + \delta Q_j^2)}}{S_{MAX}} \tag{4.13}$$

$$MER_V = \frac{\sqrt{\frac{1}{N}\sum_{j=1}^{N}(I_j^2 + Q_j^2)}}{\sqrt{\frac{1}{N}\sum_{j=1}^{N}(\delta I_j^2 + \delta Q_j^2)}} \tag{4.14}$$

and EVM and MER are related such that:

$$EVM_V = \frac{1}{MER_V} \times \frac{1}{V} \tag{4.15}$$

where

$$V = \frac{S_{MAX}}{\sqrt{\frac{1}{N}\sum_{j=1}^{N}(\delta I_j^2 + \delta Q_j^2)}} \tag{4.16}$$

If V is calculated over a large number of symbols, so that each symbol has the same probability to occur, then it is a constant for a given constellation size. The limit values of V, calculated by considering the peak to mean of all the constellation points, are reported in the third column of Table 4.2.

Relation between MTA and V

In [15], MTA is calculated for each square M-QAM constellation independently from the number of data points in the measurement sample N, assuming that all symbols have the same probability of occurring. The peak-to-mean voltage ratio V computation, as defined in [6], is instead based on the N symbols considered for the measurement of MER or EVM. Therefore, it is best suited as a conversion factor when MER or EVM are estimated over a low number of

Constellation	MTA Ratio (dB)	Peak-to-mean Voltage Ratio (V)
QPSK	0	1
16-QAM	2.55	1.341
64-QAM	3.68	1.527
Limit for infinite QAM ($M \to \infty$)	4.77	1.732

Table 4.2 MTA ratio and limit values of Peak-to-mean voltage ratio (V) for some square QAM constellations.

symbols. The limit values of V provided in [6] are bound to the MTA values provided in [15] by the following equation:

$$MTA_{dB} = 20\log(V) \tag{4.17}$$

4.4 Application Layer: Video Quality Measurements

For an exhaustive analysis of the performance of a digital transmission system, like DVB-T broadcasting, it is necessary to evaluate the quality of service (QoS) provided from the point of view of the end-user. To fulfill this purpose a third level, in addition to physical layer's RF power and modulation quality, has been considered: the application layer. In particular, for the case of television broadcasting systems, the QoS is determined by the evaluation of the video quality perceived by the end-user.

Parameters commonly utilized in the assessment of the performance of a digital communication system, like bit error rate (BER), packet loss ratio (PLR), etc., are not suited for QoS evaluation, mainly because they are not directly linked to the perceived video quality. In fact, a same BER value could lead to very different levels of perceived video quality when considering video sequences with different characteristics. For example, let's consider two sequences with the same level of BER: an highly dynamic scene, like a football match, could appear more degraded than a static scene, like a journalist reading the news.

4.4.1 Traditional methods of video quality evaluation

The most commonly used measure for video quality evaluation are based on the *Mean Square Error* (MSE) and its derivatives, i.e. Root Mean Square Error (RMSE) and *Peak signal-to-noise ratio* (PSNR). MSE is obtained by the mean square of the error between the single pixel of the transmitted frame and the corresponding pixel of the received frame, computed over all the pixel

of the frame. Let's consider two $m \times n$ monochrome frames, as represented

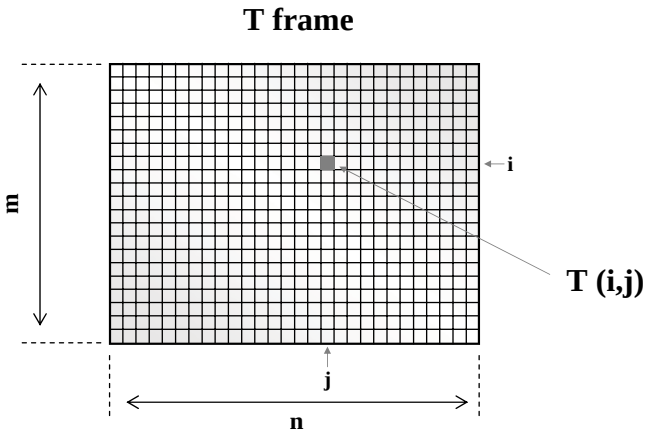

Figure 4.2 Scheme of frame with m lines and n pixels per line.

in fig. 4.2, the transmitted one T and the received one R, where $T(i,j)$ and $R(i,j)$ are the values of the j-th pixel in the i-th line. MSE then is obtained as reported in Eq. 4.18.

$$MSE = \frac{1}{m \cdot n} \sum_{i=0}^{m-1} \sum_{j=0}^{n-1} \|T(i,j) - R(i,j)\|^2 \tag{4.18}$$

For color images, where each pixel has three RGB [1] values, the MSE is the sum over all squared value differences divided by image size and by three.

PSNR is the ratio between the maximum possible power of a signal and the power of corrupting noise expressed in decibels. In the case of video signals, it is computed as the ratio between the square of the maximum possible pixel value, MAX_T, and the MSE.

$$PSNR = 10 \log \left(\frac{MAX_T^2}{MSE} \right) \tag{4.19}$$

The main drawback of these metrics, based on a frame by frame analysis, is that they do not account for the movement visual perception, which is bounded to the time-correlation of subsequent frames. Furthermore they do not account for the errors spatial distribution. Therefore, pixel errors spatially concentrated within an area of the frame may produce the same MSE of pixel errors uniformly distributed over the frame, but the visual impact is clearly

[1] The RGB color model is an additive model in which red (R), green (G) and blue (B) are combined in various ways to reproduce other colors.

different. The frames shown in Fig. 4.3 provide a good example, reported from [17]. The leftmost frame (a) is the original one, the other ones (b) and (c) are corrupted with different spatial frequency noise. They both result to have a MSE value equal to 12.5 however, due to errors spatial distribution, the rightmost image (c) seems to suffer lower distortion.

Figure 4.3 Original frame (a) and corrupted frames (b,c) with MSE = 12.5.

Due to the non-linear behavior of the Human Visual System (HVS) these metrics fail under many circumstances, as shown in the example. MSE and PSNR, in fact, are based on the assumption that human observer is sensitive to the summed squared deviations between reference and test sequences, and is insensitive to other aspects like spatial and temporal frequency or color of the deviations.

4.4.2 Perceived video quality

From the considerations above derives that only metrics considering the human visual perception can provide high accuracy in digital video quality measurements. Video quality measurements related to human visual system are referred to as *perceptual* quality measurements and can be performed by subjective or objective techniques. For subjective ones knowledge of the HVS is required to create suitable video tests for viewers, including all possible perceptible visual artifacts. For objective techniques mathematical models, emulating the response of the HVS, are indispensable to design algorithms that are able to estimate the visual component of impairments affecting a video sequence. The knowledge of the HVS was the starting point for the development of mathematical models describing most of the processing that is done from the lens of the eye to the representation in the primary visual cortex, i.e. the brain area responsible for processing visual stimuli. These models are able to predict the response from the cells in the primary visual cortex to video signals.

Subjective and objective perceptual video quality measurements

In subjective test, video quality is assessed directly by human observers. Video sequences are shown to groups of viewers, in conformity with International Telecommunication Union (ITU) standardized procedures [12]; it is asked to the viewers to indicate the type of impairment, its level of significance, time duration and spatial extent, on a predefined scale. The quality of each sequence is then determined by the average opinion, and the results produced by the tests are called Mean Opinion Score (MOS). In the recommendations a number of parameters of interest is standardized, as dimension of the screen, distance of the viewers, kind of the evaluation scale, kind and length of test sequences and others. Fundamental importance is due to the kind of service assessed, because different standards, like for example television and teleconferencing, require different evaluation parameters and procedure. This kind of approach has some heavy drawbacks: it is time-consuming, because it requires a large number of experiments performed on many test viewers, it is expensive, not very repeatable, not suitable to do in-service measurements and, obviously, unusable for real-time analysis.

Objective metrics for quantifying the performance of digital video systems (e.g. satellite and terrestrial digital television, high definition television, teleconferencing, video streaming, mobile phone video, etc.) are required, in particular by service providers, industry and government agencies in order to assess quality for specification of system performance, service level agreements, network maintenance and optimization of the use of limited network resources such as transmission bandwidth. The goal of objective techniques is to best approximate results obtained by subjective measurements. To do this, it is necessary to conduct sets of subjective measurements, in accordance with ITU recommendations, to determine relationships between objective metrics parameters and specific perceived video artifacts commonly associated with digital compression and transmission (e.g. blurring, block distortion, unnatural motion, global noise, color distortion). This kind of tests have been conducted by ITS/NTIA (Institute for Telecommunication Sciences of National Telecommunications and Information Administration) researchers. The tests, called impairments Root Cause Analysis (RCA), lead to the definition of objective metrics with a high correlation with subjective results [10]. In the Sec. 4.4.3 a description of Video Quality Metrics (VQM) and measurement techniques developed at ITS/NTIA is provided.

Perceptual objective video quality measurement techniques can be classified into three groups: Full Reference (FR), Reduced Reference (RR), which require information from both original/transmitted and processed/received video streams, and No-Reference (NR) methods.

- The FR measurement technique performs a comparison between the full

original video, used as reference, and the processed video. It can be used only when the original source video is available at the destination end. Consequently this technique is not suitable to perform in-service monitoring.

- The RR method operates by extracting low bandwidth features from the source video and transmitting these features in addition to video data. At the destination end they are used to perform the quality measurement by a comparison with the corresponding features of the processed video. RR measurement systems provide an effective method to perform perception-based in-service measurements.

- In the NR methods perceptual video quality evaluation is made video without any reference, based only on the processed video sequence.

For the purpose of this work, the availability of the DVB-T transmission platform at Digilab, Bolzano, allowed the use of a Full Reference measurement method. For the experiments, a selected video sequence of 30 seconds time length has been inserted into the transmission stream and broadcasted into the air. At the receiver side, at each measure, the sequence has been recorded and compared to the transmitted one through a software developed by ITS/NTIA, called VQM software.

4.4.3 VQM software

In this paragraph the main features implemented by the software utilized for the perceptual video quality measurements, referred to as *VQM software*, are reported. In [10] a complete description of the ITS video quality metric (VQM) algorithms and techniques is provided. The automated objective measurement algorithms provide close approximations to the mean opinion scores of digital video impairments, that have been graded by groups of viewers. The diagram in Fig. 4.4 highlights the processes required for the video quality measurements. In the figure, the video system under test is referred to as Hypothetical Reference Circuit (HRC). The processes can be summarized as follows:

1. sampling of the original and processed video streams
2. calibration of the original and processed video streams
3. extraction of perception-based features
4. computation of video quality parameters
5. calculation of VQM models

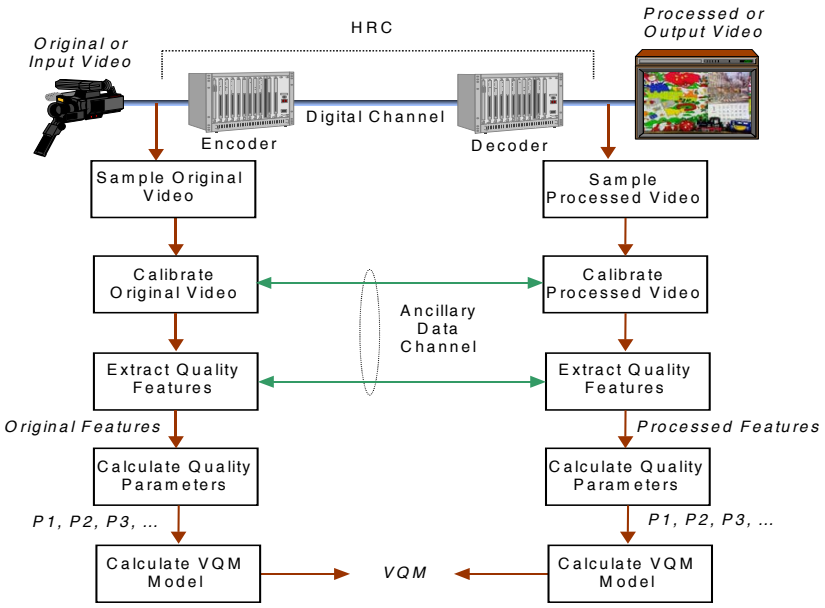

Figure 4.4 Diagram of the steps required to compute VQM.

At the final step a global index, called VQM, tracking all the perceptual changes due to the components of the transmissions system, is provided. VQM is mapped on a scale from 0 to 1, where 0 means that no impairment is perceivable and 1 that a maximum level of impairments is visible and the video sequence quality is completely degraded.

The availability of an ancillary data channel between the original and processed ends, as highlighted in Fig. 4.4, allows the VQM techniques, suitably adapted, to perform a reduced reference continuous in-service quality monitoring.

Sampling

If the original and processed videos are in analog format, they must be digitally sampled according to the standard ITU-R Recommendation BT.601 [18]. Composite video such as PAL are converted into component video that contains the following three signals: luminance (Y), blue color difference (C_B), and red color difference (C_R) [18]. Rec. 601 sampling is commonly known as 4:2:2 sampling since the Y channel is sampled at full rate while the C_B and C_R channels are sampled at half rate. A 13.5 MHz sample rate is specified, that produces 720 Y samples per video line, while the chrominance channels C_B and C_R are each sampled at 6.75 MHz. In the PAL standard 576 lines contain

picture information, consequently the complete sampled Y video frame consists of 720 pixels by 576 lines.

In the calculation of VQM, each sampled image is divided into a large number of smaller sub-regions. Rectangular sub-regions are used to control the computation of VQM. The video streams are divided into overlapping segments and each segment is independently processed. This method allows to emulate continuous quality assessments for video sequences longer than 10 seconds.

Calibration

Calibration of the original and processed sampled videos is required in preparation for feature extraction. The four steps performed are here enlisted.

1. Spatial registration estimation and correction; it determines the horizontal and vertical spatial shift of the processed video relative to the original video. It is realized by means of an iterative search process.

2. Valid region estimation; it is necessary to limit the extraction of features to those pixels that contain picture information, since the sampled videos may have a border of pixels and lines that do not contain a valid picture.

3. Gain (contrast) and level offset (brightness) estimation and correction.

4. Temporal registration estimation and correction; estimates of video delay are required to temporally align the original and processed video before making quality measurements. All video systems are treated as having a constant video delay, thus variations from this delay are considered degradations.

The calibration process prevents VQM to be sensitive to horizontal and vertical shifts of the image, temporal shifts of the video stream and changes in image contrast and brightness.

Quality Features

A *quality feature* is defined as a quantity of information associated with a spatial temporal sub-region of a video stream. The feature streams, a function of space and time, characterize the perceptual changes of video streams. By the comparison of features extracted from the calibrated processed video with the ones from the original video, a set of *quality parameters* can be computed that are indicative of perceptual changes in video quality.

Enhancement of properties of perceived video quality, such for example edge information, is applied to the video stream by means of perceptual filters.

Subsequently, features are extracted from spatial-temporal sub-regions using mathematical functions like mean, which measures the average pixel values, and standard deviation, which estimates the spread of pixel values.

Some examples of quality features. Features derived from spatial gradients can be used to characterize perceptual distortions of edges. For example, a general loss of edge information results from blurring while an excess of horizontal and vertical edge information can result from block distortion. Features that measure localized contrast information are sensitive to quality degradations such as blurring (e.g., contrast loss) and added noise (e.g., contrast gain). Features that measure distortions in the flow of motion are sensitive to quality degradations such as dropped or repeated frames (motion loss) and added noise (motion gain).

Quality Parameters

Quality parameters measure distortions in video quality due to gains and losses in the extracted feature values. They are calculated for each spatial-temporal region by comparing the original feature values with the corresponding processed feature values, to obtain an overall measure of video distortion. Error-pooling functions are applied across space and time to emulate how humans deduce subjective quality ratings. Sequential application of error-pooling functions to the stream of spatial-temporal quality parameters produces single-value quality parameters for the entire video sequence. The final parameter values may be scaled and clipped to account for nonlinear relationships between the parameter value and perceived quality.

VQM Models

VQM can suite to different applications, it includes five models: General, Developer, PSNR, Videoconferencing and Television. Each model is an algorithm to compute VQM index that has been specifically optimized to achieve maximum objective to subjective correlation by accounting for the range of quality over which the model applies. A short description and the rate processing of each model is provided in the following:

- General: allows the user to accurately evaluate video quality over a wide range of quality and bit rates, this model processes about 9 frames per second (fps);
- Developer: emphasizes processing speed at the cost of some accuracy, this model processes about 47 fps;
- PSNR: the traditional measurement of peak signal to noise ratio, it processes about 64 fps;

- Videoconferencing (e.g., MPEG-4): relative to General model is specifically optimized for lower video quality (bit rates from 10 kbits/s to 1.5 Mbits/s), this model processes about 12 fps;
- Television (e.g., MPEG-2): relative to General model is specifically optimized for higher video quality (bit rates greater than 1.5 Mbits/s), this model processes about 10 fps.

For the purpose of this work the television model, designed for digital television systems like DVB-T, is utilized. It provides five objective parameters for measuring the perceptual effects of the usual types of television impairments, typically shown when digital transmission errors are present. The five artifact indices include:

- blurring
- jerky or unnatural motion
- global noise
- block distortion
- error blocks.

4.5 Cross-layer relations

Radiofrequency signal power and carrier-to-noise ratio are the first parameters commonly considered in measurements for the determination of the coverage area of a wireless communication system. Minimum signal and C/N levels, to be used as a reference, are generally provided by theoretical analysis and simulations accounting for different channel conditions (Gaussian, Ricean, etc.), available in standards and literature [5], [11].

When applied to practical measurements, in real-life conditions, the main drawback of these parameters is that they do not always allow to predict detrimental effects on the signal: in particular, when degradation is not caused by low C/N levels or when degradation sources can't be clearly seen and detected on a spectrum analyzer display. As a consequence degradation effects due to the possible presence of impulsive interference, multipath, phase noise, etc. may not be detected. Furthermore, as digital television service coverages are characterized by a very rapid transition from near perfect reception to no reception, the definition of coverage areas becomes much more critical [11]. This could lead to different situations. In some cases a reduced quality of service (QoS) could be provided to the end-users, due to underestimation or non-detection of noise in the channel. In other situations, a useless increase of

the transmitter power level could be carried out to solve coverage problems, thus increasing the environmental impact on the population of the electromagnetic field. It is then necessary to take into consideration other indices and to investigate their correlation with RF power and C/N.

Modulation error ratio, also belonging to the physical layer, is a sort of baseband signal-to-noise ratio of the demodulated signal, which accounts for impairments, like the ones listed above, not detected by radiofrequency signal measurements. Moreover, it has a linkage to bit error rate and then, indirectly, to the QoS at the application layer. The concurrent analysis of MER and RF signal power can provide useful information on the actual performance of the system under test but may not be sufficient for a thorough analysis.

Minimum MER reference values are also required, as they do not match the corresponding RF power or C/N reference values. In the absence of interference, estimated MER at the receiver generally increases according to a linear trend upon the increasing of the received signal power, but, as highlighted in Sec. 4.3.1, saturation and statistical variation effects must be considered. Attention must be paid to the fact that, in the case of OFDM signals, MER estimates are computed over the number of independently modulated subcarriers (K) and averaged over a number of OFDM symbols (N). For this reason narrowband interference, which affects only a few subcarriers, is unlikely to be pointed out by MER measurements computed over about 2000 (2K) or 8000 (8K) subcarriers. Similarly, impulsive noise effect on the MER, due to its short-time nature, depends on the burst duration (and amplitude) and on the amount of OFDM symbols over which MER average is computed. In some cases, MER may encounter a slight decrease in the presence of short bursts, because of the average measurement over $N \cdot K$ symbols, while the quality of service is heavily degraded. An example of the possible impact of narrowband and impulsive interference on MER estimates of OFDM modulated signals, like DVB-T, is sketched in Fig. 4.5. Besides, as MER is related to the symbols coordinates on the constellation diagram, minimum MER reference values depend on the modulation scheme employed for the signal transmission [15].

A QoS index is then necessary for the definition of minimum required MER levels for optimal reception, to be used as a reference. As digital television systems are in this work dealt with, the QoS from the point of view for the end-user corresponds to the subjective perception of video quality. In the literature, DVB systems performance assessment is generally referred to BER estimation, to subjective Mean Opinion Score (MOS), or to number of uncorrectable picture errors [19]. As transmitted video are MPEG-2 compressed, a BER estimation could not be suited for perceived video quality assessment. For example, a same sequence of error bits affecting a reference frame (intra coded picture), periodically present in MPEG-coded stream, could cause different visual impairment with respect to a compressed frame. For an effective

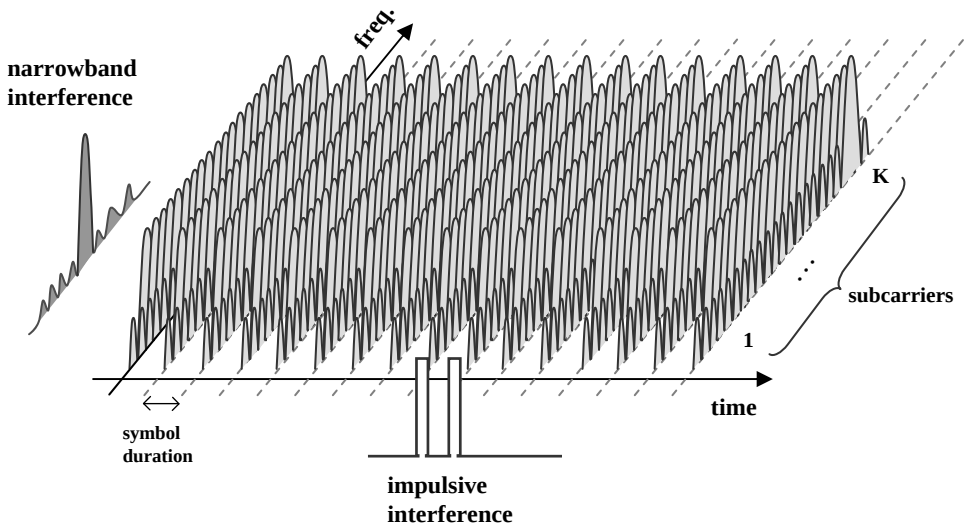

Figure 4.5 Impact of narrowband and impulsive interference on DVB-T signal.

evaluation of the QoS at application layer video quality measurement must be applied. It is necessary to use a technique providing objective metrics accounting for the point of view of the end-user, which, for the purpose of this work, has been successfully applied by means of the VQM algorithms.

In the literature, measurements at these different layers are widely described, and techniques are suggested to efficiently perform measurements in many different real-life scenarios. For instance, in [20], information and guidelines are offered for the case of PHY layer and BER measurements in digital RF communications receivers. For DVB-T systems, a similar analysis is offered by [21]. In [22], PHY layer measurements are proposed for the transmission optimization of DVB-T systems, while in [23] PHY layer parameters of DVB-T systems are assessed for indoor applications. The Video quality measurement on generic video streaming applications is treated in [24] and [25], while the case of DVB video streams is analyzed in [26]. Only a few of such contributions are referred to the case of DVB-T systems, and the measures they present are seldom investigated together and correlated with each other. In such a direction, in [27], an interesting approach based on cross-layer measurements is presented, which is specifically referred to the case of Wi-Fi communication systems. Cross-layer measurements on a DVB-T system are instead presented in [19], in which attention is mainly paid to the perturbation effects caused by impulsive interference. In this case measurements are carried out in terms of carrier-to-noise and carrier-to-interference ratio at PHY layer, while video quality is estimated though a count of visible impairments.

Chapter 5

Testbed

5.1 Introduction

The testbed has been set at *Digilab*, the competence center for digital communications of Bolzano, Italy, where the Thales DVB-T/H transmission platform, described in Sec. 5.2, is located. A simplified scheme of the testbed used in the experiments is provided in Fig. 5.1. Three main parts can be distinguished.

1. A transmission stage, including the Thales DVB-T/H transmission platform, a RF amplifier and a transmitting log-periodic antenna (A).

2. An interference generation stage, including a digital signal generator, two function generators and a log-periodic antenna (C).

3. A receiver/measurement stage, including a receiving antenna (B), a DVB-T receiver, connected to a personal computer (PC) through an USB link, a Superheterodyne Spectrum Analyzer, a Vector Signal Analyzer, exploiting data acquired by SSA, and a power splitter, which routes the output signal of the receiving antenna both to SSA and DVB-T receiver.

Each part is described in details in this Chapter. Experiments have been conducted within a non-shielded and non-anechoic room, with antennas positioned as shown in Fig. 5.1 and placed at a height of 1.5 m from the ground floor. In particular, the antennas A and C have been oriented toward B, placed at a distance from it respectively of 5 m and 4 m, and have an open line of sight.

5.2 DVB-T/H Transmission Platform

In this Section an overview of the main modules of the *Thales Broadcast & Multimedia* Digital TV platform is provided. The digital platform can exhibit

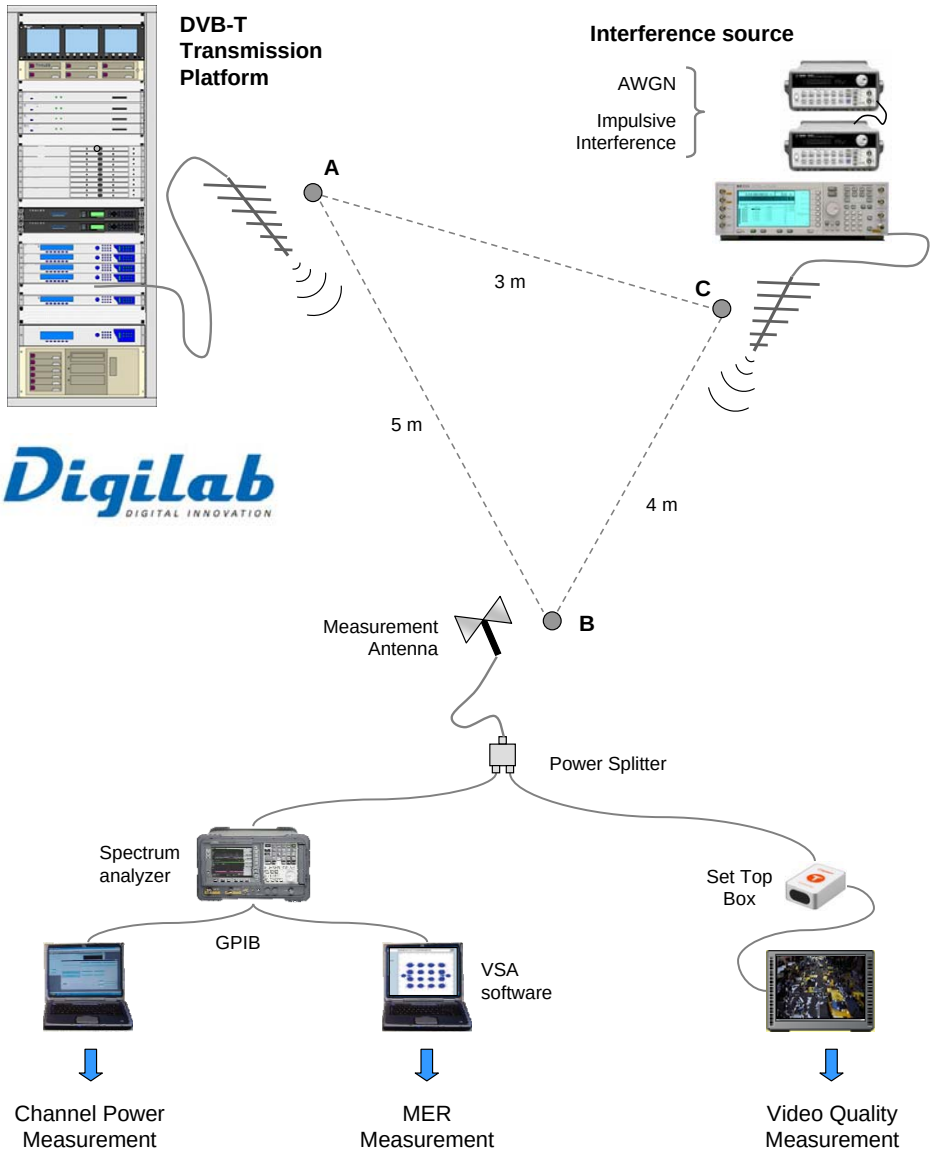

Figure 5.1 Scheme of the testbed at Digilab.

different operative configurations, through the regulation of a number of transmission parameters, such as video encoding format, video resolution, number of frames per second, number of carriers, modulation scheme, code rate, guard interval, transmission output power and central frequency.

The block diagram of Fig. 5.2 shows the architecture of the platform, the

organization of its components and the information flow from the sources to the transmitting antenna.

ARGOS: MPEG2 Encoder

Argos is a real time encoder that converts and compresses audio and video into a DVB Transport Stream (TS) by the MPEG2 format. For DVB applications MPEG-2 MP@ML 4:2:0 [1] encoding is used, in order to obtain high quality at a low data rate. The supported data rate is available from 1.5 Mbps up to 15 Mbps.

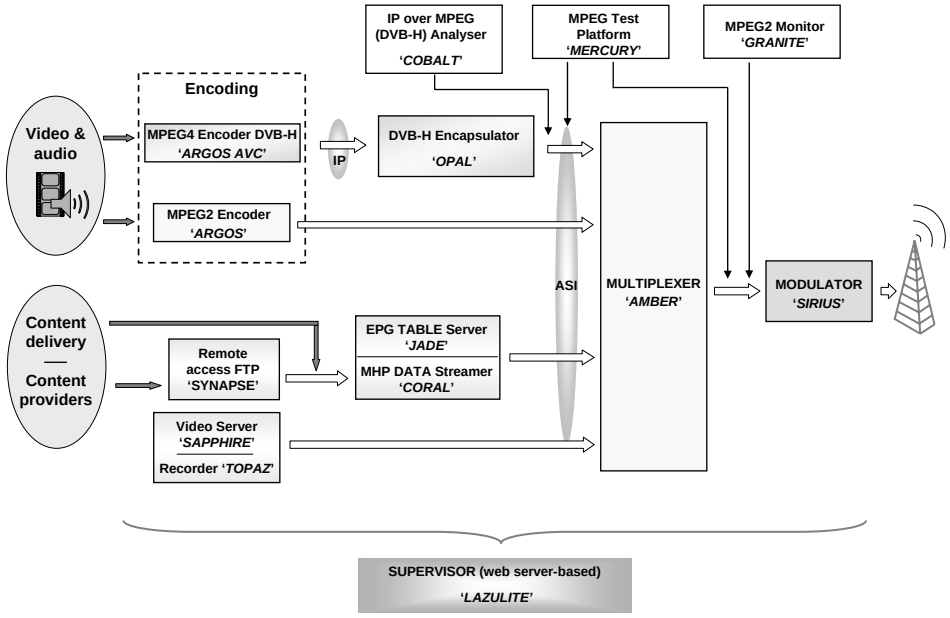

Figure 5.2 Block diagram of the DVB-T/H transmission platform.

Inputs:

- Audio channel: Input balanced analog signal

- ASI [2]: MPEG-2 transport stream

[1] MPEG-2 MP@ML (Main Profile@Main Level) 4:2:0 : encoding specifically designed for video signal distribution (DVB, DVD) in order to obtain the higher quality at the lower data rate.

[2] ASI (Asynchronous Serial Interface): DVB ASI is an interface designed to transport MPEG-2 video streams, primarily for television applications, over coaxial cable. DVB ASI

- CVBS: Composite analogue video signal

- AES/EBU: Digital audio signal

- SDI : Digital video stream which may include audio

Outputs:

- DVB-ASI : MPEG-2 transport stream, 75 ohm BNC connection

- Ethernet 10/100BT: Media (MPEG-2 transport stream over UDP), Control (SNMP monitoring)

Supervision:

- remotely manageable by a web browser through an http connection

- SNMP for remote management and reporting

- web network management system *Lazulite* [3]

Management:

- the control and the configuration of the Argos encoder are performed by means of the web management, which allows to check the Encoder status, select the audio parameters, select the video encoding configuration (video standard, horizontal and vertical resolution, transport rate).

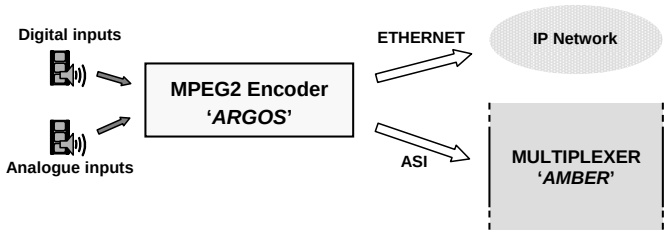

Figure 5.3 Argos inputs and outputs.

is a uni-directional service that enables to transmit up to 16 transport streams over a single circuit. There are currently two standard services: DVB ASI 34 - providing 34 Mbit/s and DVB ASI 140 - providing 140 Mbit/s.

[3]Lazulite is a web network management system. It is based on a web server, it allows to supervise each component of the platform via IP connection.

ARGOS AVC (Advanced Video Coding): H.264/MPEG4 Encoder

Argos AVC is a H.264/MPEG4 real time video encoder. H.264/MPEG4 is the standard of choice for DVB-H in order to reduce the bit rate while maintaining high video quality. The Argos AVC encoder allows to perform the encapsulation of H.264 over MPEG-2 transport streams and the distribution of H.264 over IP Networks (both directly and via MPEG2). The typical bit rates are from 256 Kbps to 10 Mbps.

OPAL: DVB-H IP Encapsulator

While other DVB transmission systems are based on the DVB Transport Stream, the DVB-H system is based on IP (Internet Protocol), in fact DVB-H data are IP data. The OPAL Encapsulator, which works on the IP domain, multiplexes IP traffic of multiple services, performs the encapsulation of IP datagrams into MPEG2-DVB packets and transmits a DVB Transport Stream out in ASI format. The OPAL Encapsulator performs IPv4 and IPv6 real time

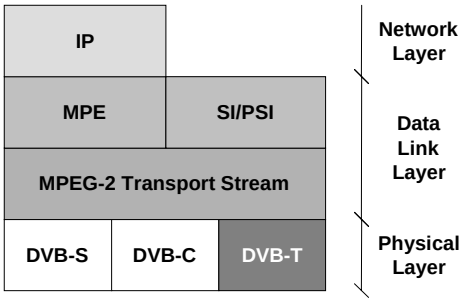

Figure 5.4 DVB-H data are IP data, IP datagrams are inside MPE sections.

MPE encapsulation, transport adaptation and the following DVB-H specific features:

- Time Slicing

- Multi-Protocol Encapsulation - Forward Error Correction (MPE-FEC)

Multi-Protocol Encapsulation (MPE) is a protocol for the adaptation of IP data into the DVB Transport Stream. In particular it is a data broadcast specification profile dedicated to transmission of IP datagrams of communication protocols via DVB compliant broadcast networks.

Time Slicing

In order to reduce the average power consumption of the mobile terminals the DVB-H services are sent in bursts, so that the receivers switch on only in the time interval when the data burst of a selected service is transmitted. The OPAL Encapsulator allows burst bandwidth definition (bits/s) and burst cycle time definition (millisecond). Mixing of fixed bandwidth services and time-sliced services is available. An example of Time Slicing is shown in Fig. 5.5, where Service 1, 2, 3 and 4 are time sliced, while Service 5 and PSI/SI tables are fixed bandwidth services.

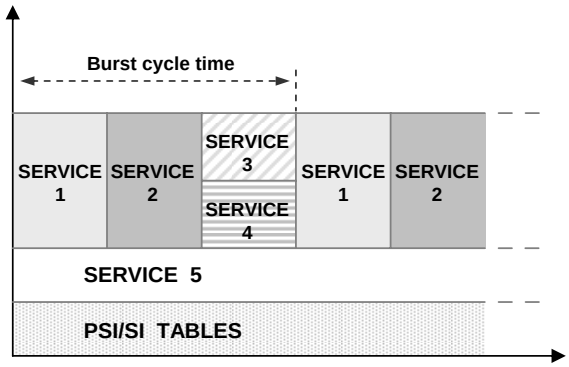

Figure 5.5 Time slicing.

Multi-Protocol Encapsulation - Forward Error Correction

Multi-Protocol Encapsulation - Forward Error Correction (MPE - FEC) is an enhanced error-protection scheme employed for reliable transmission in poor signal reception conditions. MPE-FEC employs powerful channel coding and it is based on a matrix with 255 columns. It is possible to use predefined Coding Rate ratios (1/2, 2/3, 3/4, 5/6, 7/8) or a custom ratio. The OPAL Encapsulator allows multiple configurations by selecting several parameters. Each parameter can be changed in real time: number of lines, number of padding bits, number of FEC columns, timeout.

AMBER: Multiplexer (TV Router)

Amber Multiplexer performs the multiplexing of several services from ASI and Ethernet inputs and the re-multiplexing of existing multiplexes. It allows the multiplex customization by deletion and insertion of local services and local data using the available bandwidth.

Inputs:

- 8 x 90 Mbps ASI Transport Streams
- 75 ohm BNC connection
- Ethernet 10/100 BT

Output: 1 ASI Transport Stream

Supervision:
- remotely manageable with a web browser through an http connection
- SNMP for remote management and reporting
- Lazulite

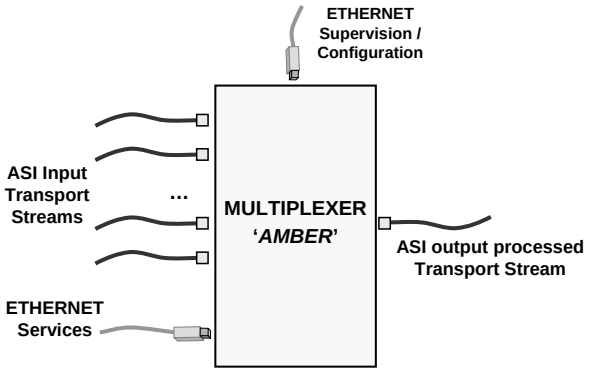

Figure 5.6 Amber inputs and outputs.

Management:
the control and the configuration of the Amber Multiplexer are performed by means of the web management. The main functionalities of the multiplexer are listed below.

1. Sources configuration: it is possible to edit both continuous sources (ASI, Ethernet) and On-demand sources (Ethernet) by means of a proper configuration panel.

2. Output configuration: it is possible to define broadcast parameters like: clock source (internal/external), packet size (188/204 bytes), global output bit rate

3. Bandwidth optimization: in order to have a constant final bit rate, some stuffing (e.g. null packets) is automatically added when the bit rate of the programs and MHP data is lower than available total bit rate.

4. Programs configuration: multiplexing and re-multiplexing of programs from the input sources.

5. Input and output photo panel: it allows to check the status of current input and output configurations.

6. Configuration panel: it enables to create a new configuration, to save and load configurations files, and check the configuration coherence.

7. Alarms and logbook panels: they display active alarms and logbook referring to the system status (equipment) and to the application status (processing).

8. Statistic panel: it shows, for each program, information on the used bit rate and global bit rate.

SIRIUS : DVB-T/H Modulator

Sirius is an exciter (modulator) supporting the required features of ETSI EN 300 744, the standard concerning DVB-T and DVB-H framing structure, channel coding and modulation. The exciter performs the digital modulation of the input signal, signal processing, up conversion of the IF digital signal to RF analogue signal, RF feedback processing.
The main transmission characteristics are the following:

- Channels : VHF I, VHF III, UHF (TV Bands)
- Bandwidth: 8, 7, 6 MHz
- Modes: 2k, 4k, 8k. Hierarchical mode option

Inputs:
- 2 ASI
- 1PPS pulse-per-second (clock reference signal)
- 10 MHz
- Ethernet monitoring, RS422 or RS232, Bus CAN
- TC input and TS dry loop
- Local Control and Monitoring
- RF Feedback Input (for this option a Thales amplifier is needed)

Output : RF output

Output power : 1mW (0 dBm)

The exciter is constituted by some sub-components that perform different parts of the modulation process. The digital board performs the DVB-T/DVB-H coding and the management of the internal communications. The TS board operates the up conversion of the IF digital signal to RF analogue signal and the down conversion of the RF feedback to a IF digital signal.

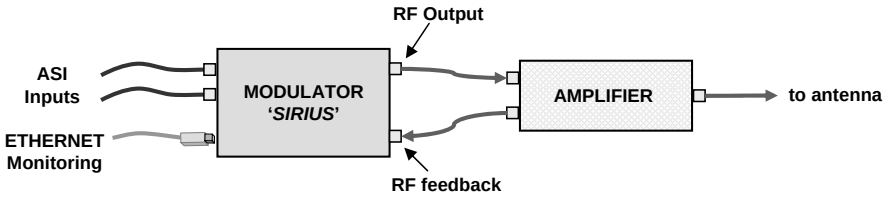

Figure 5.7 Sirius external interfaces.

TS Board :

- Up conversion of the IF Digital signal to RF Analogue signal.
- Down conversion of the RF feedback to a IF Digital signal.
- Non linear pre-correction, linear correction, clipping, Digital to Analogue RF conversion.
- Automatic non-linear and linear correction.

5.3 Interference source

The interference source stage consists of a digital signal generator, *Agilent Technologies* E4433B (250 kHz - 4 GHz, output frequency range), two function generators, *HP* 33120A, and a log-periodic antenna, *EMCO* 3146 (220 MHz - 1 GHz frequency range). It provided either in-channel AWGN interference or in-channel impulsive interference, at different power levels, according to the characteristics given in Sec. 3.3.

For the generation of AWGN signal the digital signal generators has been used, exploiting the I/Q arbitrary waveform generation function. The signal generator allows to set the carrier frequency, bandwidth and output power level. In this case an AWGN signal characterized by 8 MHz bandwidth and centered at a frequency equal to 770 MHz, has been considered.

Impulsive interference is generated as gated Gaussian noise by creating an externally triggered AWGN waveform. As reported in Sec. 3.3 gating must be performed twice: one gating defines the burst duration and the time spacing between consecutive bursts, a further gating is necessary to shape the pulses within the burst. This is accomplished by means of the HP function generators. A first HP generator provides the waveform that amplitude modulates the AWGN signal to shape the single pulses, through the external input of the Agilent E4433B. The pulse-shaping waveform has been created by means of the Agilent Intuilink Waveform editor and loaded to the HP 33120A generator via GPIB connection. The other HP generator provides a trigger signal to

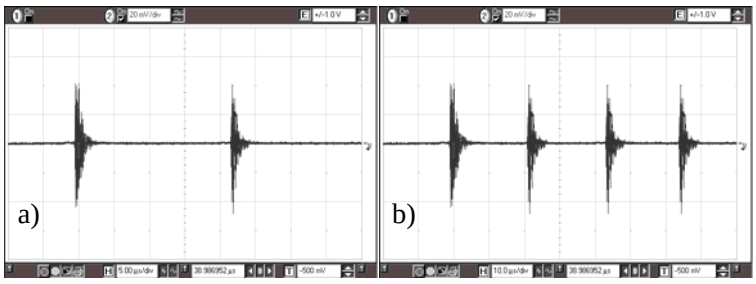

Figure 5.8 Impulsive interfering signals: a) 2-pulses per burst; b) 4-pulses per burst.

the first one that sets the time spacing between consecutive bursts. The burst duration depends on the pulse spacing and on the number of pulses per burst.

The burst-like modulated AWGN signal used as interference in this work is characterized by 8 MHz bandwidth and centered at 770 MHz. Bursts consist of a set of pulses of 1.5 μs time duration, with pulse spacing of 22 μs and burst period of 10 ms. Two different number of pulses per burst can be included in a set: i) two, and ii) four. Due to limitations of the available instruments, waveforms with higher number of pulses could not be generated. In Fig. 5.8, a time representation of the two types of burst captured by a digital oscilloscope is given.

5.4 Receiver and Measurement stage

The receiver and measurement stage consists of a receiving antenna, PCD 8250 (80 MHz - 2:5 GHz frequency range) by Seibersdorf, a DVB-T receiver by Terratec, connected to a personal computer through an USB link and emulating the operation of a Set Top Box (STB), a Superheterodyne Spectrum Analyzer, Agilent Technologies E4433B (9 kHz - 3 GHz input frequency range), a Vector Signal Analyzer software, Agilent Technologies 89600, exploiting data acquired by SSA, and a power splitter, which routes the output signal of the receiving antenna both to SSA and DVB-T receiver. A scheme of the connections to the splitter is provided in Fig. 5.9.

Superheterodyne Spectrum Analyzer

Radiofrequency signal power measurements have been performed exploiting the channel-power function of the Agilent SSA based on the post-processing formula detailed in Sec. 4.2.1. The settings of the spectrum analyzer utilized in the experiments are the following:

- center frequency: 770 MHz

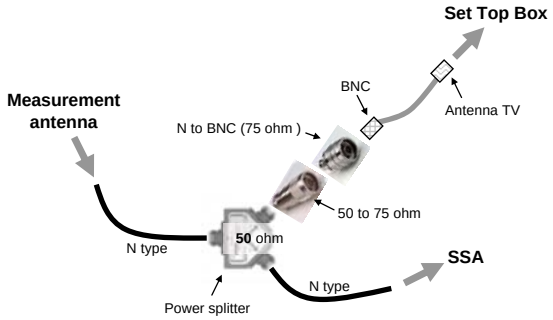

Figure 5.9 Scheme of the connections to the splitter.

- video bandwidth: 3 MHz (maximum available)
- resolution bandwidth: 100 kHz
- frequency span: 9 MHz
- sweep time: 5 ms

MER measurements

MER measurements have been performed by means of the Agilent Technologies 89600 Vector Signal Analysis software, exploiting data acquired and sampled by SSA. The data are sent to the PC via a GPIB-USB interface; this connection also allows to control the acquisition directly on the PC, after a proper setting of the SSA. The Option E9285 COFDM Analyzer used, allows to estimate modulation parameters specifically for DVB-T signals; it displays the acquired data, i.e. the symbols on the I/Q constellations diagram, the EVM magnitude spectrum, etc., and the measurement results.

Video capture and VQM measurements

VQM measurements have been performed off-line on 30 seconds sequences extracted from the video stream. For the MPEG-2 video sequences capture, a recording software tool running on the PC connected to the DVB-T receiver has been exploited.

Some pictures of the test bench at Digilab

Figure 5.10 Picture of part of the test bench at Digilab. On the left the SSA for channel power measurements is visible. The first NB on the left, connected to the SSA via GPIB, provides MER measurement by means of the COFDM analysis software. The other NB is connected to the DVB-T receiver for video streams capture. On the right side of the picture the signal generator and the function generators for AWGN and impulsive noise generation are visible.

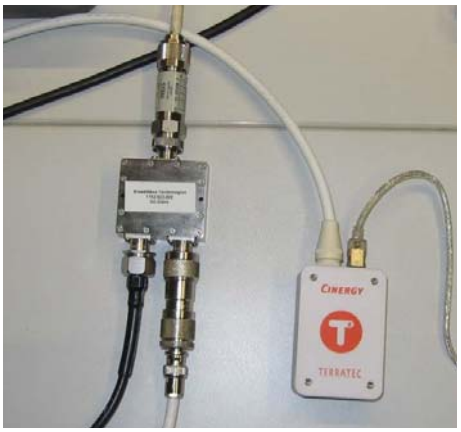

Figure 5.11 Power splitter and DVB-T reciever.

Figure 5.12 DVB-T/H platform and transmitting antenna.

Chapter 6

Experimental results

6.1 Introduction

The choice of the DVB-T signal transmission configurations to be investigated by experimental tests has been made according to several considerations, some of which are reported hereinafter. Typical configurations used by national and European broadcasters for the transmission of digital video contents have also been kept into consideration.

The main parameter determining major differences in terms of robustness of the signal and, at the same time, in terms of available useful data rate is the modulation scheme. Code rate is also a very important parameter, as the proper selection of code rate allows to trade off between the level of error correction and again the data rate. For the purposes of the conducted analysis, the comparison of the performance provided by the different modulation schemes (QPSK, 16-QAM, 64-QAM) have been firstly carried out. The effectiveness of error correction provided by some of the values of code rate defined by the DVB-T standard (1/2, 2/3, 3/4, 7/8) has been then evaluated, in particular in presence of in-channel interference.

The parameters of the DVB-T platform that have been kept constant, in the experiments described in this Chapter, are the following:

- 1/32 guard interval
- 8K mode
- 770 MHz central frequency
- 8 MHz channel bandwidth
- MPEG-2 video encoding format, 720 x 576 pixels resolution, 25 frames per second.

Since multipath effects can be considered negligible in the available test environment, a fixed value of the guard interval has been used, the one providing the lowest protection against multipath delays and the highest date rate. The number of subcarriers deployed is mainly related to the network architecture, single-frequency (SFN) or multi-frequency (MFN), and to the coverage area. The 8K mode, which is the most used by broadcasters, is suitable both for MFN and for small and large SFN networks. The central frequency has been fixed after an in-depth analysis of the VHF frequency spectrum in the test site, in order to avoid in-channel interference due to analogue or digital transmissions of local and national TV broadcasters. Video stream characteristics selected for the tests correspond to the DVD-standard quality commonly deployed in PAL systems for fixed TV reception.

Two layers at the receiver side have been analyzed: physical and application layer. At physical layer, measurements of channel power (P_R) and signal-to-interference ratio (SIR) are carried out. Measurements focused on modulation quality and performed on the received signal once downconverted to baseband, involve Modulation Error Ratio (MER). At application layer, measurements have been performed in terms of video quality of DVB-T streams by means of VQM algorithms.

The aforementioned indices have been estimated according to the considerations and conclusions provided in Ch. 4

6.2 First Experiments

The first experiments have been conducted without the addition of intentional in-channel interference on the following DVB-T signal configurations:

i) 64-QAM modulation scheme, 7/8 code rate,

ii) 16-QAM modulation scheme, 7/8 code rate,

iii) QPSK modulation scheme, 7/8 code rate.

The performance of the DVB-T system have been evaluated upon the varying of the transmitted signal power, while keeping unchanged the channel conditions. The mean values of estimated MER are reported in Fig. 6.1 upon the varying of in-channel power at the receiver input, P_R. The obtained results allowed a first analysis of the relation existing between RF power and baseband MER at the receiver side, in real-life indoor reception conditions, for the different modulation schemes. From the figure, it can be observed that:

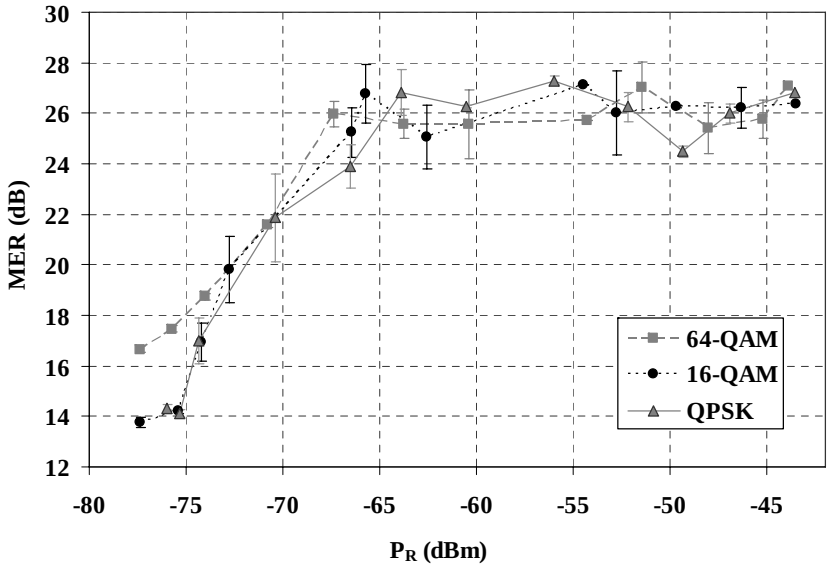

Figure 6.1 DVB-T system performance: MER vs received power P_R.

- the trend of the MER curves versus P_R is quite the same regardless of the deployed modulation scheme; they are comprised within a 4 dB wide-area;

- MER and P_R are related with each other according to a threshold-like relationship;

- MER and P_R grow quite proportionally in the range $P_R < P_\gamma$, where P_γ is the threshold value here nearly equal to -66 dBm;

- for greater values of P_R, $P_R \geq P_\gamma$, MER does not increase anymore and assume quite constant values in the range 24 - 28 dB;

- the standard deviation, represented by the vertical bars at each point of the graph, allows to account for the variability of the results, which is comprised within a 4 dB interval.

A saturation effect on MER measurements at the receiver for $P_R \geq P_\gamma$ is highlighted by the curves of Fig. 6.1. As reported in Sec.4.3, this is caused by the implementation loss of the receiver, whose noise contribution to the MER estimate is due to the front-end noise figure (e.g. imperfect time, frequency or phase tracking, round-off effects, imperfect equalization). The variability of the results highlighted by the standard deviations is mainly due to the fact that

measurements are performed within a non-shielded and non-anechoic room. The room at Digilab is in fact characterized by typical office furniture and appliances, with the presence of possible sources of uncontrolled interference like PCs, monitors, mobile phones, printers, power supplies, and light switches [19].

Stemming from these results, P_R values for the second step of experimental tests have been defined. In order to effectively investigate the DVB-T signal performance in presence of in-channel interference the maximum variability interval, $P_R \leq$ -65 dBm, has been considered, as reported in the next Sections 6.3 and 6.4.

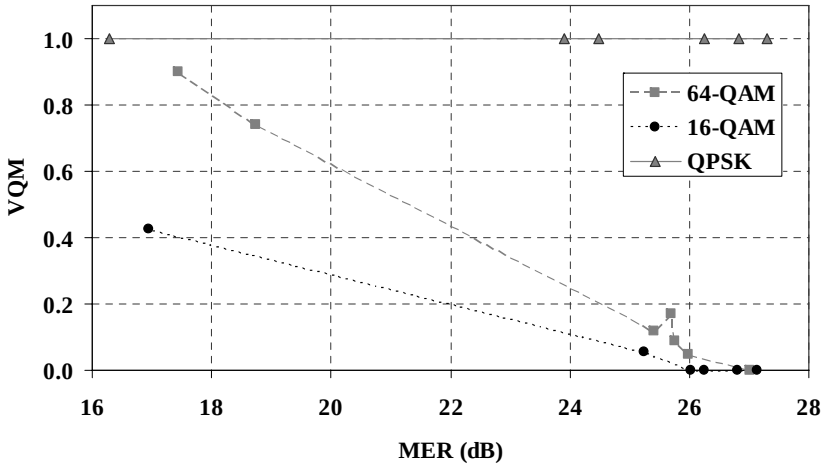

Figure 6.2 DVB-T system performance: VQM score vs MER.

A diagram showing the cross-layer relationship between MER and VQM is given in Fig.6.2. From the figure, it can be observed that the curves of 16-QAM and 64-QAM vary quite regularly upon the growing of MER, while in the case of QPSK, VQM is always unitary for any value of MER.

The visible separation of the three curves allows to deduce that at application layer, through VQM measurements, the effect of a given modulation scheme can clearly be recognized and assessed. The differences between 16 and 64-QAM VQM scores confirm that low orders of M-QAM schemes, unless setup errors, are generally better in terms of video quality perceived by end users. The minimum values of MER shown, to obtain an acceptable value of VQM (i.e. VQM $\leq$ 0.2), represent an example of how such a kind of measurements can be useful to gain helpful relationships between cross-layer parameters and practical hints for DVB-T network designers.

The presence of unitary values of VQM in the case of QPSK is instead quite strange. In fact, the QPSK scheme should be more immune to errors than any higher order M-QAM scheme. This unusual result is due to a wrong setup, and in particular to the output bit rate (15 Mbps), higher than the maximum limit (10.55 Mbps) supported by the QPSK for the DVB-T standard [5]. This setup has been chosen on purpose to clearly show that measurements at only physical layer may not be sufficient to recognize the presence of such destructive inconvenient (see Fig.6.1). Conversely, the presence of unitary VQM scores is instead a result that can be easily acknowledged and interpreted as a wrong system setup.

In these first experiments it was noticed that some interference was generated by the spectrum analyzer, during the MER measurement, when the input attenuation adaptation was performed by the VSA software. In particular, the switch of the internal attenuator caused impulsive noise affecting the acquisition of the video sequence, thus resulting in a block distortion video impairment. For this reason the VQM scores obtained have been corrected in such a way to neglect the effects of SSA interference on video quality. In the second part of the experiments, the measurement sequence has been modified in order to complete the VSA attenuation adaptation before the beginning of the video acquisition, thus avoiding the aforementioned problem.

The different MER values of Fig.6.2 have been obtained by the variation of the transmitted signal power. The lack of measured MER points in the 19 - 24 dB interval, which is due to the slope variation of the MER vs. P_R curves as reported in Fig.6.1, induced to a more accurate investigation of MER and VQM by a different choice of the transmitted power steps in that interval, to be deployed for the second step of experimental tests.

6.3 Experiments in presence of AWGN Interference

In the experiments performed on DVB-T signals affected by in-channel interference the following two scenarios have been considered:

a) 64-QAM modulation scheme, 2/3 code rate,

b) 16-QAM modulation scheme, 7/8 code rate.

They comprise both different modulation schemes and different code rates, while providing similar useful data rates; in particular 24.13 Mbps in the a) scenario and 21.11 Mbps in the b) scenario [5]. The purpose is to compare the robustness of different configurations with the same capabilities in terms of video services and contents, as it is clearly a main issue for TV broadcasters.

Transmission power at the input connector of antenna A (Fig. 5.1) has been set at a level, P_T, as high as to achieve good video quality scores (lower than 0.1) in the absence of interference, both for 16-QAM and 64-QAM modulation scheme [30]. In particular, P_T has been regulated in such a way as to receive at the SSA input a channel power level, P_R, equal to about -66.5 dBm, in the absence of interference.

Different results, summarized in Fig.6.3 for the two considered scenarios, have been achieved upon the varying of Signal to Interference Ratio (SIR), defined as P_R/P_I, where P_I is the power level measured at the SSA input with the only interference acting. For each SIR, the mean value of MER and VQM estimates is given. From the analysis of the results the following considerations can be drawn.

1) For SIR values lower than 13 dB, MER varies proportionally with SIR. The average slope undergoes variations for higher SIR values.

2) VQM varies with MER according to a threshold-like relationship. In particular, VQM = 0 (optimum video quality) for MER values greater than 18.2 and 15.8 dB, respectively in the scenario a) and b), and abruptly increases for lower values;

3) VQM varies with SIR according to a threshold-like relationship. In particular, VQM starts increasing when SIR is lower than 13.1 and 13.4 dB, respectively in the a) and b) scenario.

4) For any SIR lower MER values are achieved in the b) scenario.

5) The b) scenario exhibits better performance, in terms of VQM, in the range $12.2 \leq MER \leq 18.2$ dB. For instance, with MER = 17 dB, the maximum video quality (VQM = 0) is experienced in the b) scenario, while a null quality (VQM = 1) characterizes the a) scenario.

6) The minimum MER necessary to achieve good video quality scores, i.e. VQM lower than 0.1, is equal about to 18 and 15.3 dB respectively in the a) and b) scenario.

7) The minimum SIR necessary to achieve good video quality scores is equal about to 13 dB both in the a) and b) scenario.

8) The average slope of the edge related to the a) scenario in Fig. 6.3b is greater than that peculiar to the b) scenario. In particular, the transition region (i.e. the interval of MER values in correspondence of which VQM varies from 0 to 1) is 1 dB wide for the a) scenario, and 3.5 dB wide for the b) scenario.

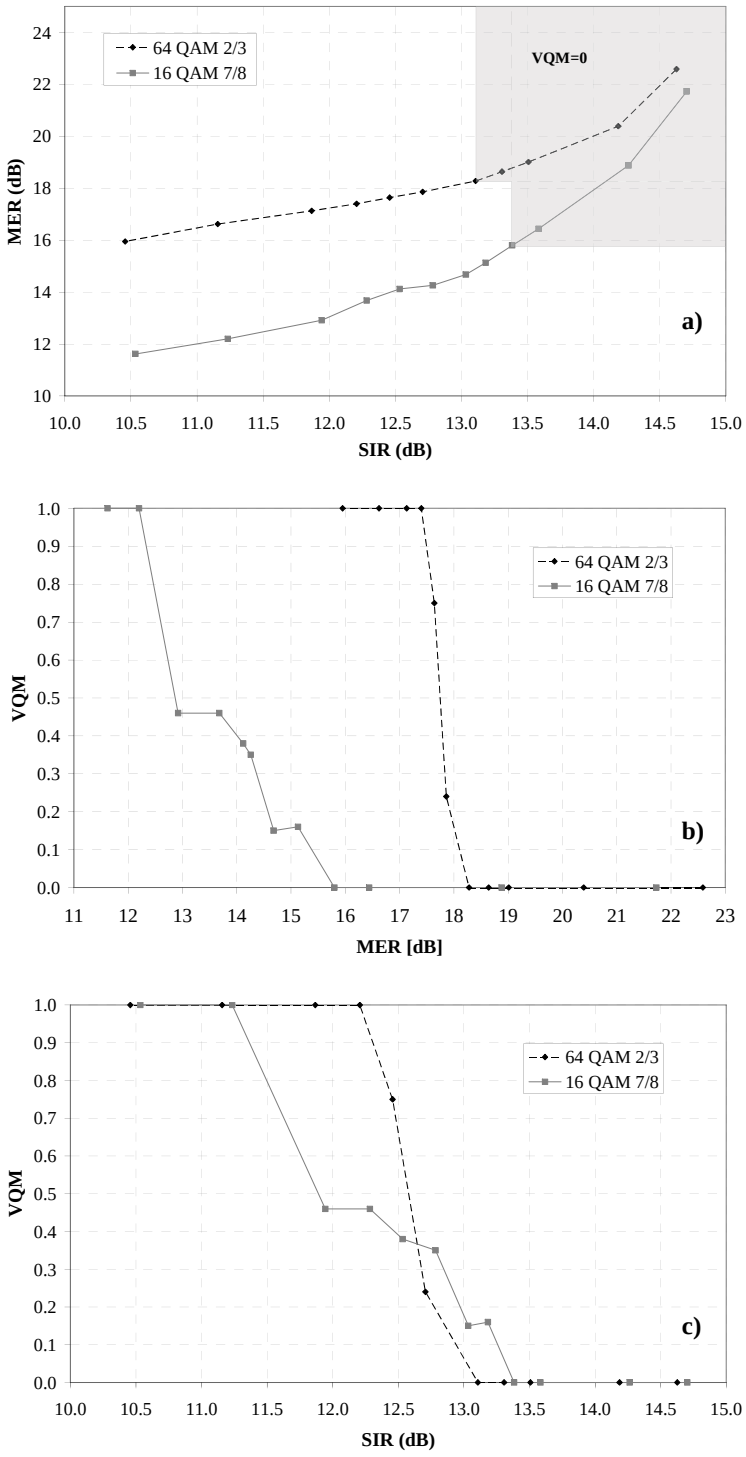

Figure 6.3 DVB-T system performance in the presence of AWGN interference: a) MER vs SIR, b) VQM vs MER, c) VQM vs SIR.

9) The average slope of the edge related to the a) scenario in Fig. 6.3c is greater than that peculiar to the b) scenario. In particular, the transition region (i.e. the interval of SIR values in correspondence of which VQM varies from 0 to 1) is 0.8 dB wide for the a) scenario, and 2.2 dB wide for the b) scenario.

The simulation results provided in Tab.2.3 for the various code rate and modulation scheme combinations, in terms of required carrier-to-noise ratio (C/N) to achieve a BER $= 2 \times 10^{-4}$, can be compared to the obtained experimental results. The a) and b) scenario have been evaluated in terms of signal-to-interference ratio (SIR), where the interference is controlled AWGN, so in this case SIR can be considered equivalent to C/N. In regard to Gaussian communication channel the simulation results suggest for the a) scenario (64-QAM, code rate 2/3) a minimum C/N equal to 16.5 dB, and for the b) scenario (16-QAM, code rate 7/8) a minimum C/N equal to 13.9 dB.

As highlighted by Fig.6.3c the threshold value is comprised within 13 – 13.5 dB for both scenarios, meaning that in the real-life test environment the a) signal configuration shows to be more robust than what expected from simulations, while for the b) signal configuration there is an higher correspondence between simulated C/N and experimental SIR results. The higher robustness that the b) scenario guarantees is confirmed by the slower transition from optimum to worse video quality.

Finally, it is interesting to notice that a 2.5 dB gap between the a) and b) scenario performance, comparable to the gap provided by simulations data in Tab.2.3, is instead present in terms of MER vs video quality as reported in the results of Fig.6.3b.

An investigation on the indices related to the specific video impairments has been also carried out. The results given in Fig.6.4 refer to the values of the five artifact indices, along with VQM, exhibit for different SIR levels, in the b) scenario and in the presence of AWGN interference. In particular, for SIR levels within the interval 11.3 – 13.7 dB, *unnatural motion* generally has greater values than those of other indices. As a matter of fact, it can be identified as the primary type of degradation arising in digital TV systems. In the same interval, *blurring* and *global noise* values are almost always negligible with respect to those assumed by the other indices; they reach high scores only in the SIR ranges in correspondence of which VQM is very high, i.e. when the video is already strongly corrupted. Blurring and global noise are in fact common impairments only for analogue TV transmissions. Finally, the trends of *block distortion* and *error blocks* curves are similar to the one presented by the global VQM score.

In Figs.6.5 and 6.6, an example of frame corruption due to AWGN interference is shown. It refers to the b) scenario accounting for a SIR value equal

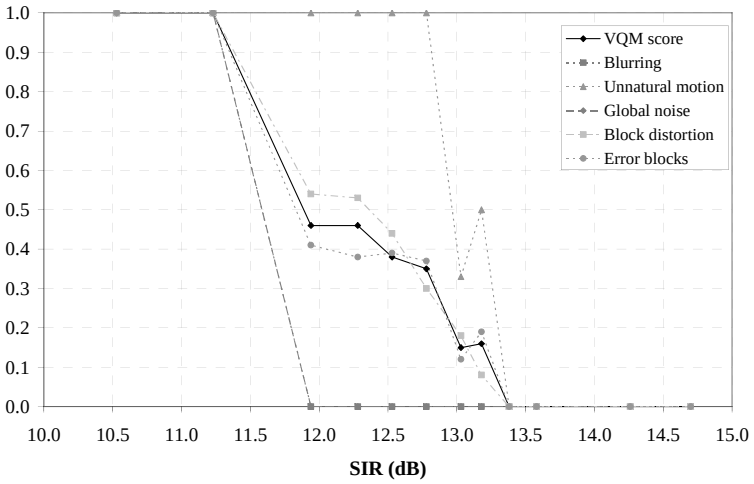

Figure 6.4 VQM vs SIR for a 16-QAM signal in the presence of AWGN interference.

Figure 6.5 Frames from the original (reference) stream.

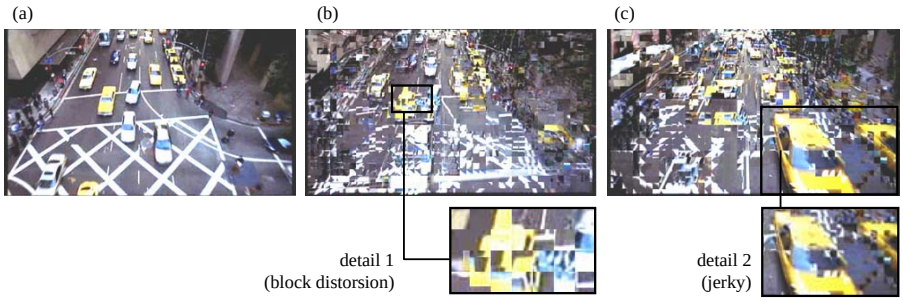

Figure 6.6 Received version of the frames sequence of Fig.6.5.

to 11.9 dB and highlights a clearly visible loss of video quality. The VQM software output provides an overall quality score equal to 0.46, and the following specific artifacts: blurring = 0, unnatural motion = 1, global noise =0, block distortion = 0.54, error blocks = 0.41. The first set of pictures represents three

subsequent frames of the original transport stream, while the second provides the corrupted version of this sequence, obtained at the receiver side. From the comparison of Fig. 6.5b and 6.6b the presence of block distortion can easily be noted. In fact, as clearly visible in the detail box of Fig. 6.6b, the frame is entirely subdivided into blocks of pixels. From the comparison of Fig. 6.5c and 6.6c, instead, the appearance of elements in Fig. 6c, not displayed in Fig. 6.5c, can be observed, like the two cars visible in the detail box of Fig. 6.6c. This inconvenient is due to a loss at the receiver side of one or more subsequent frames, with the consequent abrupt appearance of new images. Such a phenomenon is clearly visible by end users and causes unnatural (jerky) motion on the perceived video content.

6.3.1 Code rate contribution

Other experiments have been carried out with the aim of assessing the contribution on video quality of different code rates. For the purpose of these tests the 64-QAM modulation scheme has been adopted, because it is the less robust, both theoretically and experimentally, and furthermore it is subjected to the greatest changes of useful data rate upon the varying of the code rate, e.g. from 18.10 Mbps with code rate 1/2 to 31.37 Mbps with code rate 7/8, for guard interval equal to 1/32 (Tab.2.2). The obtained results are summarized in Fig.6.7.

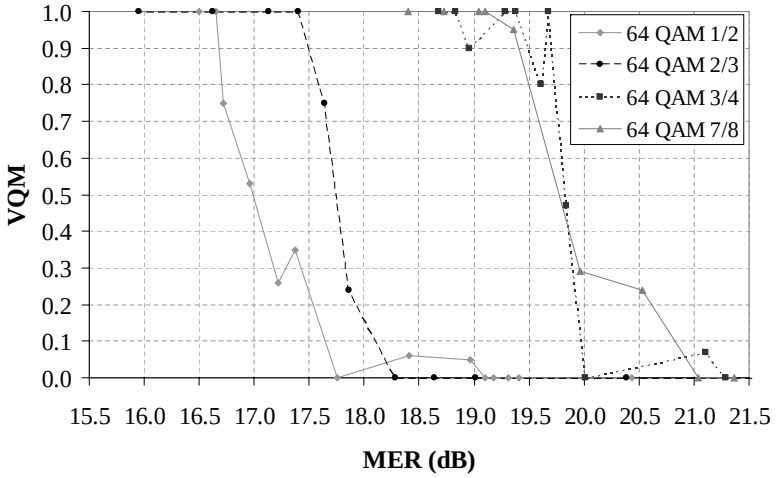

Figure 6.7 VQM vs MER for different code rates: 1/2, 2/3, 3/4, 7/8.

From the analysis the following considerations derive.

1) The VQM traces associated to the minimum and maximum code rate con-

sidered, 1/2 and 7/8, are set approximately 3 dB apart along the MER axis.

2) The minimum MER necessary to achieve good video quality scores, i.e. VQM nearly lower than 0.1, is 17.7 dB, 18.2 dB, 20.0 dB and 21.0 dB, respectively for a code rate equal to 1/2, 2/3, 3/4 and 7/8.

3) Changing the code rate from 3/4 to 7/8 does not imply a significant reduction of video quality; the corresponding traces are rather close to each other.

4) The previous consideration stays also for the traces associated to the code rates 1/2 and 2/3.

5) Each edge has roughly the same average slope.

6.4 Experiments in presence of Impulsive Interference

A burst-like modulated AWGN signal, characterized by 8 MHz bandwidth and centered at 770 MHz, has been utilized. It represents a typical interference for DVB-T household applications, arising in urban context and due to sources like housing appliances, central heating thermostats, light switches, and ignition systems [19]. Each burst consists of a set of pulses, characterized by a time duration equal to 1.5 μs, and spaced from one another of 22 μs; the burst period has been fixed to 10 ms. Two different number of pulses per burst have been considered: i) two, and ii) four.

Obtained results are summarized in Fig.6.8 for 2-pulses per burst interference and Fig.6.9 for 4-pulses per burst interference. VQM and MER have been measured upon the varying of P_U, defined as the interference signal power level in the absence of burst modulation. From the analysis of the results, the following consideration can be drawn.

1) The approximately linear at intervals trend, noticed in the previous MER vs. power (or SIR) diagrams, is not experienced in presence of impulsive interference, as highlighted by Fig.6.8a and Fig.6.9a.

2) A threshold-like relationship between VQM and MER, and VQM and P_U, similar to the one experienced in presence of AWGN, stands also in presence of impulsive interference.

3) The average slope of the edge of the VQM trace related to the a) scenario is is greater than that characterizing the b) scenario, both in Fig.6.8b

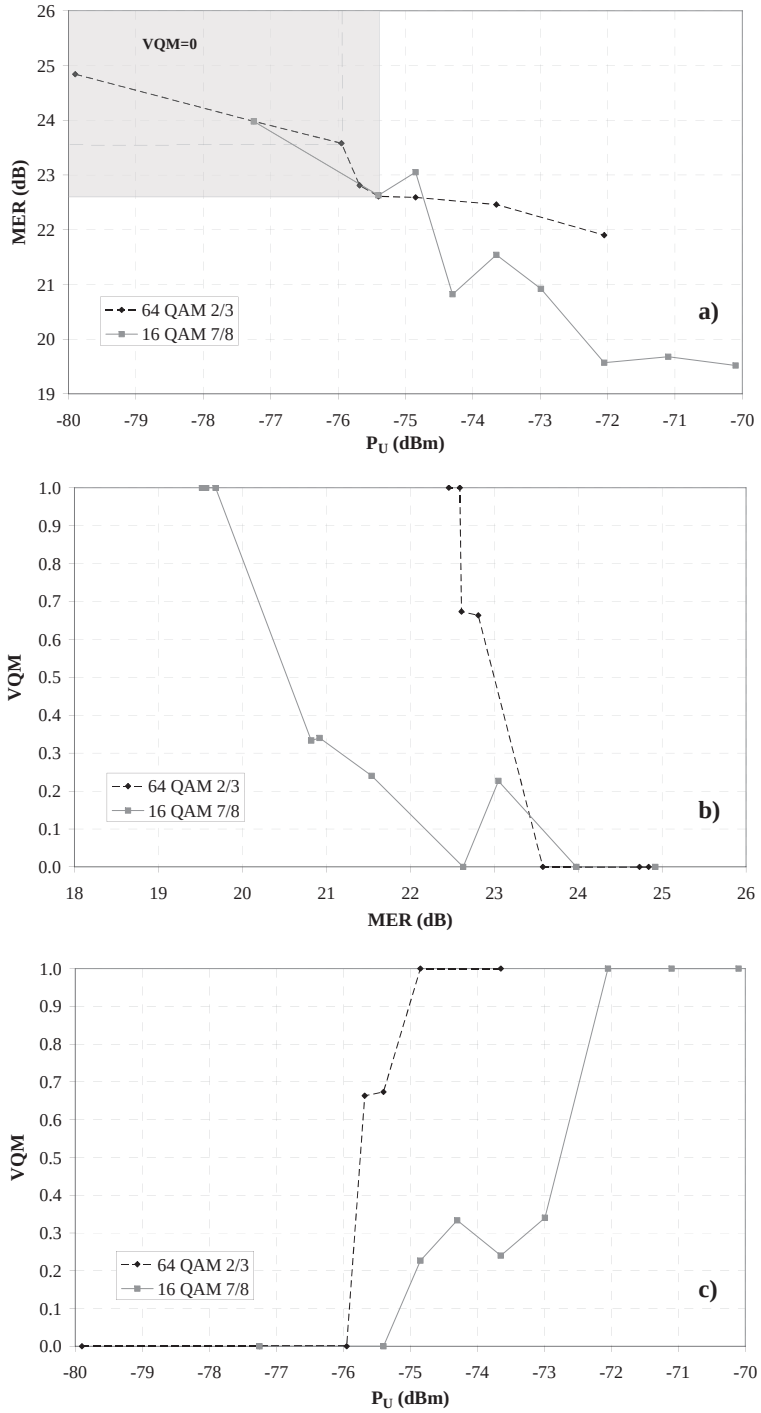

Figure 6.8 DVB-T system performance in the presence of impulsive interference (2-pulses per burst) : a) MER vs P_U, b) VQM vs MER, c) VQM vs P_U.

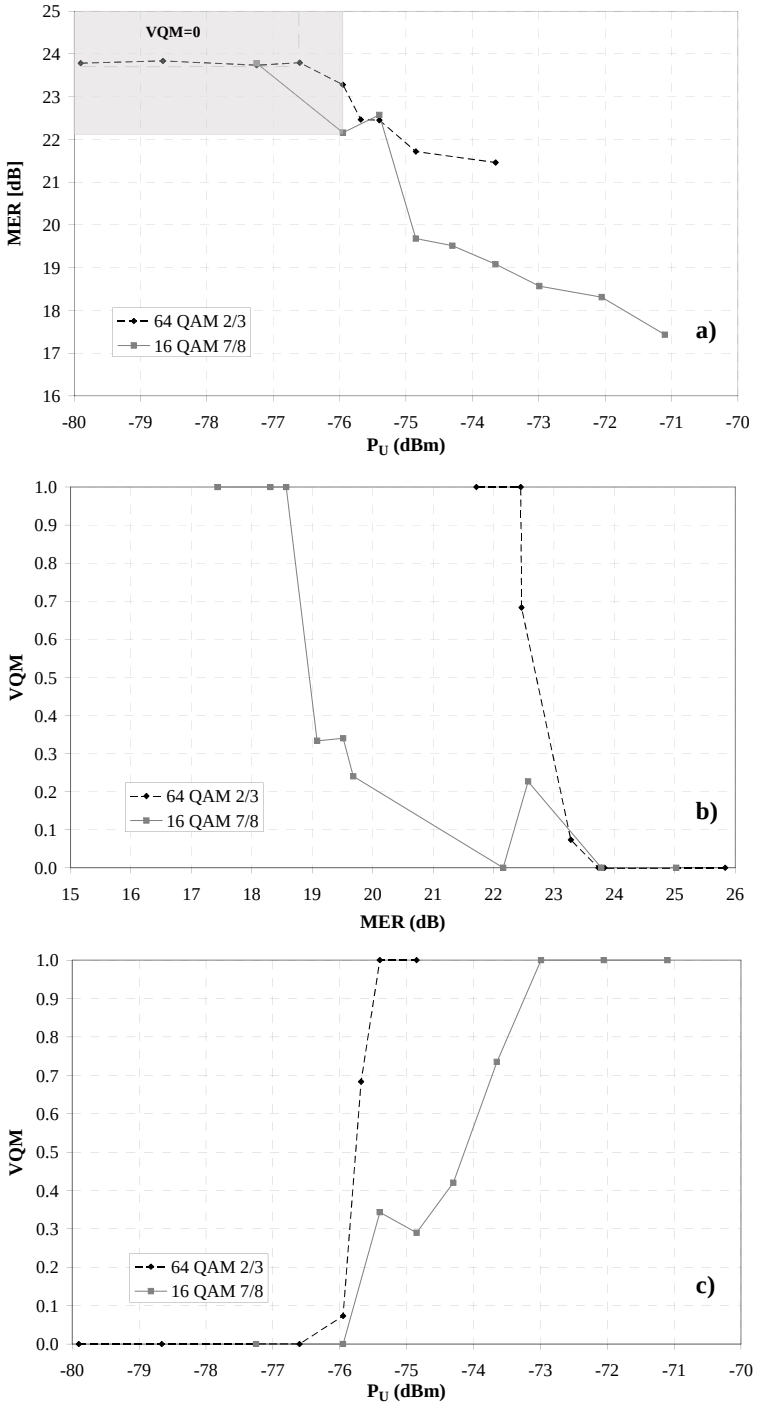

Figure 6.9 DVB-T system performance in the presence of impulsive interference (4-pulses per burst) : a) MER vs P_U, b) VQM vs MER, c) VQM vs P_U.

and Fig.6.9b in terms of MER, and in Fig.6.8c and Fig.6.9c in terms of interference power P_U.

4) MER and P_U threshold values are rather close to each other, for both the type of burst considered. With regard to MER, they are 23.6 and 24 dB in the presence of the 2-pulses per burst interference, and 23.8 and 23.7 dB for the 4-pulses interference, respectively in the a) and b) scenario. In terms of P_U, they are -76 dBm and -75.4 dBm, in the presence of the 2-pulses per burst interference, and -76.6 dBm and -76 dBm in the presence of the 4-pulses interference, respectively in the a) and b) scenario.

5) Better performance in terms of VQM is experienced in the b) scenario with MER and P_U values within respectively 19 – 23 dB and -76 – -73 dBm for both types of interference, 2-pulses and 4-pulses per burst. The transition regions result in fact from 4 to 5 dB wide for the b) scenario, thus assuring higher immunity to interference with respect to the a) scenario with 1 – 1.5 dB wide transition regions.

6) For some levels of P_U, in spite of very similar values of MER, the measured VQM's are completely different for the two scenarios. For instance in Fig.6.8, when P_U = -75.4 dBm, MER = 22.6 dB for both scenarios, but VQM = 0.68 (low quality) in the a) scenario and 0 (high quality) in the b) scenario.

6.4.1 Code rate contribution

Further tests with different code rates on 64-QAM modulation scheme signal configuration have been performed also in presence of impulsive interference, in particular with 2-pulses per burst interference. From the obtained results, summarized in Fig.6.10, the following considerations arise.

1) The curves associated to the minimum and maximum code rate considered, 1/2 and 7/8, are set approximately 2 dB apart.

2) The minimum MER necessary to achieve good video quality scores, i.e. VQM nearly lower than 0.1, is 22.8 dB, 23.4 dB, 24.2 dB and 24.8 dB respectively for a code rate equal to 1/2, 2/3, 3/4 and 7/8.

3) The major impact on video quality is noted when the code rate is shifted from 2/3 to 3/4. Similarly to the previously analyzed diagram (Fig.6.7), MER traces related to the code rates 3/4 – 7/8, and 1/2 – 2/3 are rather close to each other, separated by 0.5 dB.

4) Each edge has roughly the same average slope.

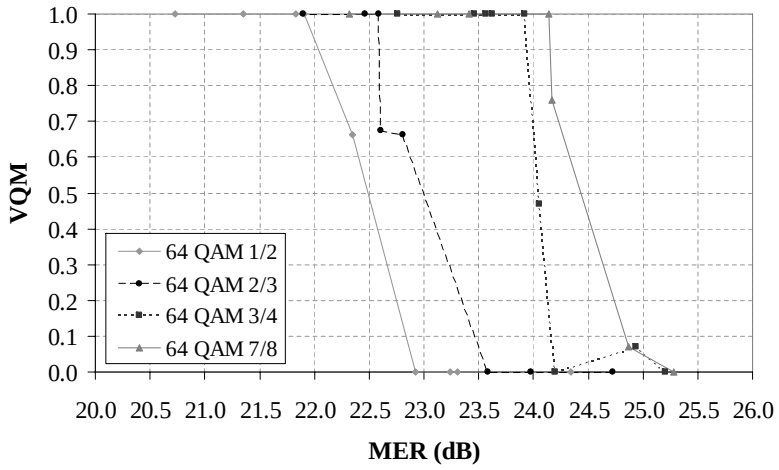

Figure 6.10 VQM vs MER for different code rates: 1/2, 2/3, 3/4, 7/8.

6.5 Comments

Some comments and useful hints can be deduced from the obtained results; the most relevant of them are given below.

As highlighted by Fig.6.1, MER does not significantly increase upon the growing of received signal power, when the saturation region is reached. Thereby, increasing signal power (or C/N, or SIR) beyond a given limit may be completely useless in terms of video quality, in case that no modulation quality (MER) improvement is present. An increment of emitted signal power to solve coverage problems would cause an addition of power consumption, which is non-trivial from the point of view of broadcasters, and furthermore a worsening of the environmental impact of the electromagnetic field on the population. A more efficient solution could be the use of transmitters front-end and amplifiers guaranteeing high linearity and reduced signal distortion (phase noise, I/Q offset, etc.), i.e. higher levels of output MER.

AWGN interference

AWGN interference has an heavy impact on DVB-T signals when SIR is lower than a given threshold. Threshold values related to each transmission configuration, are required for the coverage areas planning, as transition regions from optimum to worse video quality are rather narrow. As shown in the example of Fig.6.3c concerning the a) scenario, the displayed video stream may completely be degraded for SIR values shifting from 13 dB to values lower than 12.2 dB.

Since VQM is evaluated on the displayed video stream, the results of Figs.6.3b and 6.3c also account for the positive effect of error correction, which is evident in the scenario a) with code rate 2/3. The effect is visible in Fig.6.3c, where the two SIR thresholds, under which VQM abruptly increases, are quite the same. So, the more intense code rate in the scenario a) is sufficient to balance the intrinsic higher immunity to interference of the modulation scheme of the other scenario.

In a whole, the performance experienced in the b) scenario is better than that characterizing the a) scenario, as clearly shown in Fig.6.3b. In particular, the b) scenario requires lower levels of MER than those needed in the a) scenario and, mainly, the average slope of the edges of the traces obtained in the b) scenario is much lower than those related to the a) scenario. Unexpected decreases of MER or SIR may provoke stronger increase of VQM in that related to the a) scenario than that occurring in the b) scenario.

Regarding the specific video impairments observed in the test, unnatural motion is the one that mainly contributes to degradation of digital TV video streams; blurring and global noise, typically present in analogue TV transmissions, have instead negligible effects.

In respect to the code rate, different choices in the presence of interference may have a relevant impact on video quality perceived by the final user. The minimum value of MER needed to obtain VQM ≤ 0.1 may in fact vary up to 3 dB depending on the chosen of code rate. Adopting a 64-QAM modulation scheme and an higher code rate to enhance the data rate implies a non-negligible loss of immunity to interference. In particular, a variation of the code rate from 2/3 to 3/4 may cause the minimum MER value to obtain VQM ≤ 0.1, to increase of nearly 2 dB.

Since varying the code rate from 1/2 to 2/3, or from 3/4 to 7/8, is rather equivalent in terms of VQM in the presence of AWGN interference, the code rates with lower redundancy 2/3 and 7/8 should be preferred to 1/2 and 3/4, respectively, to favor the useful data rate.

Code rate has no influence on the average slope of the edge of the VQM traces; the same "safety margin" from MER thresholds is present regardless of the chosen code rate.

Impulsive interference

Many of the above considerations can be extended to the case of the impulsive interference.

Impulsive interference causes more detrimental effects on video quality with respect to AWGN. In particular, with impulsive interference, video quality degradation is achieved despite high MER values; threshold values result about 6 dB higher than those obtained with AWGN.

The increase of the number of pulses per burst in the impulsive signal from 2 to 4 causes a slight performance worsening. The curves result shifted of 0.5 dB, both in terms of MER vs. video quality and in terms of P_U vs. video quality.

The effect of a given level of MER on the perceived video quality strongly depends on the interference characteristics. For instance, in the b) scenario a MER level of 16 dB is sufficient to achieve full video quality in the case of AWGN interference, while it is not in presence of impulsive interference. Therefore, requirements for DVB-T systems should be given either in terms of video quality or in terms of MER, but with adequate information about the possible interference arising.

6.6 Conclusions

The developed measurement methodology allows to provide P_R values along with MER values for an efficient determination of the coverage area of a DVB-T system, since, as detailed and demonstrated in the thesis, only P_R values are not sufficient. MER threshold values however must be referred to a quality index and depend on the adopted transmission configuration. Video quality measurement are not suited to be performed in-service at the receiver side, as they require a reference video sequence and the analysis has to be carried out offline. Thus, the cross-relations highlighted by experimental results allow to correlate the quality of service to pairs of indices like P_R and MER, which instead can be quite easily and rapidly measured at reception sites, and compared to minimum required values obtained in the described experiments.

The proposed experimental analysis has highlighted significant relationships between VQM scores and values of MER, SIR, or interference power, P_U, to consider in order to achieve desired video quality levels in the presence of interference. It has also shown that two DVB-T signals characterized by the same MER value, may lead to completely different video quality indices. This confirms that VQM estimates are essential both for the characterization of a DVB-T system and for threshold values of MER, SIR or P_U to be deduced and usefully deployed in a design stage. Regarding the two analyzed DVB-T signals, 16-QAM modulation scheme with 7/8 code rate and 64-QAM modulation scheme with 2/3 code rate, providing similar data rates, the former allows better performance in the presence of interference both in terms of VQM and MER. Such differences are more clearly visible in the transition region where VQM abruptly changes from 0 to 1, or vice versa. Reducing the order of the M-QAM scheme is in general the solution that allows good video quality levels to be obtained with lower values of MER, SIR or in the presence of higher interference power levels. The analysis has also shown that impulsive

interference provides more detrimental effects on video quality with respect to AWGN disturbance.

Part II

Coexistence issues between IEEE 802.11b and IEEE 802.15.4 wireless networks

Introduction

Wireless networks are nowadays largely used in urban areas, industrial and indoor environments crowded of radio disturbances. Such interferences are due either to electrical and electronic appliances and devices, that cause unwanted and unintentional emissions, or to wireless communication systems and other networks sharing the same frequency bands, that may be considered intentional emissions. As a consequence, destructive interference may arise, and effects like loss of performance and poor reliability consequently occur. Some typical effects are loss of data packets, transmission delay, false commands, false alarms, jitter, loss of synchronization, etc.. A critical case of interference involves IEEE 802.11b wireless local area networks (WLANs) and IEEE 802.15.4 wireless sensor networks (WSNs). Such two networks exploit the same frequency band, *i.e.* the 2.4 GHz *Industrial, Scientific and Medical* (ISM) band, and may be simultaneously deployed in the same environment. Therefore, they are strongly susceptible to mutual interference and consequently to failures and loss of performance. To properly face coexistence problems, some works are available from today literature. In particular, Howitt studies in [31] the coexistence impact of an IEEE 802.15.4 network on IEEE 802.11b devices through an interesting probabilistic model, applied to specific network configurations and environmental conditions tested. Golmie et al. follow in [32] a meaningful experimental approach regarding the case of Bluetooth devices that operate in the proximity of a WLAN. In [8], Angrisani et al. measure the performance of a WLAN through a cross-layer approach, in the presence of narrowband and wideband in-channel interference.

In this second part of the thesis, coexistence problems of a IEEE 802.11b WLAN and a IEEE 802.15.4 network operating in a real-life environment are experimentally assessed by means of cross-layer measurements. The goal is to deduce helpful information and hints for designers and technicians, to efficiently operate with such networks and optimize their setup in common real-life conditions. A number of experiments have been conducted through a proper testbed, and a cross-layer measurement approach. In Chapter 7 the main features of the IEEE 802.11b and IEEE 802.15.4 standards are introduced and the

hardware and software components of the testbed are described. In Chapter 8 the results of the experiments performed upon the varying of the transmission parameters and network configurations are presented. In particular the scenarios where WLAN is victim of WSN interference and WSN is victim of WLAN interference are separately analyzed.

Chapter 7

Standards and testbed

7.1 IEEE 802.11b wireless network (WLAN)

A WLAN is generally a set of computing devices and access points (APs) communicating with one another through radio waves and over common frequency channels [34], [35]. The IEEE 802.11b standard defines a total of 14 frequency channels, each of which characterized by 22 MHz bandwidth (Fig. 7.1). In U.S.A., channels 1 through 11 are allowed by the Federal Communications Commission (FCC), while in Europe channels 1 through 13 can be used.

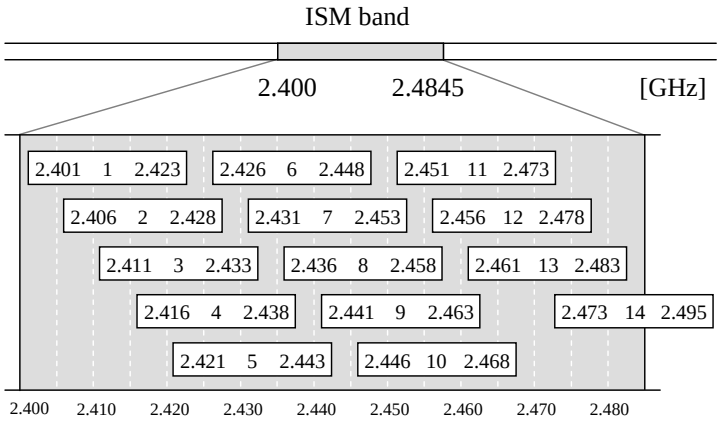

Figure 7.1 WLAN frequency channels.

Fig. 7.1 shows that channels are partially overlapped, and that only three channels at a time, *e.g.* 1, 6, and 11, do not interfere. In the design of a WLAN, the assigned channel and spatial position of each AP should be fixed in such a way as to avoid frequency overlap over the whole coverage area.

The mechanism to access the medium defined by the 802.11 protocol is the

Distributed Coordination Function (DCF), which is a random access scheme based on the *Carrier Sense Multiple Access with Collision Avoidance* protocol (CSMA/CA). The default scheme for packet transmission is a two-way handshaking technique called *basic access* mechanism. This mechanism is characterized by the immediate transmission of an acknowledgement (ACK) by the destination station, upon successful reception of a packet.

In a typical communication, an AP transmits periodically a frame called *beacon*, which contains information like a network identifier (ID), channel parameters and other traffic information. Each host station receiving the beacon, sends a request for authentication if intending to access the network. A series of tests is then performed to ensure the identity of the station. Once authenticated, the host is enabled to communicate to the AP or vice versa according to the CSMA/CA protocol. In particular, a host (or the AP) wishing to transmit senses the channel, and, if no activity is detected for a period of time equal to a distributed interframe space (DIFS), the host transmits. If the channel is sensed busy, the host continues to monitor the channel until it is sensed idle for a DIFS. Then, it waits for an additional randomly defined *backoff* interval, and transmits if the medium is still free. If the packet is received without corruption, the AP issues an ACK frame after a period of time called short interframe space (SIFS), that completes the process. If the station does not detect the ACK frame within a fixed *timeout* interval, a collision is assumed and the data packet is retransmitted after another random *backoff* interval.

To assess the channel status, the Clear Channel Assessment (CCA) technique is implemented [35]. Three CCA modes are defined by the standard; in *mode 1*, which is the one considered in this work, the channel is assumed idle if the channel power level is below a given user selectable threshold, called CCA threshold, otherwise it is assumed busy.

In addition to the basic access, an optional four way handshaking technique, *request-to-send/clear-to-send* (RTS/CTS) mechanism has been also defined. Before transmitting a packet, a station operating in RTS/CTS mode reserves the channel by sending a special Request-To-Send short frame. The destination station acknowledges the receipt of an RTS frame by sending back a Clear-To-Send frame, after which normal packet transmission and ACK response occurs [36].

A schematic representation of the described basic access mechanism is shown in Fig. 7.2a. A packet fragmentation is performed before transmission, which allows to break large packets into smaller parts, of length d, which is useful in noisy environments, singe large packets can more easily be corrupted. Two overhead frames are then added to each data packet: an *header*, h, which contains information like station identifier number, packet sequence number, sender and receiver addresses, total packet length ($d + h + c$), and a *control* field, c, which allows errors to be handled. In Fig. 7.2a, the time

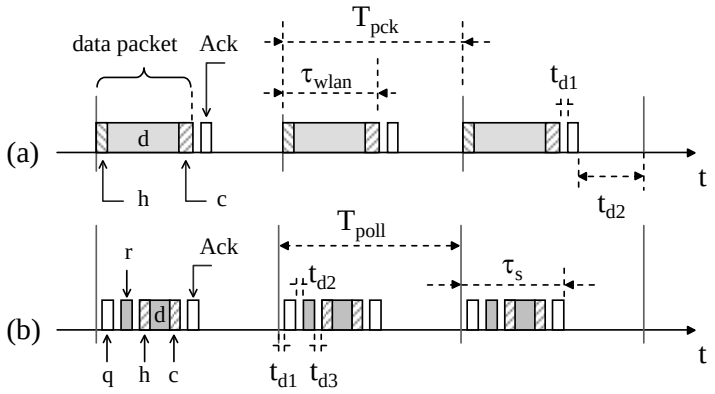

Figure 7.2 Time diagrams of WLAN (a) and IEEE 802.15.4 (b) frames.

interval covered by the packet is denoted as τ_{wlan}, while the time interval between two packets as T_{pck}. The two delays t_{d1} and t_{d2} between packets and the occurrence of ACK (DIFS and SIFS in ideal channel conditions) vary from a packet to the other, mostly depending on channel characteristics, network topology and $backoff$ time.

The actual packets interdeparture time, T_R, depends on the packet rate, R_T, set for the data transmission, in fact $T_R = 1/R_T$. In order to indicate the percentage of T_R specifically dedicated to the transmission of the whole packet, the *offered load*, also referred to as *duty cycle*, λ_{wlan}, is commonly introduced [32]. It is defined as: $\lambda_{wlan} = T_{pck}/T_R$.

7.1.1 UDP data frames in the 802.11b standard

User Datagram Protocol (UDP) is one of the core protocols of the Internet protocol suite; it is relative to the transport layer. It is a message-based connectionless protocol, where communication is achieved by transmitting information from source to destination without prior arrangement to establish a connection. The overhead added to the packets contains sufficient information to permit their independent delivery. UDP does not guarantee reliability or ordering, instead provided by TCP: datagrams in fact may arrive out of order or go missing without notice. Avoiding the overhead of checking whether every packet actually arrived makes UDP more efficient, for applications that do not need guaranteed delivery, and more simple.

In the following, the fields related to the different layers added to the payload, when the UDP protocol is applied in the 802.11b standard, are enlisted. The total overhead consists of 88 bytes.

- UDP header (8 bytes): it consists of 4 fields. Source port and destination port, which identify the corresponding ports. Length, a 16-bit field that specifies the length in bytes of the entire datagram: header and data. Checksum, a 16-bit field used for error-checking of the header and data.

- IP (Internet Protocol) header (20 bytes): it contains information for the packet routing, like the source and the destination IP addresses.

- LLC (Logical Link Control) header (8 bytes): it is necessary for the convergence of wired LAN and WLAN.

- MAC (Medium Access Control) header (24 bytes): it contains the source, the destination and the Access Point IP addresses.

- MAC FCS (8 bytes): it allows to check the received data to verify the integrity of the received packet.

- PLCP (Physical Layer Convergence Procedure) header (6 bytes): it contains information on the deployed modulation scheme.

- PLCP preamble (18 bytes): contains information required for the synchronization of the devices.

In Fig.7.3 the structure of the dataframe is schematically represented, where t_{pr} is the time necessary for the preamble transmission at fixed data rate (1 Mbps) and t_d is the time required for the frame transmission at the selected rate (11 Mbps in the experiments described), with $t_{pr} + t_d = \tau_{wlan}$.

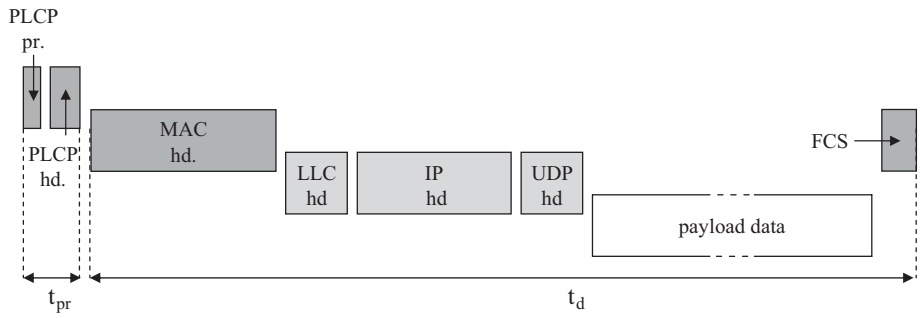

Figure 7.3 Dataframe for UDP transmissions in the 802.11 protocol.

802.11b WLAN transmission have been performed exploiting the UDP protocol, which for its efficiency and simplicity is fit for the purpose of this work. In particular, the absence of transport layer acknowledgements and packets retransmissions allows to account for values of T_{pck} and λ_{wlan} independent from

such procedures. In such a way the T_{pck} time variations may be only due to the CSMA/CA protocol, when the channel is sensed busy.

7.1.2 Throughput and goodput

The packet transmission rate, R_T, and the packet size, ps_{wlan}, (and consequently the duty cycle λ_{wlan}) influence the throughput of the network, i.e. the amount of data per second that is delivered to a certain network terminal or host computer. In communication networks, throughput is defined as the amount of digital data per time unit that is delivered over a physical or logical link, usually measured in bits per second (bps).

The *goodput* is instead the number of "useful" bits per unit of time forwarded by the network from a certain source address to a certain destination, excluding protocol overhead and retransmitted data packets. It can be considered as the application level throughput. Goodput measurements allow to determine the actual speed of a network.

Some examples of the factors that cause the gap between goodput and throughput are:

- protocol overhead;
- retransmission of lost or corrupt packets, caused by bit errors or packet dropping in congested switches and routers;
- collision avoidance using the CSMA/CA protocol, that may cause backoff waiting time (i.e. increased interframe gap) and retransmission.

7.2 IEEE 802.15.4 wireless sensor network (WSN)

IEEE 802.15.4 is a standard designed for Low Rate Wireless Personal Area Network, LR-WPAN, characterized by limited coverage area, reduced cost and low energy consumption. It is one of the most promising technology for implementing WSNs [37], allowing a variety of network topologies. In this work a star topology has been considered, where a PAN coordinator (master) cyclically queries a set of slaves (sensor nodes), one by one, and slaves reply transmitting a data packet containing the information acquired by the associated sensor. Transmission between master and slaves, with a 250 kbps data rate, exploits one of the 16 available channels in the 2.4 GHz ISM band. As shown in Fig. 7.4, the channels have a 3 MHz bandwidth and are uniformly distributed within the ISM band. In Fig. 7.4, three non-overlapped WLAN channels are also depicted with the aim of highlighting that WSNs and WLANs actually occupy the same frequencies, and that the risk of in-channel interference is very high whenever a WSN operates in presence of one or more active WLANs.

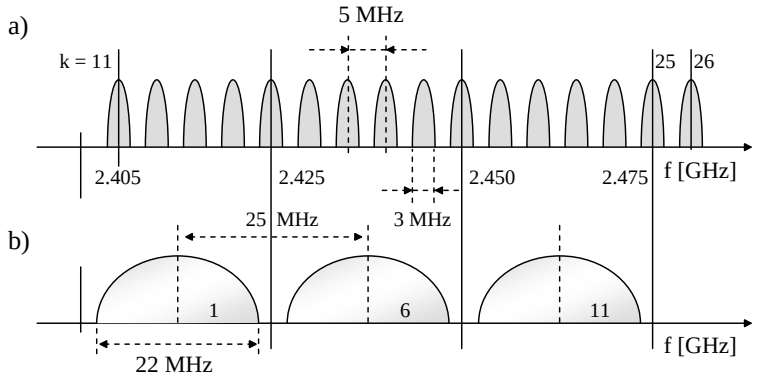

Figure 7.4 Frequency channels peculiar to a) IEEE 802.15.4 and b) IEEE 802.11.

The master dedicates a time interval, called *polling window*, of fixed time length (T_{poll}) to each sensor node. As schematically represented in Fig. 7.2b, the master starts waiting a backoff period, t_{d1}, and then senses the air according to the CSMA/CA protocol. If the channel is free, it transmits a frame (query), q, throughout the network, containing information like the destination node address, sequence number of the performed cycle and time stamps. After a pre-fixed short delay, t_{d2}, the queried sensor node replies with an ACK and waits for a second backoff period, t_{d3}. It then senses the air and, if it is free, transmits the data packet, d, with an header frame, h, and a tail field, c. In the case of correct reception, the master issues an ACK, and, at the end of the polling window, it passes to the subsequent sensor node. If the sensor does not receive the ACK from the master, it waits for another backoff period and then retries to transmit. At the expiration of the polling window, if the ACK from the master has not been issued yet, the packet from that queried sensor is considered lost.

7.3 Testbed

Experiments have been carried out on the testbed sketched in Figs. 7.5 and 7.6. It consists of an IEEE 802.15.4 WSN and a IEEE 802.11b WLAN operating in close proximity.

The WLAN is realized through a standard Access Point, AP, and a host station, ST, placed at a distance $d = 13$ m from it, which is the maximum available distance in the room used for the tests. The AP is a D-link 524 device connected to a personal computer (PC) via a wired link, while the host ST is a notebook Toshiba Satellite (Intel Centrino 1.60 GHz) with an Intel

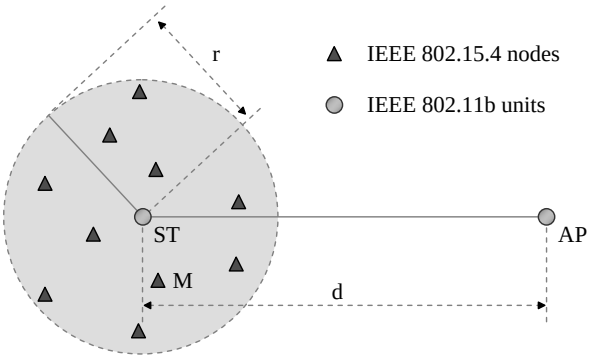

Figure 7.5 Adopted testbed.

Pro/Wireless integrated WLAN transceiver module. Two additional variable RF attenuators, Hewlett Packard 8494A and 8495A, placed between the D-link 524 output connector and its transmitting antenna, are used to vary the level of the transmitted power. Traffic is generated by means of the tool *D-ITG (Distributed-Internet traffic Generator)* [38], developed by the Department of Computer Science and Control Systems at University of Naples "Federico II". It allows the setting of the transport layer protocol (TCP, UDP, ICMP) and application layer functionality: DNS, Telnet, voice or custom. In custom mode, packet rate, packet size and inter-departure time statistical distribution can be varied according to the desired configuration. Also, it allows measurements of Quality of Service parameters, like packet rate, packet loss ratio (PLR), packet average delay and packet jitter, both at receiver and transmitter side. For the WLAN transmission setup UDP protocol, described in Sec.7.1.1, with inter-departure time constant distribution has been chosen. Packet rate and packet size have been instead varied in order to evaluate the performance of different transmission configurations, as detailed in Ch.8.

The IEEE 802.15.4 network is a set of *TmoteSky* sensor nodes (motes), available from Moteiv, randomly distributed inside a circumference of radius $r = 2$ m and centered around ST. The motes operate according to a general purpose high-layer protocol, based on a master-slave relationship. The network includes one master, M, and $N = 4$ slaves, each of which equipped with the following basic elements: (i) one micro-processor, (ii) one or more analogue input sections, to be interfaced with one or more sensing elements, (iii) a buffer for acquired data, (iv) a radio communication module, (v) a Received Signal Strength Indicator (RSSI[1]), which provides estimates of the received

[1]Received Signal Strength Indication. It is the received signal strength in a wireless environment, used in wireless networking devices to determine the amount of radio energy

in-channel power level. M is connected to a PC via a wired link, for storing collected data and post-processing. As described in Section 7.2, it executes a periodical polling of each slave for receiving data from monitoring sensors. All transmissions are handled by the Medium Access Control (MAC) layer, which allows the radio channel to be accessed, and data packets to be retransmitted in case of losses or missing acknowledgments. Traffic is generated and monitored through a specific software, *WSN tool*, developed by the EMC Laboratory at the University of Padova [39]. It allows the configuration of master and slaves, the setup of the output RF power and the central frequency of the transmission channel. It handles the data collected from the nodes, the post-processing and the displaying of the data (i.e. number of successful packets, sensor readings and RSSI readings). Different configurations of WSN parameters have been analyzed. In particular, different values of T_{poll} have been taken into account, where $T_{poll} = 30$ ms is the minimum allowed value below which the number of lost packets, in the absence of interference, abruptly worsens (about 100 %) [40].

The analysis of coexistence issues between WLAN and WSN has been performed considering the following two scenarios:

a) WLAN is victim of WSN interference,

b) WSN is victim of WLAN interference,

in both of which the two networks have been forced to operate on overlapped frequency channels, i.e. channel 11 for the WLAN (central frequency 2.460 GHz) and channel 22 for the WSN (central frequency 2.462 GHz).

For both WSN and WLAN, experiments have been executed in CCA *mode 1*, with a CCA threshold level, P_{th} equal to -76 dBm (default value). Moreover, measurements have been performed inside a non-shielded and non-anechoic room, hence with the potential occurrence of external interference and collateral phenomena like reflections from near metallic objects and structures. To properly account also for this phenomena, different positions of sensor nodes have been considered.

Measurements have been performed following a cross-layer methodology, with the same approach of the analysis described in Part I. For the purpose of this work physical and network/transport layer indices have been evaluated. Moreover, an application layer parameter, goodput, has been considered for the WLAN only.

At physical layer, because of the burst nature of the WLAN and WSN transmissions, care must be taken in the signal power measurements. When a

in the channel.

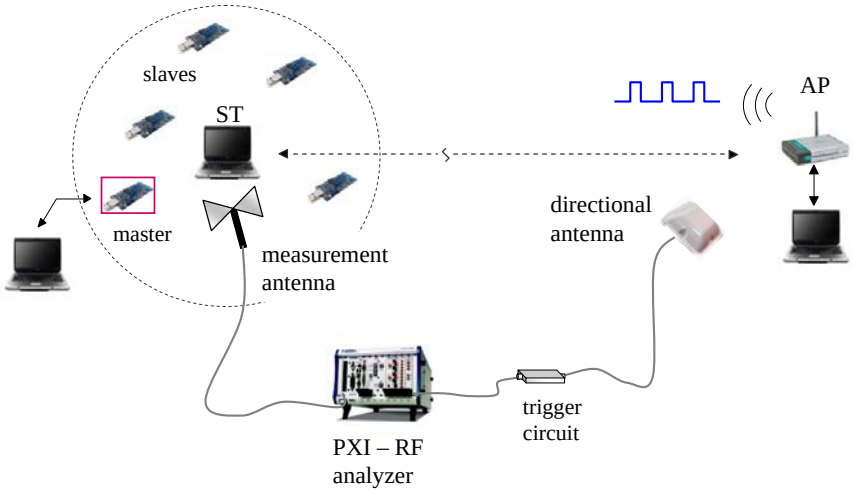

Figure 7.6 Placement of measurement instrumentation on the testbed.

spectrum analyzer is used to measure SIR, the duty cycle must be accounted for, in order to relate the estimates only to the time intervals where the channel is active and to avoid to include in the averaging the ones where the signal is off. A different approach could be to measure signal power in maximum-hold mode, but this method provides the highest packets power estimates, not the average signal power.

In the experiments described in Ch.8, measurements of channel power and signal-to-interference ratio (SIR) have been executed by means of a National Instrument PXI 5660 RF signal analyzer and a receiving measurement antenna, Seibersdorf PCD 8250 biconical dipole (Fig. 7.6). The PXI 5660 is a modular RF signal analyzer optimized for automated test, with a Spectral Measurements Toolkit (SMT), which provides spectral analysis functions including in-band power, adjacent-channel power, and power and frequency-peak-search ability. It is constituted by a 2.7 GHz downconverter and a digitizer module. The PXI 5660 allows to import a TTL trigger signal from an external source, using a front-panel connector, to synchronize RF measurements. Thus, to solve the burst power measurement problem, an external trigger circuit has been suitably realized, in order to perform estimates of the average power in the channel in correspondence to the packet transmission. Since the WLAN signal power has been varied during the test in order to emulate different reception conditions, in some cases the signal strength at the receiver side wasn't sufficient to generate a trigger signal. For this reason the input signal of the trigger circuit has been acquired by a directional antenna located in proximity

of the transmitting device, like sketched in Fig.7.6.

A different meaning has been given to SIR in the two analyzed scenarios. In the a) scenario, $SIR = P_{wlan}/P_{wsn}$, where P_{wlan} is the WLAN useful power, and P_{wsn} is the WSN interference power, both measured over the 22 MHz WLAN channel adopted and at the position where the receiving device is located. In the *b*) scenario, $SIR = P_{wsn}/P_{wlan}$, where P_{wsn} and P_{wlan} are measured over the 3 MHz WSN channel, averaging the power readings achieved at any sensor node position.

At network/transport layer, packet loss ratio, PLR, i.e. the ratio between the number of lost packets and the number of transmitted packets, has been estimated by D-ITG [38] and the WSN tool [39], running on the PCs. In particular, PLR_{wlan} has been estimated as the ratio between the number of packets not received and the total number of packets that should have been transmitted within a time interval of the duration of 60 s. The number of lost packets in turn accounts for two contributions: packets sent but not correctly received by the terminal, and packets not sent within the available time interval.

At application layer the goodput (Sec.7.1.2), which can be considered a QoS parameter, has been mathematically estimated, by means of a *Matlab* routine, for the different values of WLAN transmission parameters deployed in the tests.

Chapter 8

Experimental results

8.1 Experiments in the case of WLAN victim

Preliminary tests, not reported here for the sake of brevity, have been performed upon the varying of the WLAN signal power, while keeping the WSN signal power at the maximum level. The purpose was the definition of a SIR values interval corresponding to high variability of the WLAN performance. This allowed to emulate critical reception conditions to be investigated in the subsequent experiments. Moreover, these test pointed out that, for a thorough analysis of WSN interference effects on the WLAN, the two cases of one-way transmission from AP to ST and one-way transmission from ST to AP needed to be separately evaluated.

8.1.1 Transmission from AP to ST

The conducted experiments have aimed at assessing the effects of the WSN on the near operating ST, in the time interval during which ST is receiving data packets from AP, located at distance d. A typical situation has been thus emulated, in which the WLAN transmitter, being located at a certain distance from the WSN, receives an interference power below its CCA threshold, hence it always finds the channel free and can transmit continuously. Therefore, the two signals (useful and interfering) are received by ST at the same time, with detrimental effects in terms of packet collisions and signal degradation.

The first set of experiments have been conducted monitoring the average WLAN packet loss ratio, PLR_{wlan}, with the SIR fixed to -5.5 dB, and upon the varying of the aforementioned duty cycle λ_{wlan}.

The obtained results are summarized in Fig. 8.1, in which three diagrams are shown, each referred to a specific payload, of 512, 1024 and 1475 bytes, to which correspond the following WLAN packet size: $ps_{wlan} = 600$ (diagram a), 1112 (diagram b) and 1563 bytes (diagram c). Different operative conditions

of the testbed have been enlisted: WSN *off*, WSN *on* with $T_{poll} = 30$ ms and WSN *on* with $T_{poll} = 100$ ms. The solid lines represent the average PLR_{wlan} estimates, while the dashed lines give the percentage of packets not transmitted by AP within the 60 s time interval. Vertical bars are also reported to indicate the standard deviation experimented under different positions of the sensors.

From the analysis of the results, the following considerations can be drawn.

- In the absence of WSN interference, a non-negligible degradation of WLAN performance is visible, which could be attributed to the AP implementation features. In particular, PLR_{wlan} is constant and nearly equal to 5 % up to a given threshold level of λ_{wlan}, equal to 75 %, 75 % and 53 % respectively for diagram *a*), *b*), and *c*), while it increases, even abruptly in diagram *c*), for greater values. This test allows to evaluate the actual performance degradation due to the WSN interference effects, and to distinguish them from losses due to AP's non-idealities.

- In the absence of WSN interference, PLR_{wlan} assumes similar values for $ps_{wlan} = 600$ and 1112 bytes, while higher losses are experienced with $ps_{wlan} = 1563$ bytes. For instance, with $\lambda_{wlan} = 75\%$, WSN *on* and $T_{poll} = 30$ ms, the resulting PLR_{wlan} is 15 %, 10 % and 100 %, respectively.

- In the presence of WSN interference with $T_{poll} = 30$ ms WLAN performance degrades further. For $ps_{wlan} = 600$ and 1112 bytes there is a maximum PLR_{wlan} increase of about 10% and 15% respectively. In the case of $ps_{wlan} = 1563$ bytes and $\lambda_{wlan} \simeq 53\%$, PLR_{wlan} changes from nearly 5 % (without interference), up to 70 %.

- In the presence of WSN interference, the threshold values of λ_{wlan}, beyond which PLR_{wlan} increases, reduce from 75 %, 75 % and 53 % down to 65 %, 60 % and 30 %, respectively for the diagram *a*), *b*), and *c*).

- Increasing T_{poll} of 100 ms, a much weaker interference effect on WLAN is always observed. In particular, quite the same results in terms of PLR_{wlan} have been achieved with respect to the case of WSN *off*.

- The dispersion of PLR_{wlan} estimates around the corresponding mean values, is almost always negligible. The only exception is given in the diagram *c*), with WLAN *on*, and $T_{poll} = 30\ ms$.

- In the diagrams *a*) and *b*), the number of packets not-transmitted is always null, regardless of the chosen λ_{wlan}. This confirms that AP always finds the channel free, and it can transmit continuously.

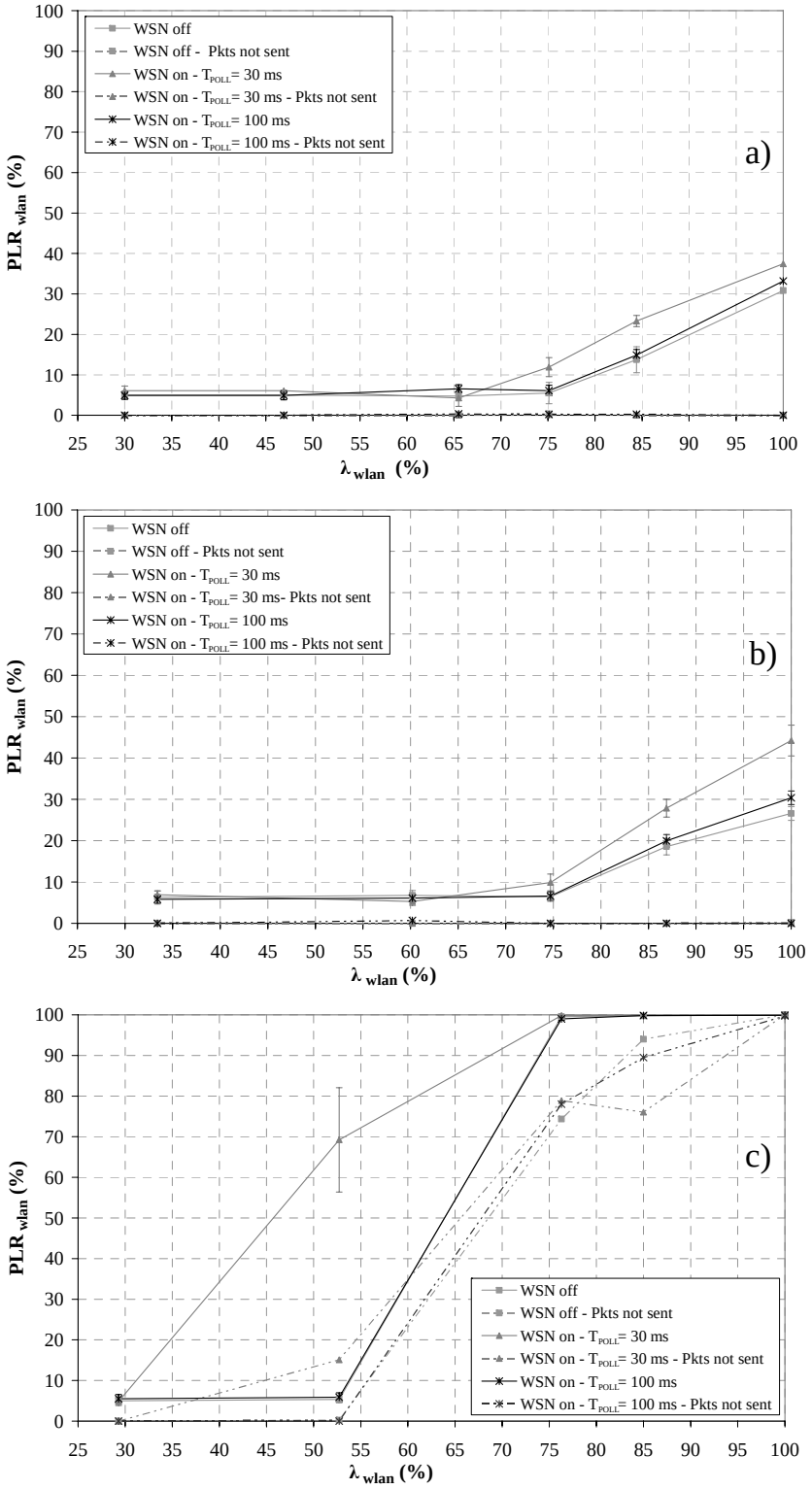

Figure 8.1 PLR of WLAN versus λ_{wlan} for different packet sizes: a) 600 bytes, b) 1112 bytes, c) 1563 bytes.

- In the diagram c), the number of packets not transmitted by AP is not always null, and increases upon the growing of λ_{wlan}. This means that, despite the channel is always assessed free, AP encounters problems to manage so long packet sizes.

In order to cross-correlate the transmission parameters to physical layer and network/transport layer indices, two duty cycle values, $\lambda_{wlan} = 56$ % and 75 %, for the intermediate payload ($ps_{wlan} = 1112$ bytes), have been chosen from the previously described tests. Experiments have been carried out with different level of SIR from -13 dB up to -3 dB. From Fig.8.1b, $\lambda_{wlan} = 56$ % corresponds to a good transmission condition, while and $\lambda_{wlan} = 75$ %, is related to a critical condition as it is the obtained threshold value. The purpose is to investigate the effects of WSN, with $T_{poll} = 30$ ms and 100 ms, on WLAN upon the varying of signal-to-interference ratio, by a comparison between a critical and a good transmission configuration. SIR has been changed by acting only on P_{wlan}, by means of the variable attenuators, placed between the output connector of the AP and the input connector of the external antenna.

The obtained results are summarized in Fig. 8.2, and the following considerations arise.

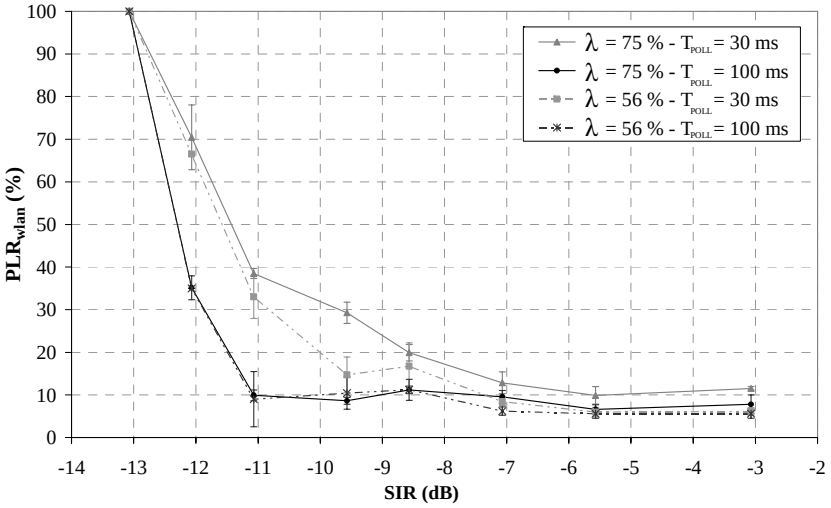

Figure 8.2 PLR of WLAN versus SIR for different λ_{wlan}.

- In the transition range, $-13 \leq SIR \leq -7$ dB, PLR_{wlan} increases from low levels up to 100 % upon the decreasing of SIR.
- In the same range, the effect of T_{poll} on PLR_{wlan} is rather significant; stretching T_{poll} from 30 ms to 100 ms, PLR_{wlan} decreases considerably.

For instance, with $SIR = -11$ dB and $\lambda_{wlan} = 56$ %, PLR_{wlan} lowers from 34 % down to 10 % by increasing T_{poll} from 30 to 100 ms.

- In the upper range, $SIR > -7$ dB, the effect of T_{poll} and λ_{wlan} on PLR_{wlan} is negligible. In fact, quite the same values of PLR_{wlan}, within 5 – 12 %, are achieved regardless of the chosen T_{poll} and λ_{wlan}.

- For levels of SIR below -13 dB, WLAN packets are completely lost, $PLR_{wlan} = 100$ %, regardless of the chosen value of λ_{wlan} and T_{poll}. This is due to the reduced level of P_{wlan} that, for the considered SIR values, is comparable with or lower than the sensitivity level of ST, which is typically at about -84 dBm (in the case of data rate = 11 Mbps).

- The standard deviation is almost always negligible, *i.e.* below 10 %, with the exception of the highest PLR_{wlan}, where higher variability of the estimates is noticed.

8.1.2 Transmission from ST to AP

Further experiments have aimed at assessing the effects of the WSN on the near operating ST, in the time interval during which ST is transmitting data packets to the AP. The typical situation in which the WLAN transmitter, being located in close proximity of the WSN, receives levels of interference power higher than its CCA threshold P_{th}, has been emulated. Consequently, when WSN transmits, ST finds the channel busy and is forced to wait, with effects in terms of delays and consequent packet losses.

The same procedure described in the previous subsection has been applied, and only the meaningful case of $ps_{wlan} = 1112$ bytes has been considered. The obtained results are summarized in Fig. 8.3, from the analysis of which other considerations are of concern.

- In the absence of WSN interference, PLR_{wlan} is constantly lower than 5 %, up to a given threshold level of λ_{wlan}, equal to 75 % (the same value obtained in AP to ST transmission). This can be attributed to the implementation features of the host (ST), resulting more efficient than the AP.

- With respect to the diagram *b)* of Fig.8.1, similar values of PLR_{wlan} have been achieved in the presence of interference.

- The percentage of packets not transmitted is not always null, and it grows upon the increasing of λ_{wlan}.

- The three dashed lines completely overlap to the corresponding solid lines, obtained with the same value of T_{poll} and with WSN *on/off*. The

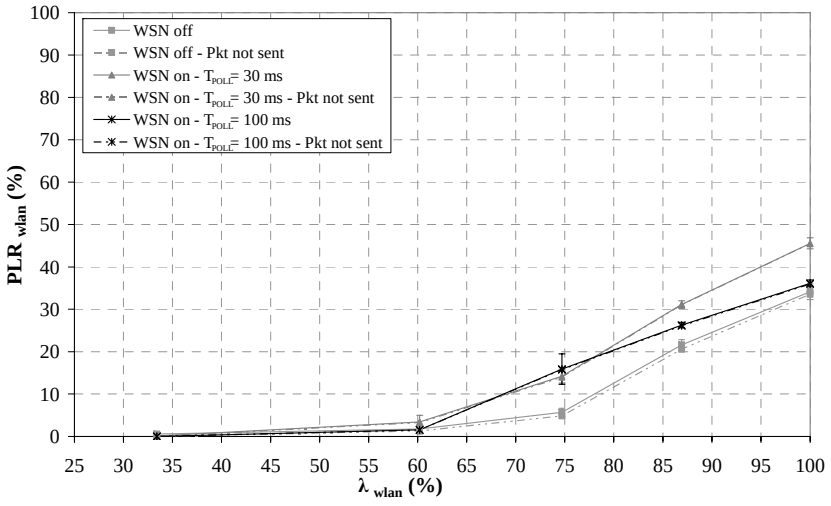

Figure 8.3 PLR_{wlan} versus λ_{wlan} for a packet of 1112 bytes.

percentage of lost packets is equal to the percentage of WLAN packets not delivered. Performance degradation can be thus entirely attributed to the delays introduced by CSMA/CA backoff time, i.e. packets not sent within the available time interval.

- In the presence of WSN interference, the number of lost packets increases significantly for higher λ_{wlan} values. For instance, with $\lambda_{wlan} = 87\%$, PLR_{wlan} is equal to about 27 % and 31 % respectively for $T_{poll} = 100$ ms and $T_{poll} = 30$ ms.

- The variation of T_{poll} from 30 ms to 100 ms, produces a reduction of the interference effect on PLR_{wlan}, in particular for $\lambda_{wlan} \geq 75\%$.

8.1.3 Comments

Both with and without WSN interference, WLAN packet loss ratio strictly depends on λ_{wlan}. It linearly increases for λ_{wlan} values greater than a given threshold, and also depends on the device implementation. It is advisable to set λ_{wlan} below such a threshold, which represents a key parameter in the design stage, to be accurately known and, if necessary, measured as reported above. Furthermore, WLAN packet loss ratio also depends on packets size. In particular, while very similar results have been achieved with $ps_{wlan} = 600$ bytes and 1112 bytes, much higher values have been experienced with $ps_{wlan} =$ 1563 bytes, for $\lambda_{wlan} > 55\%$. The use of 1024 bytes payload (corresponding to a packet size of 1112 bytes) is suggested; it allows the improvement of PLR_{wlan}

in the presence of interference with respect to $ps_{wlan} = 1563$ bytes, and higher throughput with respect to $ps_{wlan} = 600$ bytes.

WLAN packet loss ratio strictly depends also on SIR. In particular, PLR_{wlan} worsens for SIR values below a given threshold, while for upper values it assumes low levels and becomes quite independent to WSN polling time. SIR should be always greater than this threshold, which can in turn be efficiently measured as described before.

In the deployed testbed the effects of WSN interference, in terms WLAN packet loss ratio, are quite the same regardless of the communication direction between AP and ST. However, a different interference phenomenon arises depending on the case of AP transmitting to ST or vice versa. In particular, in the case of AP transmitting to ST, i.e. with WLAN source located at a certain distance from WSN, interference comes out as collisions between WSN and WLAN packets. In the case of ST transmitting to AP, i.e. WLAN source closely located to WSN, interference becomes visible through the CSMA/CA mechanism, which senses the channel always busy.

The increase of WSN polling time from 30 ms to 100 ms allows the mitigation of interference effects of WSN on WLAN in all the cases analyzed, especially for λ_{wlan} and SIR values in correspondence of which the estimated PLR_{wlan} is critical.

In all the analyzed cases, very low standard deviations have been experienced. External interference or collateral phenomena, like reflections, have not introduced significant perturbations on conducted measurements.

8.2 Experiments in the case of WSN victim

A second set of experiments have been carried out on WSN with WLAN acting as interferer. Only the configuration of AP transmitting to ST has been considered. It allows the interference effects of the WLAN on WSN to be better investigated, avoiding the effects of the CSMA/CA mechanism on the interfering signal transmission. In fact, since the AP senses low power levels from WSN, below its CCA threshold, AP always finds the channel free and, consequently, it can transmit continuously, interfering the WSN without interruption.

8.2.1 Results

Measurements have been conducted with three different WLAN packet sizes: $ps_{wlan} = 600$ bytes, 1112 bytes and 1563 bytes, at the same level of sensor nodes output power $P_{mote} = 0$ dBm, and with $T_{poll} = 30$ ms, which guarantees, in the absence of radio interference, a null WSN packet loss ratio [40], here denoted

as PLR_{wsn}. The first experiments have been carried out with $SIR = -3$ dB, and P_{wlan} greater than the CCA threshold of WSN nodes, P_{th}.

In Fig.8.4, the obtained results in terms of WSN packet loss ratio, PLR_{wsn}, upon the varying of WLAN duty cycle, λ_{wlan}, are summarized. The diagram

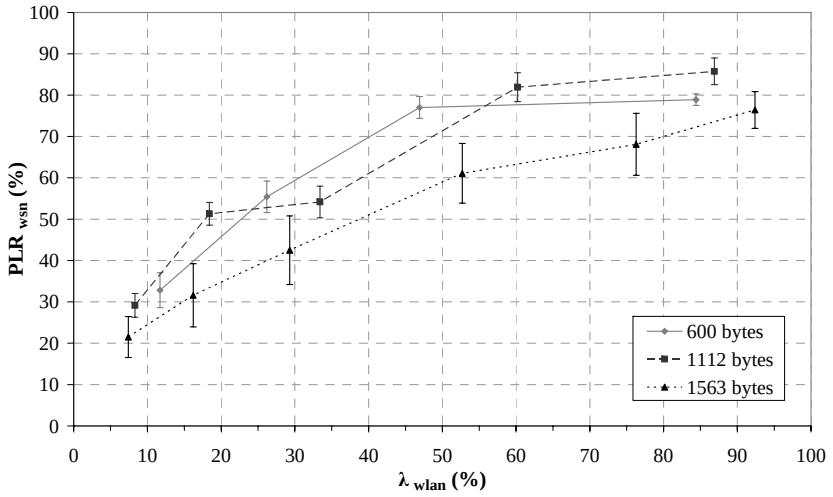

Figure 8.4 PLR_{wsn} versus λ_{wlan}, for different WLAN packet sizes: 600 bytes, 1112 bytes and 1563 bytes, and $T_{poll} = 30$ ms.

clearly shows that, in the presence of WLAN interference, PLR_{wsn} abruptly degrades from 0 % (with WLAN *off*) up to values always greater than 50 %, when λ_{wlan} is set beyond 40 %. Moreover, PLR_{wsn} increases quite linearly and quickly toward a saturation level comprised within 75 – 85 %. In these cases, the probability for a WSN to find the channel free, hence to begin transmission, is very low, and it worsens for shorter WLAN packet sizes. This phenomenon is due to the fact that, for a same value of duty cycle λ_{wlan}, the time interval $(T_R - \tau_{wlan})$ between two consecutive WLAN packets, is greater for bigger size packets. Therefore, a larger time interval is available for WSN transmissions.

To avoid such a critical degradation of WSN performance in the presence of WLAN interference, an efficient solution consists on increasing T_{poll}, for instance from 30 ms to 100 ms. Some tests have been performed with the suggested solution and the obtained results are summarized in Fig.8.5; only one packet size, 1112 bytes, and two values of T_{poll}, 30 ms and 100 ms, have been taken into account. Fig.8.5 highlights that in the case of $T_{poll} = 100$ ms, a reduction of PLR_{wsn} estimates is obtained; the minimum gap is 15% and the maximum gap is 45%, achieved in correspondence of $\lambda_{wlan} \simeq 35\%$.

A further cross-layer analysis involving physical and network/transport layers has been performed on selected WLAN and WSN transmission configura-

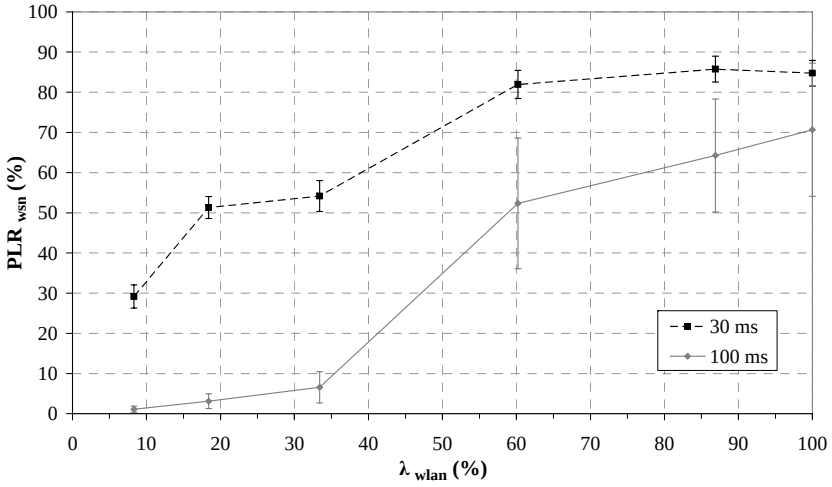

Figure 8.5 PLR_{wsn} versus λ_{wlan} for two values of T_{poll}: 30 ms and 100 ms.

tions. In particular from the previously described tests $ps_{wlan} = 1112$ bytes, $\lambda_{wlan} = 60\%$ have been chosen. This setup guarantees minimum PLR_{wlan} values (Figs.8.1b and 8.3) for the WLAN transmissions, while it is critical when acting as interferer towards the WSN. The results obtained upon the varying of SIR are given in Fig.8.6. The diagram shows that PLR_{wsn} decreases proportionally upon the increasing of SIR, up to a given threshold. Such a threshold value is nearly 16 dB and 8 dB respectively for $T_{poll} = 30$ ms and 100 ms. Beyond the threshold, PLR_{wsn} assumes quite constant values, i.e. nearly 10 % and 0 % respectively for $T_{poll} = 30$ ms and 100 ms. The variation of T_{poll} from 30 to 100 ms reduces the PLR_{wsn} also in this case; the gap varies from 10% to 45%. The maximum PLR_{wsn} reduction is achieved in correspondence of the 100 ms curve threshold value. The trend of the curves remains approximately unaltered.

8.2.2 Comments

Time-sharing of the communication channel is a main issue in coexistence problems, especially in the case of WSN undergoing WLAN interference. A WLAN may considerably degrade the performance of a nearby operating WSN, increasing the values of PLR_{wsn} even for reduced duty cycle, λ_{wlan}, values. Interference effects of a WLAN on a WSN can be mitigated increasing T_{poll} and reducing λ_{wlan} below a suitable threshold. Therefore, a WSN may coexist with a near operating WLAN, but at the detriment of the throughput of both WLAN (lower λ_{wlan}) and WSN (higher T_{poll}), which could be not always

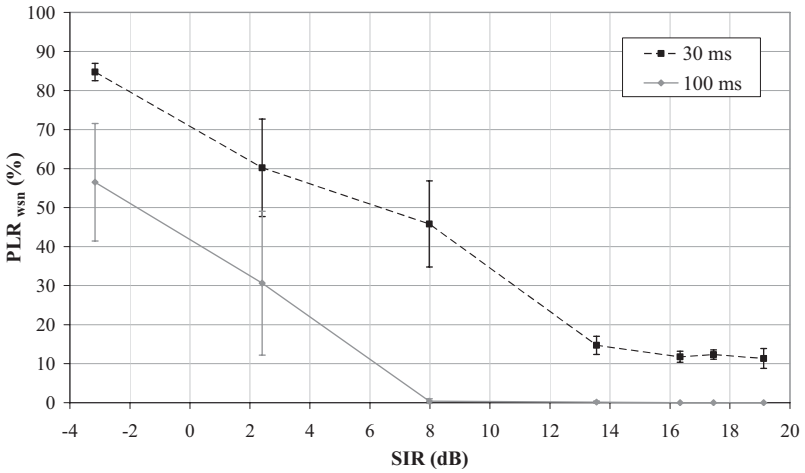

Figure 8.6 PLR of WSN, P_{wsn}, vs SIR for different polling window values: 30 ms, 100 ms.

acceptable. The maximum λ_{wlan} and the minimum T_{poll} to guarantee the desired levels of PLR_{wlan} are essential parameters to be taken into account in a design stage. They can be determined through measurements, like those described above.

PLR_{wsn} strictly depends on SIR, which should be not lower than a given threshold. Such a threshold varies upon the varying of T_{poll} and can be determined experimentally as shown above.

8.3 WSN setup optimization

In this Section, interference effects produced by the WLAN on the WSN are further investigated, with the aim to gain information for the optimization of WSN parameters setup: polling time and nodes density, i.e. number of nodes within the area to be monitored [41].

An additional mote, PM, have been placed at the center of the network coverage area. This node does not cooperate with other motes, and is specifically used to provide power estimates through its embedded RSSI device. It allows the estimation of the received in-channel interference power, P_I, in the area covered by the WSN under test.

8.3.1 Results

A first set of experiments has been carried out with N = 10 motes, three different values of polling time: T_{poll} = 30 ms, 50 ms and 100 ms, and output

power level P_{mote} = 0 dBm. The WLAN has been configured with payload of 1024 bytes and packet rate of 310 packets/s (λ_{wlan} = 38.6 %). In the experiments, only transmission from AP to ST has been activated.

The results obtained in terms of WSN packet loss ratio, PLR_{wsn}, are summarized in Fig.8.7, upon the varying of the WLAN interference power, here denoted as P_I.

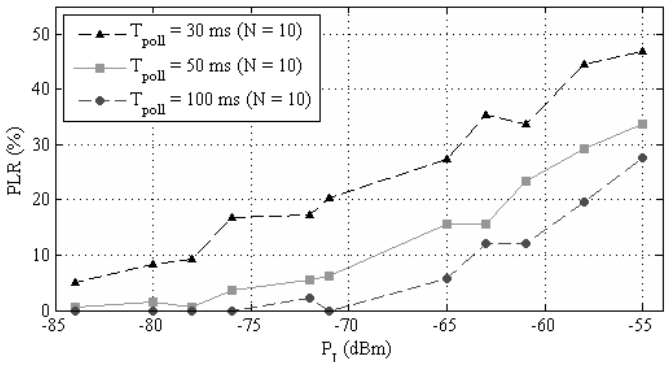

Figure 8.7 PLR_{wsn} vs interfering WLAN power, P_I.

The graph highlights that WSN susceptibility to interference is related to polling time, and decreases upon the growing of T_{poll}. The immunity level of the network, P_{Imax}, i.e. the maximum value of P_I needed to guarantee PLR_{wsn} values below a given threshold, can easily be inferred. For instance, for a maximum allowed PLR_{wsn} of 10 %, P_{Imax} is equal to -78, -68.5, and -63.5 dBm respectively for T_{poll} = 30 ms, 50 ms, and 100 ms. Such values clearly show that for T_{poll} values close to 30 ms, which is the minimum allowed value needed to guarantee PLR_{wsn} = 0 % in the absence of interference, the reduction of P_{Imax} may be considerable. In fact, P_{Imax} lowers of 9.5 dB upon a T_{poll} variation from 50 to 30 ms. Therefore, T_{poll} should never set too close to its minimum allowed value, defined in the absence of interference. On the other hand, upon the varying of T_{poll} from 50 to 100 ms, P_{Imax} increases of only 5 dB. Therefore, increasing T_{poll} beyond a given limit, e.g. hundreds of milliseconds, may be not so useful in terms of P_{Imax}, since P_{Imax} variation entity is lower. Fig.8.7 also shows that PLR_{wsn} grows rather regularly upon the increasing of P_I. This phenomenon allows to deduce that two interference effects simultaneously arise. In particular, a first effect, at Medium Access Control (MAC) layer, is due to the fact that the WLAN occupies the channel and the WSN is obliged to wait for the expiration of interference. In this case, for P_I values greater than CCA threshold, PLR_{wsn} should remain constant upon the increasing of P_I. So, a second interference phenomenon appears. It is due to the fact

that the WLAN may begin its transmission during WSN communication thus causing signal overlapping, and consequent detrimental effects on WSN signal modulation quality. This interference effect, at physical layer, is dependent of P_I, and it increases quite proportionally upon the increasing of P_I. This sort of proportionality is also due to the fact that the higher P_I the greater the number of nodes are interfered, at MAC layer, by AP.

A second set of experiments has been carried out with a number of nodes N = 15, and with T_{poll} = 32 ms and 64 ms. Such values have been chosen to keep the same cycle time T_{cycle} with respect to the previous network setup, N = 10 (Fig.8.7). The cycle time is the total length of the time interval the master node requires to perform the polling of the N-1 nodes: $T_{cycle} = (N-1) \cdot T_{poll}$. Therefore, cycle time can be considered a more general parameter to compare the WSN performance (PLR_{wsn} upon the varying of P_I in this case), for different values of N and T_{poll}.

The obtained results are summarized in Fig.8.8 together with those of Fig.8.7.

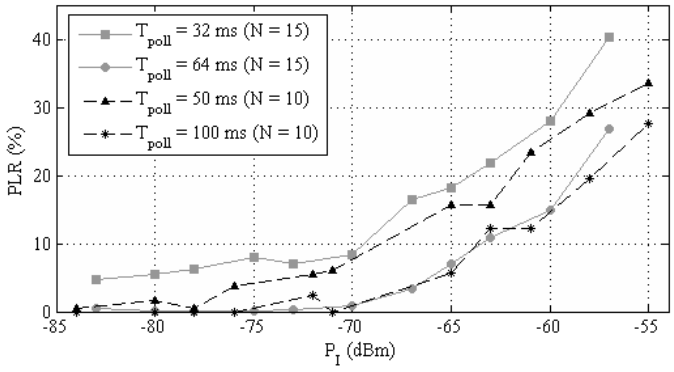

Figure 8.8 PLR_{wsn} vs P_I with two values of N (10 and 15) and different T_{poll} values.

Fig.8.8 shows that the performance of a WSN in the presence of WLAN interference is also related to the nodes density within the area to be monitored. From the comparison of the performance of the two setups providing a $T_{cycle} \simeq$ 450 ms, N = 15 with T_{poll} = 32 ms, and N = 10 with T_{poll} = 50 ms, higher PLR_{wsn} are noticed with N = 15 nodes for any P_I value, with an average 5 % gap between the curves. Similar PLR_{wsn} have been instead achieved for the two setups providing $T_{cycle} \simeq$ 900 ms, N = 15 with T_{poll} = 64 ms, and N = 10 with T_{poll} = 100 ms. The corresponding curves in Fig.8.8 are in fact almost overlapping for any P_I.

In Figs.8.9 and 8.10, the values of PLR_{wsn} measured at each node (represented by $*$ symbols), for the cases of T_{poll} = 50 ms and 100 ms, with N = 10,

are summarized. The solid lines represent the total PLR_{wsn}, already shown in Fig.8.7, obtained averaging the corresponding N readings of PLR_{wsn} provided by the nodes.

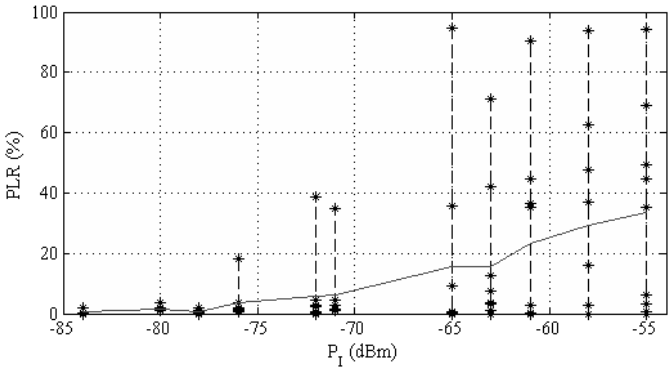

Figure 8.9 PLR_{wsn} vs P_I for N = 10, and T_{poll} = 50 ms.

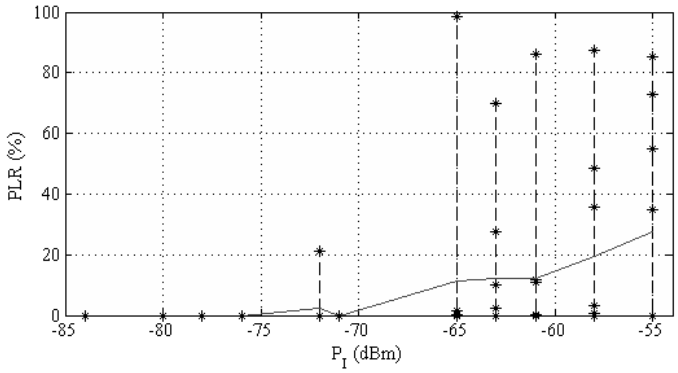

Figure 8.10 PLR_{wsn} vs P_I for N = 10, and T_{poll} = 100 ms.

The graphs show that for interference power levels P_I greater than roughly -72.5 dBm and -65 dBm, respectively for T_{poll} = 50 ms and 100 ms, more than one node may be severely affected by WLAN interference. For instance, in Fig.8.9, for P_I = -65 dBm, despite a mean PLR_{wsn} value not excessively high (i.e. below 20 %) two nodes are strongly affected by interference, i.e. PLR_{wsn} = 36 % and 95 %. In many practical situations, e.g. in case of WSN for industrial monitoring, similar performance losses, even if related to a couple of node, can not be accepted. In these cases, a network designer should accurately know the maximum value of P_I allowed to avoid failures of one or more nodes.

From Figs.8.9 and 8.10, such values are equal about to -72.5 and -65 dBm, respectively for T_{poll} = 50 ms and 100 ms, while in the cases of P_I = -76 dBm and -72 dBm, respectively, only one node presents PLR_{wsn} nearly equal to 20 %.

8.3.2 Comments

The obtained experimental results have confirmed that the high packet loss ratio arising in the presence of WLAN in-channel interference, can be effectively reduced by increasing the polling time, when it is close to the minimum allowed value (30 ms in this case). In general, network degradation worsens quite regularly upon the increasing of the interference power level. This appears to be due both to interference effects at physical layer and to interference at MAC layer. WSN immunity against WLAN interference also depends on the number of nodes deployed to monitor a given area, and may worsen upon the increasing of it. The maximum allowed interference power to avoid packet loss at each WSN node is then an essential parameter to be known by for the network design and optimization. In the test reported in this Section, it has been effectively estimated by means of the nodes' RSSI.

8.4 WLAN goodput estimation

For the estimation of throughput and goodput in ideal channel conditions, two different aspects have to be taken into account. The first one is related to the overhead, i.e. the addition of bytes (fields) to the payload, which are required for the correct transmission and routing of the data. The second one regards the medium access protocols and the handshaking procedures [42].

The total overhead applied to the data when the UDP protocol is utilized in 802.11b transmissions consists of 88 bytes, as reported in Sec.7.1.1. The time required for sending the entire frame, τ_{wlan}, can be computed as reported below:

$$\tau_{wlan} = t_{pr} + t_d = \frac{24 \cdot 8\ [bit]}{1\ [Mbps]} + \frac{64 \cdot 8\ [bit] + Payload}{11\ [Mbps]} \tag{8.1}$$

where t_{pr} is the time necessary for the preamble transmission, consisting of 24 bytes, at 1 Mbps, and t_d is the time required for the frame (64 bytes + payload) transmission at 11 Mbps. The goodput could be obtained by the following equation:

$$G_{pkt} = \frac{Payload}{\tau_{wlan}}\ [Mbps] \tag{8.2}$$

However, for the effective goodput estimation the time intervals required by the medium access protocol must be considered. In the experiments described

in this Chapter the default basic access mechanism has been set. The global time interval requested for the transmission of a packet is then:

$$T_{pck} = DIFS + \tau_{wlan} + SIFS + t_{ack} \tag{8.3}$$

where t_{ack} is the time required for the ACK transmission. The ACK consists of 14 bytes plus the preamble, consequently its time duration is:

$$t_{ack} = t_{pr} + \frac{14 \cdot 8\ [bit]}{11\ [Mbps]} \tag{8.4}$$

The goodput can be then computed as:

$$G = \frac{Payload}{T_{pck}}\ [Mbps] \tag{8.5}$$

In order to perform a cross-correlation between the PLR of the analyzed networks and the WLAN effective goodput, the latter has been mathematically estimated for the same values of WLAN duty cycle ($\lambda_{wlan} = T_{pck}/T_R$) and packet size, ps_{wlan}, employed in the experiments. It must be noted that the transmission packet rate and packet size, selected by means of the D-ITG software, have been set according to values up to a maximum $\lambda_{wlan} = 100\%$. Pointedly, when the combination of packet size and packet rate produces a λ_{wlan} equal to 100%, no time margin is left for medium access procedures occurring in non-ideal channel conditions, characterizing real-life environments like the one used for the previously described tests. This clarifies the reason why packet losses are encountered for high duty cycle values even in the absence of WSN interference.

To the purpose of 802.11b WLAN goodput estimation a *Matlab* routine has been developed. The obtained results are reported in Fig.8.11. For a fixed packet size, the goodput clearly increases upon the increasing of the duty cycle. For a fixed duty cycle, the higher the duty cycle value, the more rapid is the rise of the goodput upon increasing of the packet size. One may also note that the maximum rate achieved by a 802.11b network exploiting the UDP protocol is roughly 8 Mbps.

8.5 Coexistence issues

The obtained results have underlined the importance of the two parameters ps_{wlan} and λ_{wlan} in the optimization of both IEEE 802.15.4 and IEEE 802.11b networks performance, when operating in the same environment and sharing the same frequencies. To optimize their choice, diagrams like the one in Fig.8.12 can be usefully exploited.

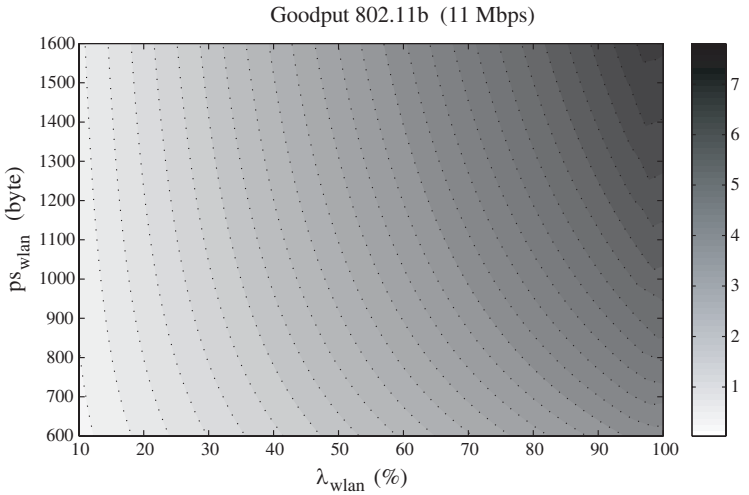

Figure 8.11 WLAN goodput (Mbps) upon the varying of ps_{wlan} and λ_{wlan}.

The diagram shows two sets of curves: the dashed ones represent values of ps_{wlan} and λ_{wlan} corresponding to a constant level of PLR_{wsn} (vertically-oriented labels), while the solid ones represent the values of ps_{wlan} and λ_{wlan} that guarantee a given level of PLR_{wlan} (horizontal-oriented labels). The two sets of curves refer to $T_{poll} = 30$ ms, which is the most critical WSN setup both in the case of WSN victim and in the case of WLAN victim.

The diagram fixes the couple of ps_{wlan} and λ_{wlan} values allowing to trade-off between the increase of WLAN goodput (which can be pursed increasing ps_{wlan} and/or λ_{wlan}, see Fig.8.11) and the minimization of PLR of both networks.

- It is clearly visible from the diagram that the predominant interference effect is due to WLAN towards WSN. WSN performance cause a PLR_{wsn} equal to 50% even when the WLAN duty cyle is rather low, i.e. λ_{wlan} is about at 25%.
- The WLAN provides the best performance for packet sizes lower than 1200 bytes. The WSN instead generally shows lower packet losses when the WLAN packet size is higher than 1200 bytes.
- If an high PLR_{wsn} can be admitted (about 70%), the optimal choice for the WLAN requires a payload of 1024 byte ($ps_{wlan} = 1112$ bytes).
- If priority is given to WSN performance, a considerable reduction of WLAN duty cycle is mandatory, with $\lambda_{wlan} < 25\%$. A consequent packet size increase is necessary to optimize the goodput of the WLAN, as pointed out by Fig.8.11.

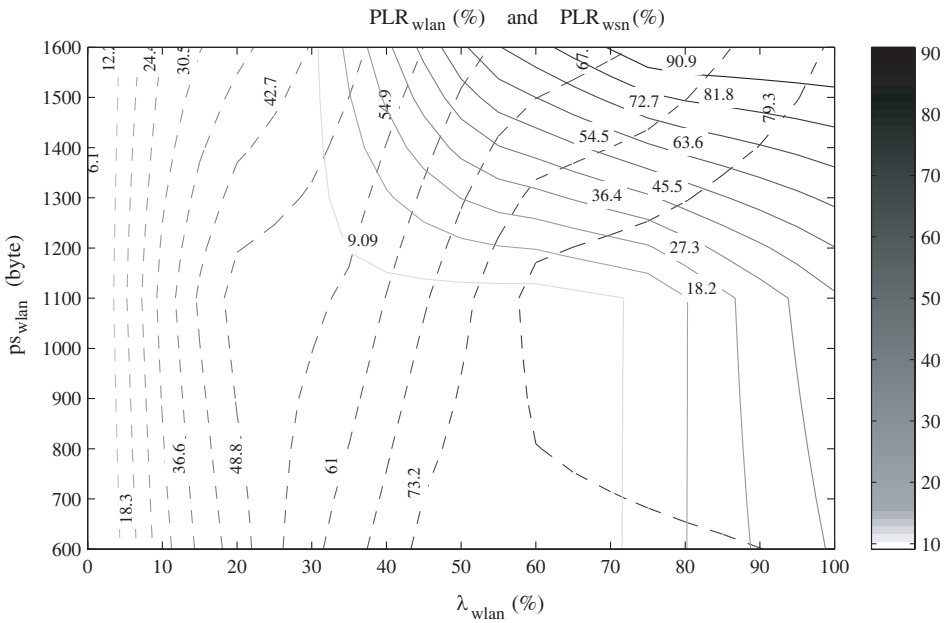

Figure 8.12 PLR_{wsn} (dashed lines) and PLR_{wlan} (solid lines) for different setup of a WLAN.

The data related to the WLAN application layer, provided in Sec.8.4, allow to cross-correlate the network transmission parameters to the performance in terms of packet loss ratio and to the goodput, i.e. the actual speed of the network, which both are quality of service indices. The information deduced leads to an overall optimization of the wireless networks when coexistence issues are encountered.

As an instance, in case that higher priority is given to the WLAN, the $PLR_{wlan} = 9\%$ solid line could be taken into account (and high PLR_{wsn} be accepted). Let's consider the two crossing points of the $PLR_{wlan} = 9\%$ solid line and the $PLR_{wsn} = 79.3\%$ dashed line on Fig.8.12; their coordinates approximately are:

a : $\lambda_{wlan} = 60\%$, $ps_{wlan} = 1112$ bytes

b : $\lambda_{wlan} = 71\%$, $ps_{wlan} = 710$ bytes

and they both guarantee same values of PLR_{wlan} and PLR_{wsn}. From the results obtained in Fig.8.11, it can be clarly noticed that the most convenient choice in terms of goodput maximization corresponds to point a, with $\lambda_{wlan} = 60\%$ and $ps_{wlan} = 1112$. In case that higher priority is given to the WSN, if for example the $PLR_{wsn} = 36.6$ dashed line is considered, a corresponding

$PLR_{wlan} < 9\%$ results. Contextually, a choice of $ps_{wlan} = 1600$ bytes is required, as it allows an higher duty cycle value ($\lambda_{wlan} > 20\%$) if compared to shorter packet sizes. In fact, as pointed out by Fig.8.11, this setup leads to the maximization of the WLAN goodput.

8.6 Conclusions

The measurement methodology described in Part II of the thesis allowed to effectively evaluate different transmission configurations of an IEEE 802.11b WLAN and an IEEE 802.15.4 network operating in a real-life environment. In particular it has been applied to coexistence issues between such networks. Helpful information for designers and technicians, to efficiently operate with such networks and optimize their setup in real-life conditions can be deduced by the employment of analogous techniques.

The proposed experimental tests pointed out physical layer's (SIR) and network/transport layer's (PLR) indices cross-relations with transmission parameters both of WLAN (duty cycle and packet size) and of WSN (polling window and nodes density). Furthermore, the obtained results have been related to the application layer throughput (goodput) optimization, which is a main issue especially for WLAN.

The experimental analysis has confirmed that WLAN and IEEE 802.15.4 WSN may coexist when operating in the close proximity, but at the detriment of the achievable performance, mainly in terms of packet loss ratio and goodput. In the case of WLAN victim, WLAN duty cycle must be always set lower than a given threshold value, which depends on WLAN packet size and decreases in the case of WSN interference. In the opposite case, WSN victim, a much more visible loss of WSN packets arising when WLAN transmits has been observed. In particular, at the beginning of WLAN operation, PLR increases abruptly from 0 % to values beyond 70 %. In this case, to enhance WSN reliability, a solution may be either to increase the time duration of the polling window, in such a way as to have more possibilities to correctly retransmit, or to reduce the WLAN duty cycle. This solution causes a lower throughput of the WSN, when a longer polling window is set, or of WLAN, if the duty cycle is reduced.

Bibliography

[1] R. Van Nee, R. Prasad *OFDM for wireless multimedia communication*, Artech House.

[2] L. Litwin, M. Pugel *The principles of OFDM*, RF signal processing, January 2001.

[3] N. Benvenuto, G. Cherubini *algorithms for Communications Systems and Their Applications*, J.Wiley & Sons, 2002.

[4] DVB Project, *Introduction to the DVB Project*, DVB Fact Sheet, March 2007.

[5] ETSI EN 300 744, *Digital Video Broadcasting (DVB); Framing structure, channel coding and modulation for digital terrestrial television*, v. 1.5.1, June 2004.

[6] ETSI TR 101 290, *Digital Video Broadcasting (DVB); Measurement guidelines for DVB systems*, v. 1.2.1, May 2001.

[7] U. Ladebusch, C.A. Liss *Terrestrial DVB (DVB-T): A Broadcast Technology for Stationary Portable and Mobile Use*, Proc. of the IEEE, Vol. 94. NO.1, January 2006.

[8] L. Angrisani, M. Vadursi *Performance Assessment of Wireless Communication Networks through Cross-Layer Measurements*, Proc. of IMTC 2006, Sorrento, Italy, pp. 201-206, April 24-27, 2006.

[9] ITU-R BT.1683, *Objective perceptual video quality measurement techniques for standard definition digital broadcast television in the presence of a full reference.*

[10] S. Wolf, M. Pinson *Video Quality Measurement Techniques* NTIA Report 02-392, June 2002.

[11] *The Chester 1997 Multilateral Coordination Agreement relating to Technical Criteria, Coordinatio Principles and Procedures for the introduction of Terrestrial Digital Video Broadcasting (DVB-T)*, Chester, 25 July 1997.

[12] ITU-R BT.500, *Methodology for the subjective assessment of the quality of television pictures.*

[13] M. Bertocco, A. Sona, P. Zanchetta *Uncertainty of Channel Power Measurements with Spectrum Analyzer* Proc. of IMTC 20045, Ottawa, Canada, pp. 947-951, May 17-19, 2005.

[14] M. Bertocco, A. Sona, *On the power measurement via a spectrum analyzer*, Proc. of IMTC 2004, Como, Italy, pp. 958-963, May 18-20, 2004.

[15] R. Hranac, B. Currivan, *White Paper: Digital Transmission: Carrier-to-noise Ratio, Signal-to-Noise Ratio, and Modulation Error Ratio*, Broadcom Corporation and Cisco System, 2006.

[16] Simon, Hinedy and Lindsey, *Digital Communication Tecniques.*

[17] F. Xiao, *DCT-based Video Quality Evaluation*, Final Project for EE392J, 2000.

[18] ITU-R Recommendation BT.601, *Encoding parameters of digital television for studios.*

[19] J. Lago-Fernandez and J. Salter, *Modelling Impulsive Interference in DVB-T*, EBU Technical Review, July, 2004.

[20] Application Note 1314 - *Testing and Troubleshooting Digital RF Communications Receiver Designs*, Agilent Technologies, 2002.

[21] C. Weck, *Validate Field Trials pf Digital Terrestrial Televison, DVB-T Field Trials around the World* DVB Project Office, Geneva, Switzerland, June 1999.

[22] R. Raulefs, J. Cosmas, K. Loo, M. Bard, G. Pousset, D. Bradshaw, Y. Lostanlen, I. Defee, P. Kasser, and S. Kalli, *Physical Layer DVB Transmission Optimisation (PLUTO)*, Proc. of 15th IST Mobile Summit 2006, Mykonos, Greece, June 2006.

[23] J.T.Ong, S.V.B.Rao, Yan Hong, and G.Shanmugam, *Measurements and Analyses of Digital TV Signals in an Indoor Environment*, Antennas and Propagation, 2003. (ICAP 2003). Twelfth International Conference on (Conf. Publ. No. 491).

[24] I. Haratcherev, J. Taal, K. Langendoen, R. Lagendijk, and H. Sips, *Optimized Video Streaming over 802.11 by Cross-Layer Signaling*, IEEE Communications Magazine, January 2006.

[25] O. Nemethova, M. Ries, M. Zavodsky and M. Rupp, *PSNR-Based Estimation of Subjective Time-Variant Video Quality for Mobiles*, Proc. of MESAQIN 2006, Prague, Czech Republic, June 2006.

[26] P. Brétillon, J. Baïna and G. Goudezeune, *Video Quality Monitoring in Digital TV networks*, EBU Technical Review, September 2000.

[27] L. Angrisani and M. Vadursi, *Cross-Layer Measurements for a Comprehensive Characterization of Wireless Networks in the Presence of Interference*, IEEE Trans. Instrum. Meas., vol. 56, no. 4, pp. 1148-1156, August 2007.

[28] M.G. Sanchez, L. de Haro, M.C. Ramon, A. Mansilla, C.M. Ortega and D. Oliver, *Impulsive Noise Measurements and Characterization in a UHF Digital TV Channel*, IEEE Transaction on Electromagnetic Compatibility, vol. 41, NO.2, May 1999.

[29] X. Puig, S. Barrera *Interferences in DTT (Digital Terrestrial television)*, Proc. of EMC Europe 2006, Barcelona, Spain, pp.306-309, September 4-8, 2006.

[30] M. Bertocco, M. Farias, D. Fortin, A. Sona, *Cross-Layer Measurement for the Analysis of a DVB-T System Performances at the End User Level*, Proc. of IMTC 2006, Sorrento, Italy, pp.196-200, April 24-27, 2006.

[31] I. Howitt, *WLAN and WPAN Coexistence in UL band*, IEEE Trans. on Vehicular Technolgy, vol. 50, no. 4, pp. 1114–1124, Jul. 2001.

[32] N. Golmie, R. E. Van Dyck, A. Soltanian, A. Tonnere, O. Rebala, *Interference Evaluation of Bluetooh and IEEE802.11b Systems*, Wireless Networks, vol. 9, pp. 201–211, 2003.

[33] L. Angrisani, M. Bertocco, D. Fortin, A. Sona *Assessing coexistence problems of IEEE 802.11b and IEEE 802.15.4 wireless sensor networks through cross-layer measurements*, Proc. of IMTC 2007, Warsaw, Poland, May 1-3, 2007.

[34] ANSI/IEEE Std 802.11 Part 11: *Wireless LAN Medium Access Control (MAC) and Physical Layer (PHY) Specifications*, 1999 Edition (R2003).

[35] IEEE Std 802.11b 1999/Cor 1-2001 Part 11: *Wireless LAN Medium Access Control (MAC) and Physical Layer (PHY) specifications.*

[36] G. Bianchi *Performance Analysis of the IEEE 802.11 Distributed Coordination Function*, IEEE Journal on selected areas in Communication, vol. 18, no. 3, pp. 535–547, March 2000.

[37] IEEE Std 802.15.4, Part 15.4: *Wireless Medium Access Control (MAC) and Physical Layer (PHY) Specifications for Low-Rate Wireless Personal Area Networks (LR-WPANs)*, October 2003.

[38] http://grid.unina.it/software/ITG

[39] http://www.dei.unipd.it/ricerca/gmee

[40] M. Bertocco, G. Gamba, A. Sona, S. Vitturi, *Performance Measurements of CSMA/CA-Based Wireless Sensor Networks for Industrial Applications*, Proc. of IMTC 2007, Warsaw, Poland May 1-3, 2007.

[41] L. Angrisani, M. Bertocco, D. Fortin, A. Sona, *Experimental Analysis of WLAN Interference Effects on IEEE 802.15.4 Wireless Sensor Networks*, Proc. of EMC Europe Workshop, Paris, France June 14-15, 2007.

[42] P. Zanchetta, *Misure di tipo cross-layer per la valutazione delle prestazioni di reti 802.11 in presenza di interferenti*, Istituto di Elettronica e di Ingegneria dell'Informazione e delle Telecomunicazioni IEIIT-BO/CNR, Sept. 2007.

List of Figures

List of Tables